Creep response of Ti–6Al–4V alloy produced by additive manufacturing: Effect of annealing at 1050 °C

Materials Science & Engineering A

Creep response of Ti–6Al–4V alloy produced by additive manufacturing: effect of annealing at 1050 °C

--Manuscript Draft--

Manuscript Number:	MSEA-D-22-04178R1
Article Type:	Research Paper
Keywords:	Additive manufacturing; Phase Transitions; Creep; Microstructure; Titanium alloys
Corresponding Author:	Eleonora Santecchia UNIVPM Ancona, ITALY
First Author:	Stefano Spigarelli
Order of Authors:	Stefano Spigarelli
	Chiara Paoletti
	Emanuela Cerri
	Eleonora Santecchia
	Marcello Cabibbo
Abstract:	The present study mainly aims at investigating the creep response of a Ti–6Al–4V alloy produced by additive manufacturing and annealed above the β-transus, and at rationalizing the differences observed when comparing its behaviour to that of the same alloy annealed at lower temperatures. Herein, the creep response of this alloy produced by additive manufacturing and subsequently annealed at 1050 °C is investigated at temperatures ranging from 500 to 650 °C. The heat treatment produces the typical Widmanstätten microstructure with thin β-lamellae interposed between coarse α-lamellae. The minimum creep rate dependence on the applied stress and temperature is compared with literature data of tests of alloys with Widmanstätten microstructures produced by traditional technologies. A modified form of an equation, successfully used to describe the creep responses of the Ti–6Al–4V alloy with different initial microstructures, was here proposed. The suggested modification introduces a threshold stress, which is related to the presence of finely spaced α–β interfaces and α2-Ti3Al particles. This threshold stress is considered to be negligible when the distance between the α–β interfaces is long and the α2-Ti3Al particles are absent or excessively spaced. In contrast, in the materials with Widmanstätten microstructures, even minor differences in the heat treatment conditions and/or the processing history cause considerable variations in the distance between the α–β interfaces. This coupled with the occasional precipitation of α2-Ti3Al particles results in different threshold stress values.
Suggested Reviewers:	Michael Kassner kassner@usc.edu
	Elisabetta Gariboldi elisabetta.gariboldi@polimi.it

UNIVERSITÀ
POLITECNICA
DELLE MARCHE

Dipartimento
di Ingegneria
Industriale e Scienze
Matematiche
DIISM

Ancona, October 17th, 2022

Dear Editor,
the present paper is the revised version of the first-submission manuscript and deals with the creep response of a Ti-6Al-4V alloy produced by additive manufacturing and annealed at 1050°C.
A file with the detailed answers to the Reviewers' comments and the actions taken has been included; all the changes have been highlighted in the marked-up manuscript.
The text underwent proofreading by the Elsevier service (certificate LE-244504-E13D7F6F518B).
We thank you in advance for considering our research and we await your response and the comments of Reviewers to our modifications and replies.

Yours Sincerely,

Eleonora Santecchia
Corresponding Author

Dr. Eleonora Santecchia
Assistant Professor
Department of Industrial Engineering and Mathematical Sciences (DIISM)
Marche Polytechnic University
Via Brecce Bianche 12
60131 Ancona
Italy

Phone: +39 071 2204731
E-mail: e.santecchia@staff.univpm.it

Reviewer #1: amendment in marked-up text in green

…….. it seems that this new manuscript is an accessory to the author's previously published article Ref. [2], not a complete work. Some conclusions cannot be made based on the results of this manuscript, if without considering Ref. [2]. Even the summary (Section 4.3 Summary of possible roles of different phases in creep response) of this new manuscript is concluded based on the results of this new manuscript and this Ref. [2] together. Also, the authors frequently cite the self-article Ref. [2] in many discussions, citing this Ref. [2] without appropriate descriptions. In this case, readers will have to read Ref. [2] carefully while reading this new article.

REPLY: Reviewer 1 rises an interesting problem. The case will be also discussed in our REPLIES to points 7 and 8. The reviewer's objection that the draft is not a complete work, from our point of view, is not correct. The paper contains a full dataset of experimental results, described in details, accompanied by accurate microstructural analysis. What is correct, is that the new manuscript relies on the constitutive model proposed in [2]. The point is that the "conventional" approach for publishing a paper is to present a set of data for a specific initial material state, and discuss these data by an ad-hoc constitutive model. This implies that we find in the literature a number of different descriptions for Ti64 creep response, scarcely compatible one each other. Our aim is to overcome this problem. We would like to propose a constitutive model which is able to describe, or, even, predict, the material response, irrespective of the heat treatment. Reference [2] demonstrated that this is possible, since the resulting constitutive model only required the estimate of the UTS to properly work and describe a many different datasets obtained by different labs. The only major exception was the behavior of the alloys with Widmanstatten microstructure. Literature, in this case, provides a sort of "cloud" of data, a significant problem. The present draft aims at covering this gap. To obtain a reliable description, a good set of data spanning over decades of strain rates (not available in the literature) was a prerequisite, and the model in [2] should be amended to take into account the differences in microstructure. This is exactly what is addressed in this draft.

1. Abstract: What is the significance of this article? What problem this article is solving? What can be the contribution of this article to the research/engineering community? These points can be highlighted in the Abstract. These points are also what the journal MSEA calls for.

REPLY: we believed that the main task of the study was already well expressed in the last sentence of the Introduction, but we nevertheless included a new sentence which illustrates the aims of the study.
ACTIONS: The initial part of the Abstract was rewritten.

2. Material and Experimental procedures: what's the geometry of the dog-bone creep samples?

REPLY: We do not think this is an essential information, since "dog-bone" is a self-illustrating concept, and dimensions of the gauge length were already provided. Nevertheless we included a new figure.
ACTIONS: a new figure (Figure 1) was included.

3. Figure 1 and 2: Suggest to point out which parts are α, β, and α' respectively.

ACTIONS we included a new caption for Figure 1 and added relevant information to Figure 2 and Figure 3 captions to indicate the existing different phases.

4. Figure 6: the caption may need to be modified to highlight what data is compared in this figure. Also, the symbol can be modified or necessary instruction can be added. The current symbol may confuse readers, for example, the black square and the white square both represent the data obtained under 500 °C?

ACTIONS: we thank the Reviewer that highlighted an error in Figure 6a. We corrected the mistake, and included a new sentence in the caption to further clarify symbols meaning.

5. Table I. How the volume fractions of phases are calculated?

REPLY: The following was added to the Materials and Method 2.4 Microscopy sub-section:

ACTIONS: Converged-beam electron diffraction (CBED) was used to identify the different detected phases, using a nominal electron beam of 5-6 nm. Volume fraction of detected phases (namely, α', α_2, and β) was evaluated by the Schwartz–Saltykov method. The method, was adapted to the TEM thin foil analyses by consider the bias introduced by the TEM thin foil and the precipitate morphology, i.e., lamellae (α), thin ribbon-like structures (β), and coarser lenticular morphological phase (α', α_2).

6. The authors frequently cite the self-article Ref. [2] in many discussions. Ref. [2] is a good article, but I suggest to describe it briefly when Ref. [2] is cited in this new manuscript, not just simply citing it. Otherwise, readers will have to read Ref. [2] carefully while reading this new article. For example, "Based on these observations, creep response was considered in [2] to be is primarily driven by the deformation of the α-phase, which accounts for approximately 90 % of the overall alloy structure." Here, what is the creep response? This can be simply described here besides just citing this article.

"Moreover, based on the findings presented in [2], it provides supplementary material in form of additional microstructural analyses." Here, what are the findings?

"However, an important issue, already presented in [2] worth describing here…". Here, what is the important issue

REPLY: we tried to pack as much information as possible in the draft, without duplicating the previous study. The Reviewer's suggestion was already implemented in the draft (Section 4.2 is a summary of the microstructural findings in [2]). Albeit we are not fully convinced that to describe in details the results in [2] is a good solution, we included a new Appendix II for illustrating how the model worked for different microstructures.

On the other hand, the reviewer objections are sometimes debatable. For example, the "important issue" is clearly illustrated in the rest of the quoted sentence, which reads "However, an important issue, already presented in [2] worth describing here <u>is the extremely large scatter of the minimum creep rate data observed when comparing different batches [3–8] of Ti–6Al–4V alloys having Widmanstätten structures</u>". This scatter is clearly presented in Figure 7a, and is self-explaining.

ACTIONS. A new Appendix 2 was included, to recall some of the findings in [2]. The sentence "Moreover, based on the findings presented in [2], it provides supplementary material in form of additional microstructural analyses" was omitted, since the sentence is ambiguous.

7. It seems that this new manuscript is an accessory to the author's previously published article Ref. [2], not a complete work. Even the summary of this new manuscript has to be concluded based on the results of this new manuscript and this Ref. [2] together.

"The results presented in this study and in a recent similar study by the authors [2] allow to draw some important qualitative inferences on the possible roles of the different phases in the creep response of the studied Ti-6Al-4V alloy."

Here, I may suggest to only summarise the points that the results from this manuscript can support.

REPLY: here, the comments and suggestion are worth discussing. The point of the reviewer, is that "this new manuscript is an accessory to the author's previously published article Ref. [2], not a complete work". We already addressed this view in the opening of this letter. It seems that the reviewer would like reading only about the results of this specific study. This actually goes against our aim. The point is that the usual approach is exactly the one suggested by the reviewer. We find in the literature a plethora of studies which illustrate the behavior of alloy A in state A, or in state B, or in state C…..each study reporting a limited picture of the same material response. In the case of the present alloy, we have investigations of the creep response of Ti64 with equiaxed, duplex, lamellar microstructures, but no

efforts to obtain a unified description of the material response which rationalize the differences…at least until ref.[2] was published. We am at obtaining a set of constitutive equations which can be used to describe ALL the datasets. Thus, quoting/summarizing the results obtained in the previous study is essential, to provide a broader picture of the material response. The model, as provided in [2], does not work for a specific microstructure. In the form here modified, it seems to work for ALL the microstructures.
ACTIONS: A new appendix II was included; this appendix reports few examples of the finding in [2].

8. In this manuscript, it seems that the self-article Ref. [2] is overused.
REPLY: the same comments apply here. Reference [2] illustrates a model that described the Ti64 creep response in a broad range of initial states, the only partial exception being the Widmanstatten structure investigated in this draft. This paper aims at filling this gap, so a discussion of previous finding cannot be overlooked. We are well aware that the reading of the text is demanding, but, in the meantime, we believe that the behavior of a complex alloy cannot be described by "simple" approaches.
ACTIONS: none

Reviewer #5, amendments in marked-up manuscript in yellow

1. Above the β-transus temperature, why was the annealing temperature determined to be 1050℃? What temperature range was the modified form of equation suitable for?
REPLY: as reported in the text, production and heat treatment was carried out on an industrial plant. The annealing temperature is the obvious compromise to obtain a treatment above beta-transus, without increasing the cost. As for the second part of the question. In principle, the constitutive model was devised to be useful in the WHOLE range of annealing temperatures. What you must know is the beta distribution and the UTS. As obvious, microstructural data are lacking, and no information is available on the typical alpha-beta interface distance for the different treatments, so this study only represents a first step to really solve this intriguing problem.
ACTIONS: a sentence was modified in Section 2.1.

2. What was the purpose of the variable-load creep experiments? Were VLE and CLE experiments did at the same time? It seems that the curves of VLE and CLE cannot be distinguished.
REPLY: VLE were carried out to obtain multiple data-points from a single test, and to evaluate is a significant softening or hardening occurred after prolonged creep exposure. The reviewer is correct, VLE data roughly align with CLE results, in this case, although in one case, the VLE test at 500°C, a moderate hardening was observed.
ACTIONS: We included few comments on this regard in Section 3.2, and we used different symbols for VLE and CLE.

3. The Figure 4b mentioned in the text cannot be found.
ACTIONS reviewer is correct, the text should read "Figure 4" (now Figure 5). Text was amended.

4. How the data points in Figures 5 and 6 were obtained?
REPLY: data for Fig.5 and 6 were obtained, as usual, from the strain-strain rate curves obtained in the present study , i.e. from Figure 3 and 4 which show most of the experiments (figure 5, solid symbols in Figure 6, all belong to the same dataset) and from literature (open symbols in Figure 6), as indicated in the caption.
ACTIONS: none, except that we added the somewhat pleonastic statement "the minimum strain rate as a function of the applied stress obtained from experimental curves".

5. Why Figure 8 only showed the results of the 650°C experiment? What about 500℃ and 600℃?
REPLY: This is the highest temperature, the one under which more extensive changes of the structure could be expected. Yet, we concluded that TEM provides more interesting results than SEM, and for this reason we carried out only a limited amount of SEM observations. Under this regard, we could even omit Figure 8 without impairing the conclusions of microstructural analysis.
ACTIONS: Figure 9b (old Figure 8b) was omitted (see Reviewer's 6 comments).

Strong recommendation for increasing the readability of this paper:
1. Try to use colorful marks and curves to draw the figures (fig 5, fig 6, fig 12 ……), if not, it is hard for readers to get the key information.
REPLY: under this regard we do not agree with the reviewer. We used the same format previously used in many other papers of ours on creep. Our senior author still prefer the use of BW plots, which can be printed by any potential reader without needing a color printer.

ACTIONS: none

2. Please mark which the α, β, α' phases are in SEM and TEM micrographs.
REPLY: In Figure captions and/or in SEM and TEM micrographs labels of detected and existing phases were added throughout the manuscript.

3. Page 4, explain briefly about the "…comparing different batches[3-8]…" and "the full temperature range considered in [2]."
ACTIONS: we tried to explain by replacing "batches" with "lots"….we could not find more exhaustive descriptions to illustrate different sets of samples with similar microstructure

4. Simplify and shorten the section "2.4 Microscopy".
REPLY: Section 2.4 provides all the details required to repeat the measurements, and under this regard we do not think it is appropriate to shorten or reduce this part of the text.
ACTION: none

Reviewer #6: **amendments in marked-up manuscript in light blue**

1. Abstract：The abstract should be further concise.
ACTIONS: This comment goes against reviewer 1's request, since he asked for additional information in this section. We nevertheless tried to shorten a bit the text.

2. Experimental procedures.
1) After annealing, whether the alloys would be further aging or not? If not the aging process, the annealing microstructure maybe a metastable microstructure, such microstructure usually can not be used in engineering.
REPLY: As a matter of fact, this statement is highly debatable. Metastable microstructure are ALWAYS used, even the most demanding engineering applications: think about Ni_3Al rafting in Ni-based superalloys, or recovery and precipitates evolution in tempered 9Cr-1 Mo steels, just to quote to significant examples for creep. Yet, the negligible importance of prior ageing at the highest temperatures can be directly obtained from Figure 5 (previous Fig.4). The Figure clearly shows that a long permanence at 650 °C before loading, only results in a barely perceptible increase in the creep rate and in a reduction in the strain to fracture. Somewhat conflicting results could be obtained at 500°C, Figure 4, where a long permanence under 225MPa caused a moderate hardening of the alloy. Figure 8 indeed shows that the microstructure undergoes a change in hardness. We thus have a clear indication that the microstructure is not fully stable. Yet, as a whole, the effects of ageing, in this case, are scarce and are possibly mostly limited to a moderate precipitation of Ti_3Al at 500°C for long times of exposure, since all the experimental data, either obtained by CLE, VLE or even after 145h annealing at 650°C, roughly align on the same curve.
ACTIONS: none, the point was already discussed, and further additions were made following Reviewer's comments.

2) What is the reason for choosing two loading modes (constant load/variable load)? For variable loads, the measurement of minimum creep rate may not be accurate, which will greatly affect the fitting results of subsequent stress index and constitutive equation. On the one hand, it is impossible to determine whether some curves have reached the minimum creep rate before changing load. For example, the curve of 500 ℃/225 MPa in Fig. 3(a) cannot accurately determine whether the curve has entered the lowest point. On the other hand, the creep behavior before changing load may affect the subsequent creep experiment results. For example, in Fig. 3(b), the minimum creep rate of 600 ℃/400 MPa is higher than that of 600 ℃/409 MPa. Is it reliable to select the minimum creep rate of variable load samples under high stress? The lack of reliability in data selection will distort the constitutive equation, especially in the high-stress part.
REPLY: VLE were carried out to obtain multiple data-points from a single test, and to evaluate if a significant softening or hardening occur after prolonged creep exposure. The objection that VLE COULD result in an overestimation of the creep rate is correct, at least as far the first loading condition is considered, but we can cite the same curve at 500°C to prove that this effect is quite negligible. The first value of the creep rate under 225MPa is obviously a bit overestimated, but a subsequent loading under a nominal stress of 225 MPa (actual stress 233 MPa) provides a quite similar value of the strain rate. The point is that omitting the datum from the first loading step, will not change the slope of the strain rate vs stress curves of Figure 6. Yet, we choose to omit this datum, but as anticipated the overall curve did not change. As for the 400-409 MPa difference, we are discussing data to be presented in double logarithmic

coordinates, and the two data points overlap, as shown in Figure 6. We can conclude that in this dataset there is no "reliability problem" to be accounted for.
ACTIONS: the symbol for the test at 500°C-225MPa has been omitted; different symbols were used for CLE and VLE data.

3. Results
1) Which one phase is α'-martensite in Fig. 2? There is not any symbol or any evidence of α'-martensite in Fig. 2.
REPLY: A label in the TEM micrograph of the Figure was added.

2) The text of Fig. 4b should be Fig. 3b? or where is the Fig. 4b?
ACTIONS: the reviewer is correct, the text was amended.

3) The symbols in Fig. 6 and Fig. 12 are confusing.
ACTIONS: we thank the Reviewer that highlighted an error in Figure 6a. We corrected the mistake, and included a new sentence in the caption to further clarify symbols meaning.

4) The quality of Fig. 8b is low. The characteristics are not obvious even not visible.
ACTIONS: we omitted fig.8b, since it was deemed as not essential for text understanding.

5) In Fig. 9, is the sample with parameter (500 °C/225 MPa) under variable load (500 °C, 225/577/233/368 MPa) or constant load (500 °C /225 MPa)?
REPLY: As reported in the text, the figure illustrates the microstructure of the VLE experiment.
ACTIONS: We included this information in the caption.

4. Discussion
1) Are you sure that "the volume fraction of the b-phase in the material annealed at 1050 °C was much higher than that in the alloy annealed at 740 °C."
REPLY: as far as the measurements are correct, and we do not have reason to doubt it, this is what appears from tables I (annealed at 1050°C, volume fraction 9.5-12%) and II (annealed at 740°C, 3-8%).
ACTIONS: we just omitted "much", for the sake of clarity

2) In Section 4.2, What is the proportion of β phase before creep? The content of β phase after creep seems to be different under different parameters, and the results in Table 1 and Table 2 are quite different. With the conclusion of Page 20, "the reported amounts of the beta phase were not significantly marketers from those in the initial uncrept condition. ", the above results do not match.
REPLY: Table I and II are for different initial states. Table I was for the alloy for annealed at 1050°C, Table II for the alloy annealed at 740°C. Section 4.2 refers to the material annealed at 740°C; in this material, the initial volume fraction of beta phase did not exceed 5% (see ref.[2]), and ranged between 3 and 8% after creep. Thus, the amount of beta phase did not significantly change during creep. The annealed uncrept alloy had a mean volume fraction of beta of 4 ± 1 %.
ACTIONS. we included the information about the initial volume fraction of beta phase

3) In section 4.3, The UTS of the alloy used in this paper (922 MPa) is about 100 MPa smaller than that of the alloy aged at 740 ℃ (1015 MPa). Is Formula 1-4 still applicable?
REPLY: the answer is YES. For the sake of simplicity, we used the same UTS value (1000 MPa) for both states in Figure 13, since the difference in UTS is quite negligible (roughly 10%). Actually, one can appreciate that the minimum strain rate data at high strain rates converge, and at 500°C the strain rates for the alloy annealed at 1050°C are even slightly higher than after annealing at 740°C.

ACTIONS: none.

4) In section 4.3, What's meaning of this sentence: "For the samples annealed at 740 °C, the fragmentation process was unnoticeable, because the β-phase did not form long lamellae as under the heat treatment at 1050 °C"
ACTIONS: for the sake of clarity, we modified the text.

5) In section 4.3. Generally speaking, creep threshold stress phenomenon appears in the second phase particle reinforced alloy. A high stress index is usually considered as a sign of threshold stress. 7), when the applied stress is lower than the threshold stress value, no measurable strain will be generated. Does the creep test in this paper satisfy the condition of threshold stress?
REPLY: From a theoretical point of view, the reviewer is correct. Nevertheless, a very high value of the (apparent) stress exponent can be observed only when the applied stress closely approaches the value of the threshold stress, the source of threshold stress is thermically stable and, last but not least, creep data spanning over several orders of magnitude are available. When the threshold stress is much lower than the applied stress, the apparent stress exponent is higher than theoretical values (3-5), but not dramatically high.
ACTIONS: no amendments are required, the Reviewer's question makes sense only in "model materials" of some sort, observed in a range of stress very close to the threshold stress.

6) In section 4.3. How is threshold stress determined? What is the true creep stress index and the true creep activation energy? The threshold stress is different at different temperatures, so choosing a temperature (650 ℃) is not representative and there is a large error.
REPLY. The reviewer seems to address the problem as if we used the conventional power law, following a procedure that needs the selection of proper values of the true stress exponent and of the true activation energy. We did not. We here used a different approach. Equations 1-4 do not contain free-parameters. They only need the substitution of the UTS to provide the model curve for the strain rate dependence on applied stress and temperature. Yet, the model does not work very well for the alloy with Widmanstatten structure. We thus introduced a "back stress" or "threshold stress", if you prefer, that represents the additional stress required for the dislocation to overcome alpha-beta interfaces or Ti_3Al particles. Introduction of this new term results in the presence of a single free parameter (the back/threshold stress) in the model equations, all the other parameters remaining exactly the same. Thus, the back/threshold stress was calculated to obtain a good fit of the experimental data at 650°C, and then the same value (actually, the same σ_0/G value) was used for all temperatures, assuming that threshold stress does not significantly changes with temperature, as clearly stated in the text. The description is excellent.
As for the variability of the threshold stress value with temperature: this variability exists, but is not universal. When the threshold stress is equivalent to the Orowan stress, it depends on temperature through the G=G(T) dependence alone. In many other cases, a significant temperature-dependence (hard to be explained, indeed) has been observed, see, for example, as an example,
https://doi.org/10.1016/j.compositesa.2018.06.021
which is also representative of a "model behavior" as quoted by the Reviewer in his comment 5, with experimental data spanning over 8 orders of magnitude, a feat seldom observed in industrial materials. This fact does not imply that a temperature dependence necessarily exists, and, rather the fact that it was not observed here is a remarkable result.
ACTIONS: none.

7) In section 4.3. The authors attributed the threshold stress to the distance between α/β interface and the precipitation of α2 phase. What are the precipitation conditions of α2 phase? In which creep stage does it precipitate? Generally speaking, the first stage of creep is very short. If precipitated after entering the second stage, it will not affect the minimum creep rate and cannot be used as the source of threshold stress. The minimum creep rate is generally the creep rate at the steady state stage, which has little relation with the microstructure evolution in the subsequent creep process.

8) In section 4.3. the β phase is a hard phase in β transformed microstructure, which plays a strengthening role. What is the mechanism of threshold stress induced by β lamella? (Is the dislocation partially climbing? Load transfer? Or something else?) Need to focus on discussion and provide more effective evidence? The fracture of small lamellae usually occurs under high strain. The explanation of the fracture of β lamellae should be based on two perspectives: stress and deformation.

REPLY. Points 7 and 8 will be addressed together. We thank the Reviewer for his/her trust in our knowledge, but we are fully aware that these questions remain unsolved, nor can be solved by a single study as the one here presented. We rather aim at arising in the audience a renewed interest on these materials. As we clearly stated in the text, no model exists that could convincingly address the strengthening role of alpha/beta interfaces. We cannot derive any theories on this subject, simply because experimental data are lacking. What we can do is simply to suggest that, once a number of microstructural data are collected, the model could be further developed to describe the strengthening role of the interfaces in combination with precipitation of Ti_3Al particles. For the sake of discussion, also the Reviewer statement on the potential role of precipitation is not correct. Precipitation could be fast at high temperature, and could thus occur well before a minimum creep range is approached, in particular if the test in carried out under low stresses (long tests). In addition, if particles play a significant hardening role, the peak-ageing time should roughly correspond to the minimum in creep rate, unless the damage mechanisms overcome the strengthening role of the particles. Further, dislocations can provide nucleation sites, which can accelerate precipitation. On the other hand, the same dislocations could accelerate also coarsening, as demonstrated in 9Cr-1Mo steels. This short analysis demonstrates that the problem cannot be solved by a single study, as the reviewer seems to suggest. Here, a number of different researches on Ti64 microstructural evolution during creep should be planned, a feat never undertaken in the past. The same complexity should be addressed when discussing the role of the interfaces and the fragmentation of the beta particles. Please, note that fragmentation is here driven by temperature, strain/stress do not have a role, since, as clearly stated in the text, TEM samples were obtained from the heads of creep specimen (the gauge length dimensions were too small to reliably obtain TEM samples).
ACTIONS: no amendments were made, since reviewer's requests go well beyond the possibilities of any single study. The point was already clearly illustrated in the final part of the Discussion section

9) In section 4.3. The difference of minimum creep rate disappears under high stress, and the new model is not applicable under high stress. What is the main reason? The UTS of the sample before creep is 922 MPa, lower than 1000 MPa, which is attributed to the reliability of low UTS estimation (whether α2 phase affects the minimum creep rate) and the strengthening effect of β phase under high stress (load transfer?). Loss related?
REPLY: we NEVER stated that the model does not work. We wrote: "The correlation between the experimental and model results is good, except in the very high-strain rate region, where the model overestimates the strain rate. This deviation can be PARTLY attributed to the underestimation of the UTS, in particularly at 500 °C, where a limited precipitation of the α_2-particles slightly increases the tensile strength.". Again, microstructural data and models for precipitation are lacking, so we must

content ourselves with only qualitative explanations. Last, but not least, we must remember that the high-strain rate part of the curve is governed by the R_{max} term, ROUGHLY quantified by Eqn.4. This equation is purely empirical, and does not take into account of any hardening/softening phenomena occurring during creep, so we can be happy of the relative accuracy we obtained with so rough data in input.
ACTIONS: none

5. English should be further improved. The whole article should be checked carefully especially the spelling and grammar errors. Such as "the present study reports new data on the creep responses at 500 and 600 °C of the AM Ti-6Al-Ti-6Al-4V annealed at 1050 °C." in the last part of Introduction.
REPLY: We have full confidence that the Elsevier Language Editing Service made a good job in correcting the draft before first submission, i.e. before Review (Certificate Serial number: LE-244504-E13D7F6F518).
Actions: no further actions were made, language was already certified by Elsevier Language Editing Service

Creep response of Ti–6Al–4V alloy produced by additive manufacturing: effect of annealing at 1050 °C

S. Spigarelli[1], C. Paoletti[2], E. Cerri[3], E. Santecchia[1,*], M. Cabibbo[1]

1. DIISM, Università Politecnica delle Marche, via Brecce Bianche, 60131 Ancona, Italy

2. Faculty of Engineering, Università degli Studi eCampus, Via Isimbardi 10, 22060 Novedrate, Italy

3. DIA Università di Parma, V.le G. Usberti 181/A, 43124, Parma, Italy

*E. Santecchia: corresponding author

Abstract

The present study mainly aims at investigating the creep response of a Ti–6Al–4V alloy produced by additive manufacturing and annealed above the β-transus, and at rationalizing the differences observed when comparing its behaviour to that of the same alloy annealed at lower temperatures. Herein, the creep response of this alloy produced by additive manufacturing and subsequently annealed at 1050 °C is investigated at temperatures ranging from 500 to 650 °C. The heat treatment produces the typical Widmanstätten microstructure with thin β-lamellae interposed between coarse α-lamellae. The minimum creep rate dependence on the applied stress and temperature is compared with literature data of tests of alloys with Widmanstätten microstructures produced by traditional technologies. A modified form of an equation, successfully used to describe the creep responses of the Ti–6Al–4V alloy with different initial microstructures, was here proposed. The suggested modification introduces a threshold stress, which is related to the presence of finely spaced α–β interfaces and α_2-Ti_3Al particles. This threshold stress is considered to be negligible when the distance between the α–β interfaces is long and the α_2-Ti_3Al particles are absent or excessively spaced. In contrast, in the materials with Widmanstätten microstructures, even minor differences in the heat treatment conditions and/or the processing history cause considerable variations in the distance between the α–β interfaces. This coupled with the occasional precipitation of α_2-Ti_3Al particles results in different threshold stress values.

Keywords: Additive manufacturing; Phase Transitions; Creep; Microstructure; Titanium alloys

1. Introduction

Ti–6Al–4V alloy is a commercial material well suited for processing by additive manufacturing. In particular, selective laser melting (SLM), also known as laser-beam powder-bed fusion, is an excellent candidate for industrial-scale production of Ti–6Al–4V components. Consequently, several recent studies, accurately reviewed by Liu and Shin [1], thoroughly investigated the microstructural features and mechanical properties of the additively manufactured (AM) alloy. Notably, the creep response of the AM alloy has not received equal attention. Thus, in a previous study all recently available data on the creep behaviour of Ti–6Al–4V produced by different technologies and having different initial microstructures were collected [2]. Moreover, they were compared with new experimental results obtained by testing a Ti–6Al–4V alloy produced by SLM and subsequently annealed at 740 °C for 130 min. Furthermore, an additional effort was made to rationalise the creep responses of the alloys produced by traditional technologies and AM, respectively. This analysis demonstrated that the same equation can be successfully used to describe the creep response of Ti–6Al–4V alloy, irrespective of the initial microstructure and the production technique. The minimum strain rate ($\dot{\varepsilon}_m$) dependences on the stress (σ) and temperature (T) of "traditional" materials with both equiaxed and duplex microstructures and annealed or as-deposited AM alloys were expressed by

$$\dot{\varepsilon}_m = A\frac{D_0 G b}{kT}\left(\frac{\sigma_\rho}{G}\right)^3 exp\left(\frac{\sigma_\rho b^3}{kT}\right) exp\left\{-\frac{Q_L}{RT}\left[1-\left(\frac{\sigma_\rho}{R_{max}}\right)^2\right]\right\}, \quad (1)$$

where b was the Burgers vector; G was the shear modulus; k was Boltzmann's constant; A was a constant, and D was the self-diffusion coefficient, which was expressed as:

$$D = D_0 exp\left(-\frac{Q_L}{RT}\right), \quad (2)$$

where D_0 was a material parameter and Q_L was the activation energy (for lattice self-diffusion in pure metals). The σ_ρ term (dislocation hardening) was calculated by handling the equation:

$$\sigma = \sigma_\rho + \sigma_{ss} = \sigma_\rho + \delta\sigma \quad (3)$$

where σ_{ss} was the solid solution strengthening term and δ is a constant (= 0.4) introduced to represent its effect.

The R_{max} parameter (maximum strength) was expressed as

$$R_{max} = 1.5UTS\frac{G_T}{G_{RT}}, \quad (4)$$

where G_{RT} and G_T were the shear moduli at room temperature and the testing T, respectively.

For any interested reader, Equations (1)–(4) are described in detail in [2], although Appendix 1 provides a synthetic description of the genesis of their formulation. This set of constitutive equations provided an excellent description of the minimum creep rate dependence on applied stress for equiaxed and duplex microstructures, the input parameter being the UTS (see Appendix II for few non-exhaustive examples of the findings reported in [2]). However, an important issue was the extremely large scatter of the minimum creep rate data observed when comparing different lots of Ti–6Al–4V alloys having Widmanstätten structures [3–8]. This peculiar microstructure forms after annealing the alloy above the β-transus temperature and subsequently cooling at a relatively high cooling rate. Equations (1)–(4) provide curves that bisect the 'clouds' of experimental data; however, the scatter is extremely large to conclude that the model is perfectly adequate for describing the creep response. This discrepancy suggests broadening the study on the creep response of AM Ti–6Al–4V by also annealing the alloy at 1050 °C, which is well above the β-transus temperature, to obtain a Widmanstätten structure. A few creep results at 650 °C, a temperature above the predictable range of α_2-Ti_3Al precipitation, have recently been reported by the authors of the present study [9]. The aim of that preliminary investigation was limited to comparing the creep responses of the alloy with a Widmanstätten structure before and after annealing below the β-transus temperature. The experimental results proved that at this temperature, the alloy with a Widmanstätten microstructure exhibited lower creep rates than after annealing at 704 or 740 °C. This behaviour cannot be explained by Equations (1)–(4), in particular, owing to the ultimate tensile strength (UTS) of the alloy annealed above the β-transus temperature being slightly lower than that of the material annealed at 704–740 °C. These observations indicated the need to enlarge the range of the experimental conditions to be investigated to cover the full temperature

range considered in [2]. Thus, the aim of the present study was twofold: i) present a much more extensive set of experimental data obtained by testing the AM alloy annealed at 1050 °C at different temperatures by both constant-load and variable-load creep experiments (CLEs and VLE, respectively) and ii) provide a model on a wider scale applicable to alloys produced by traditional technologies and able to describe the creep response of Ti–6Al–4V with a Widmanstätten structure. Therefore, the present study reports new data on the creep responses at 500 and 600 °C of the AM Ti–6Al–Ti-6Al-4V annealed at 1050 °C.

2. Material and Experimental procedures

2.1 Material and sample production

In this study, commercial gas-atomised Ti–6Al–4V grade 23 extra-low-interstitial powders (5.5–6.5 % Al, 3.5–4.5 % V, 0.25 % F, 0.1 % O, 0.05 % maximum N, 0.08 % maximum C, 0.011 % maximum H, and Ti balance wt.%) were used. The powder particles had sizes ranging from 15 μm to 45 μm. An SLM280 machine (SLM Solutions AG, Lübeck, Germany) equipped with a 400 W IPG fibre laser was used for the production of dog-bone creep samples, with a square section of area A_0 = 3 mm × 3 mm and a 25 mm gauge length (Figure 1).

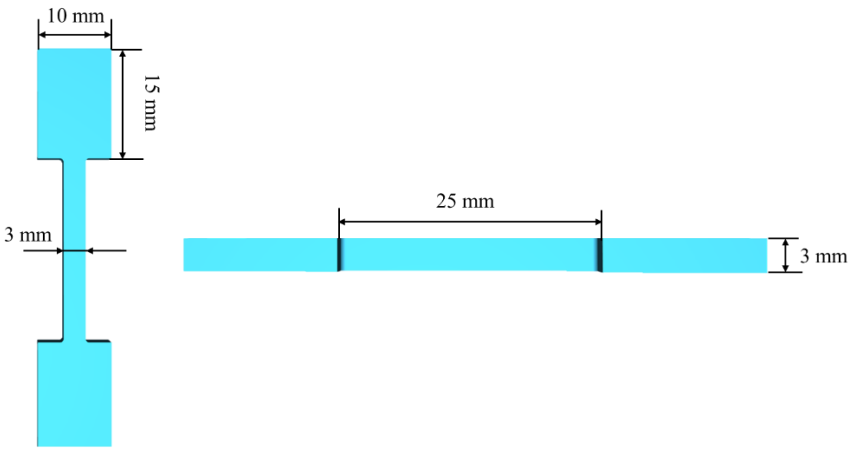

Figure 1. Geometry of the creep sample.

A powder bed was preheated at 80 °C, and deposition was performed in argon (Ar) to reduce oxygen concentration to 0.05 %. The building direction was parallel to the gauge length of the specimen. The deposition was conducted to a thickness of 60 μm at a scanning speed of 1250 mm/s, with hatch spacing of 120 μm, and laser power of 340 W. The post-processing treatment consisted of annealing at 1050 °C, which is sufficiently above the β-transus temperature to ensure the full transformation of the microstructure, for 1 h, followed by cooling in Ar at 0.4 °C/s. This relatively slow cooling was expected to lead to the formation of a Widmanstätten structure with reduced internal stress [10]. Both sample production and post-processing heat treatment were performed by BEAMIT (https://www.beam-it.eu/, Fornovo di Taro 43045, Italy).

2.2 Creep experiments

CLEs and VLEs were conducted at 500, 600, and 650 °C in air on samples whose surfaces were in the as-deposited state. In a CLE, a load *P* was applied immediately after a short soaking time at the testing temperature and maintained until rupture or test interruption in the tertiary stage. In a VLE, a sample was loaded similarly to in a CLE under a given initial stress; however, after the minimum creep rate range was presumably attained, the load was abruptly changed.

The soaking time at temperature before loading was typically 0.5–1 h, except before a CLE test, in which the soaking time was 145 h.

The test temperature was measured using four thermocouples, and the elongation was continuously measured using a linear variable displacement transducer.

2.3 Room-temperature mechanical properties

To evaluate the UTS, tensile tests at room temperature were performed on samples having the geometry of a creep experiment specimen. The surfaces of the samples used for the tensile tests were in the as-deposited state. The test strain rate was 3×10^{-2} s^{-1}. The UTS after heat treatment at 1050 °C was 922 ± 2 MPa.

Rockwell hardness (HRC) tests were performed on as-heat treated and crept sample heads. Because these tests were merely aimed at assessing the age-hardening responses of the alloy, the hardness was measured in these (almost) unstressed portions of the samples. The dislocation substructures introduced by loading and straining considerably influenced the hardness of the gauge lengths, thus masking the possibly considerably limited effects of age hardening. The HRC value after heat treatment was 38.1 ± 0.5 for the alloy after annealing.

2.4 Microscopy

Samples for light microscopy analyses were mechanically ground and polished with a colloidal suspension and subsequently etched using Kroll's reagent (100 mL H_2O + 2 mL HF + 4 mL HNO_3). Following this, the samples were observed under a Leica DMi8 optical microscope (Germany).

Scanning electron microscopy (SEM) observations were conducted using a Tescan Vega 3 scanning electron microscope (Brno, Czech Republic) at an accelerating voltage of 30 keV.

For transmission electron microscopy (TEM) analyses, thin foils were obtained from untested and crept sample heads. The samples were prepared by mechanical grinding and polishing to a thickness of 150 µm. This was followed by twin-jet electro-polishing to reach 60 µm thickness using a Struers™ Tenupol-5® device (Struers Inc., Westlake, Cleveland, OH, USA) with a solution consisting of 5 % perchloric acid, 35 % butanol, and 60 % methanol at −35 °C and voltage V = 24 V. The discs were dimpled to a reach a thickness of 20–25 µm and ion-milled to electron transparency using a Gatan© precision ion polishing system (Gatan Inc., Pleasanton, CA, USA) operating at 8 keV (incident beam angle progressively reduced to 8°, 6°, and 4°). The TEM analyses were performed using a Philips™ CM-20 microscope (Philips It, Milano, Italy) working at 200 kV and equipped with a double-tilt liquid nitrogen cooling specimen holder. Selected area diffraction patterns (SAEDPs) were recorded using a converged beam. Based on the SAEDPs, The crystallographic structures of the α, α′, and α_2-phases were found to have α-[0001] or α-[$2\bar{1}\bar{1}0$] directions parallel to the beam direction. Converged-beam electron diffraction (CBED) was used to identify the different detected phases, using a nominal electron

beam of 5-6 nm. Volume fraction of detected phases (namely, α′, α_2, and β) was evaluated by the Schwartz–Saltykov method. The method, was adapted to the TEM thin foil analyses by consider the bias introduced by the TEM thin foil and the precipitate morphology, i.e., lamellae (α), thin ribbon-like structures (β), and coarser lenticular morphological phase (α', α_2).

3. Results

3.1 Initial Microstructure

Figure 2 shows the initial microstructure of an annealed SLM-manufactured-alloy (referred as SLM-alloy) (light microscopy and SEM images). A Widmanstätten microstructure is noticeable as thin layers of light α-phase-decorating prior β-grains.

Figure 3 shows a representative TEM micrograph of the annealed SLM-alloy. The microstructure consists of thin and long β-lamellae interposed between much thicker α-lamellae. The thicknesses of the β and α-lamellae are in the ranges of 110–140 and 390–460 nm, respectively. In addition, remote α'-martensite colonies having essentially the same thickness as the α-lamellae are uniformly distributed in the α-phase of the Widmanstätten microstructure.

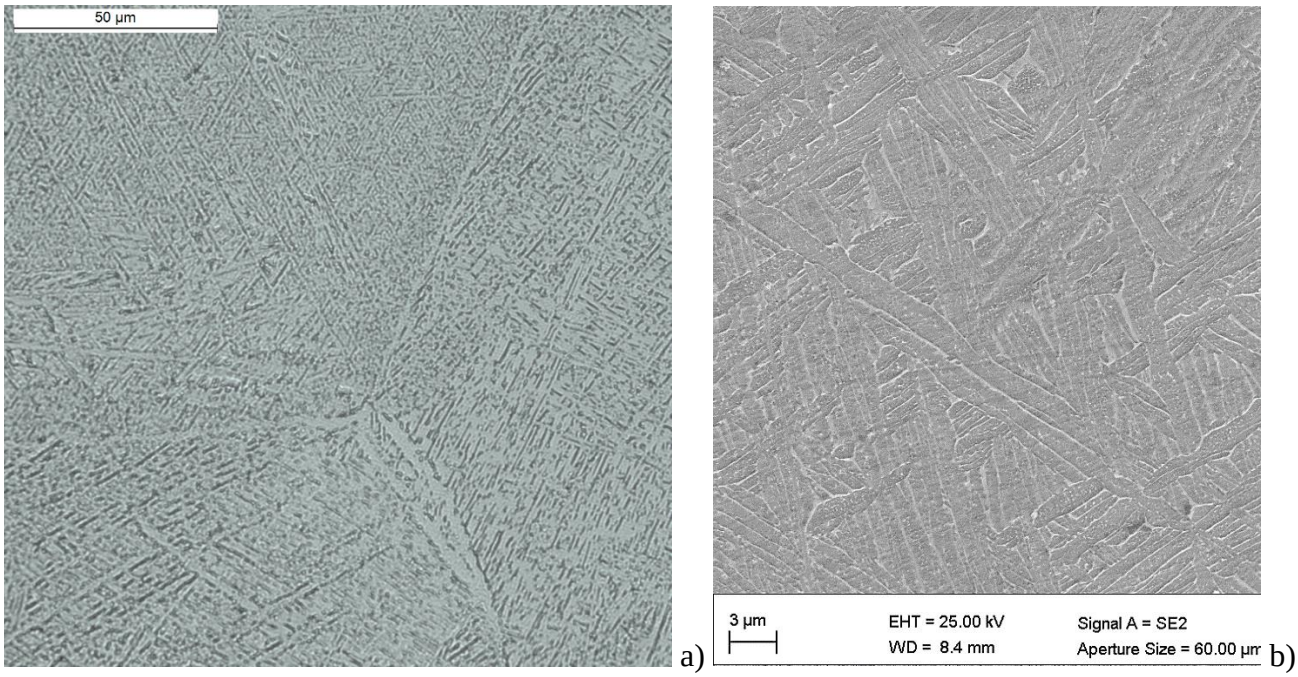

Figure 2. Microstructure of SLM-alloy after annealing at 1050 °C observed by a) optical microscopy and b) SEM; the α-phase is bright in Figure 2a, and dark-grey in Figure 2b; β-phase is dark-grey in a), and light-grey in b).

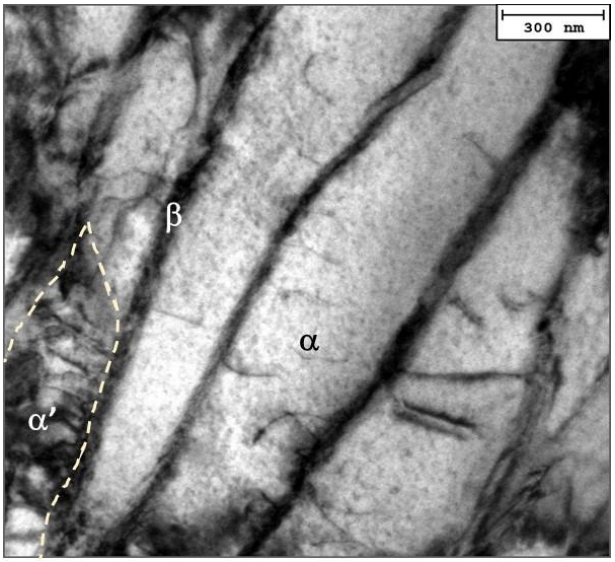

Figure 3. Microstructure of SLM-alloy after annealing at 1050 °C observed by TEM, showing α (the broad lenticular region), β (the long narrow features in-between), and α' (region included in the dashed line).

3.2 Creep response

Figure 4 shows the strain rate versus strain creep curves obtained in the present study at 500 and 600 °C (from CLEs and VLEs). Figure 5 displays the creep curves at 650 °C from [9] and supplemented by one additional VLE curve obtained in this study at this temperature. Figure 5 compares the curves obtained after short (0.5 h) and very long (145 h) soaking times at the testing temperature before loading.

In general, the shapes of the creep curves are similar to that observed when testing the alloy after annealing at 740 °C [2], and consist of a well-defined primary stage, a minimum creep rate range, and an extended tertiary stage. Figure 5 clearly shows that a long permanence at 650 °C before loading only results in a slight increase in the creep rates and a reduction in the strain to fracture.

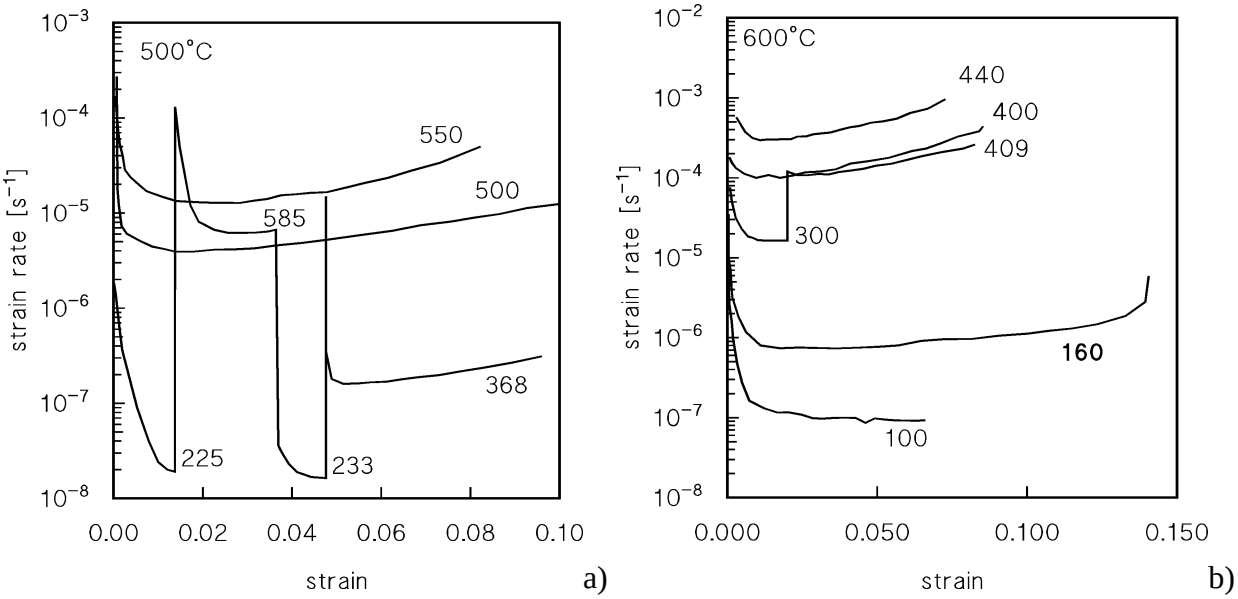

Figure 4. Strain rate versus strain creep curves from CLEs and VLEs at 500 and 600 °C of AM alloy annealed at 1050 °C. Numbers are nominal stresses in MPa. Test conducted under 100 MPa is interrupted.

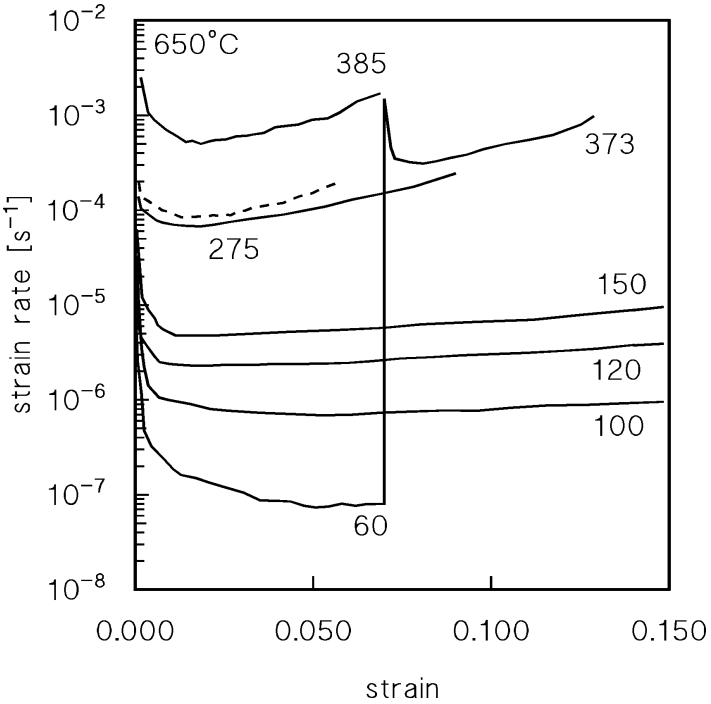

Figure 5. Representative strain rate verses strain creep curves from CLEs and VLEs at 650 °C of AM alloy annealed at 1050 °C [9]. Numbers are nominal stresses in MPa. Broken line corresponds to test conducted under 275 MPa after 145 h annealing prior to loading.

Figure 6 shows the minimum strain rate as a function of the applied stress obtained from experimental curves; the data approximately align on straight lines with slopes 7, 5.2, and 4.8 at 500, 600, and 650 °C, respectively. The datum for the VLE at 500°C, under 225 MPa was omitted, since presumably the

minimum creep rate range was not reached. The other data from VLE experiments (open symbols) roughly align with CLE results, except in the case of the test at 500°C. As illustrated in Figure 4a, long exposure at high temperature under a low stress, seems to result in a moderate hardening of the alloy, possibly due to a limited Ti_3Al precipitation. Yet, this effect will be here neglected, since the deviation between CLE and VLE data is fairly negligible. The data displayed in Figure 6 cover over three orders of magnitude of strain rates, and do not present a large scatter; therefore, they present an excellent basis for the search of a reliable constitutive model.

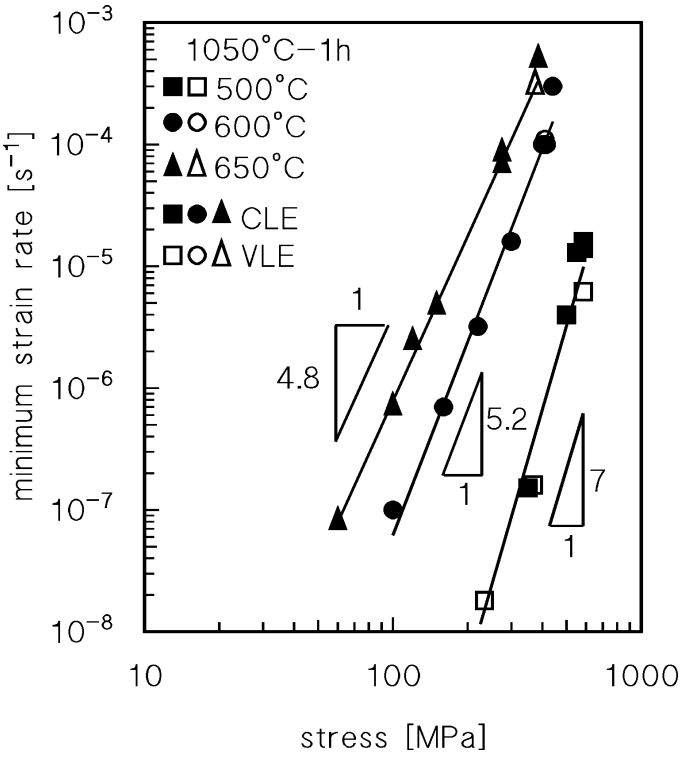

Figure 6. Minimum creep rate as function of applied (nominal) stress.

Figure 7a shows the data obtained in the present study and the literature data on alloys with Widmanstätten structures [3–8] produced by traditional technologies. The data obtained in this study cross the 'cloud' of the literature data. The drastic scatter of the latter causes occasionally a substantial deviation between the solid (this study) and open (literature) data points.

Figure 7b presents a comparison of the minimum creep rate measured in this study and those reported for the AM alloy annealed at 740 °C in [2]. As already noted in [9], compared to annealing at 740 °C,

annealing at 1050 °C results in lower creep rates in the entire investigated stress and temperature ranges; however, the difference progressively vanishes in the high-stress regime.

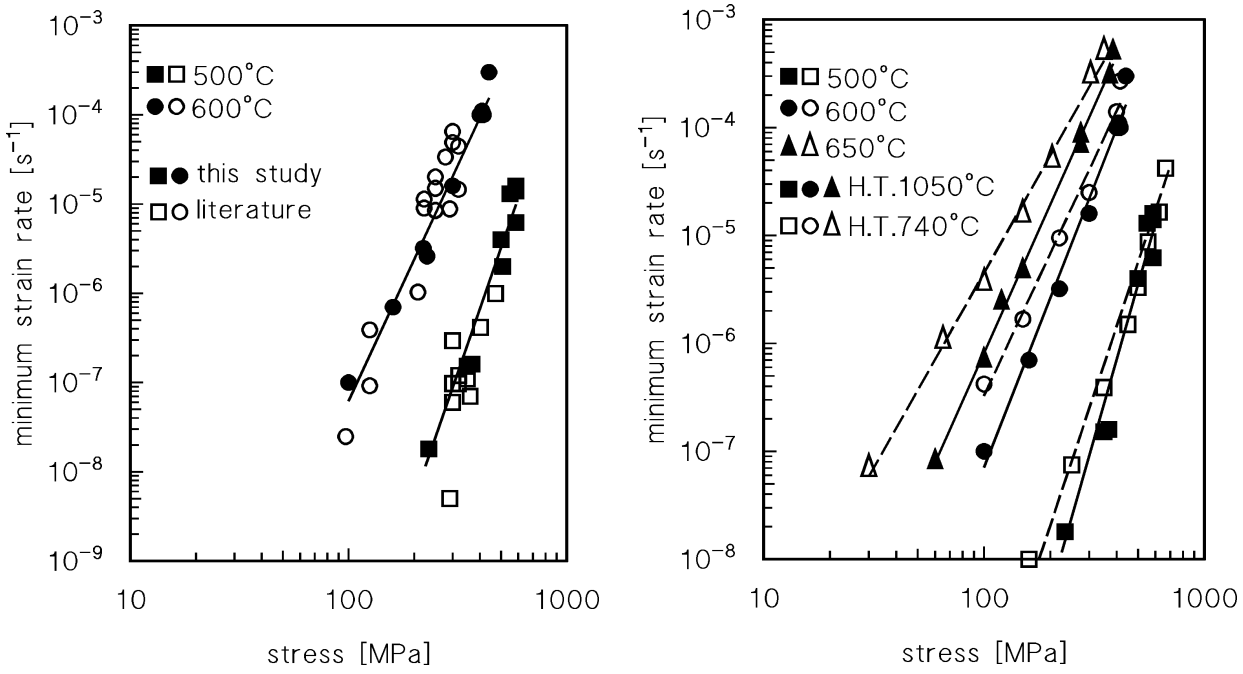

a) b)

Figure 7. Comparison of data obtained in present study by testing AM alloy annealed at 1050 °C with a) literature data of traditionally processed Ti–6Al–4V with Widmanstätten microstructure [3–8] and b) data of same alloy produced by additive manufacturing and annealed at 740 °C [2]. Squares, circles and triangles represent tests carried out at 500, 600 or 650°C respectively. Open symbols represent literature data in a), and creep results obtained by testing the alloy of the present study after annealing at 740°C in b).

3.3 Hardness after high-temperature exposure

Figure 8 shows the HRC measurement results of the heads of crept samples. The data approximately present curves typical of age-hardening materials. Although this behaviour does not necessarily fully represent the phenomena occurring in the gauge lengths, where the dislocation activity significantly affects the microstructural evolution, it can be considered of interest for the description of the present model. At 500 °C, the hardness increases above 200 h of exposure, a possible indication of α_2-Ti_3Al precipitation. At 600 and 650 °C, the hardness decreases for the sample heads after a long time of exposure. At 650 °C, the hardness continuously reduces with the time of creep exposure. Because the dislocation activity considerably alters the microstructural evolution in the gauge length, the hardness trend showed in Figure 8 cannot be used to qualitatively predict the creep response of the alloy.

However, the results in Figure 8 remain significant as they show that the alloy is unstable at high temperatures. Permanence at high temperatures causes a moderate variation in the properties of the alloy.

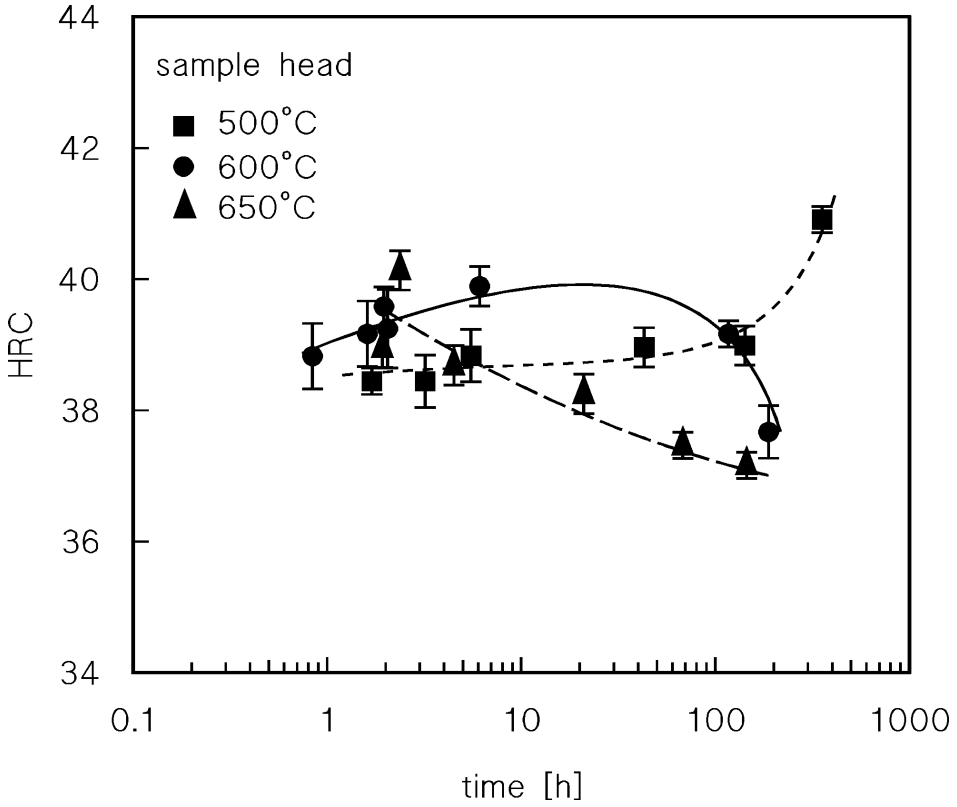

Figure 8. HRC hardness measured on crept sample heads.

3.4 Microstructure after creep experiments

Figures 9–11 show the microstructures of the crept samples observed using SEM and TEM. The most straightforward finding of the analysis shown in Figure 9 is the fragmentation of the β-lamellae at 650 °C. The micrographs obtained by TEM are more relatively interesting (Figures 10 and 11). They reveal that the microstructure of the alloy crept at 500 °C under an initial stress of 225 MPa (VLE in Figure 4a, at high-temperature exposure for 355 h) is still characterised by diffused long and thin β-lamellae (Figure 10a). Their thickness is approximately four times lower than those of the α-lamellae. Within the α-phase, the precipitation of α_2-Ti_3Al is evident (Figure 10b). This precipitated phase exists in the form of both long precipitates and much smaller cube-shaped particles, as presented in Figures 10b and

10c, respectively. The long particles have an average length of 450–480 nm and an average width of 55–60 nm, whereas the square-shaped particles are 180 nm in size. The dislocations bow around these particles, indicating a remarkable strengthening effect due to the dislocation–particle interactions (Orowan bowing and/or climbing above the particles). The formation of the α_2-Ti_3Al phase, as also reported by other studies (see [11]), is expected, because the testing temperature is in the range where its precipitation is probable. The crystallographic relationship between the α_2 and α-phases is found to be was α_2-$[01\bar{1}1] \parallel \alpha$-$[01\bar{1}1]$, as shown in the insets of Figures 10b and c.

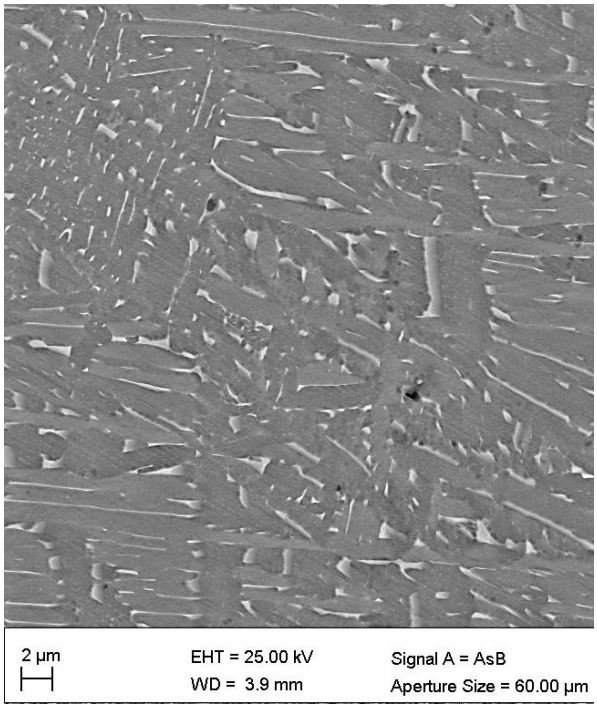

Figure 9. SEM micrograph of the sample tested at 650 °C/275 MPa, where α is the darker region and β the bright needle-like structure.

The distinctive microstructural feature is the β-lamellae fragmentation phenomenon, as shown in Figure 10d. It is activated by long holding times at high temperatures, as noticeable in Figures 9 and 10d, and has been described in other studies [10]. The dislocation activity due to creep straining is ultimately responsible for the progressive β-lamellae fragmentation.

The lamellar microstructure of the alloy crept at 650 °C under an initial stress of 60 MPa (VLE in Figure 5, total exposure time of 187 h) is shown in Figure 11. In particular, in the α-phase, dislocation sliding primarily occurs along $\boldsymbol{g}$ = *(0002*) and $\boldsymbol{g}$ = $(0\bar{1}10)$ [13], as shown in Figure 11b. These two sliding directions form a local network of dislocations. Similar results have been reported by Li *et al.* [11].

Occasionally, α'-martensite colonies are still observed. Dislocation accumulation occurs in the α′ to α lath interfacial region owing to local strain accommodation followed by both β to α and β to α′-phase transformations. Stacking faults (SFs) are formed in the α-lamellar structures, which was also reported by Li et al. [11] and Su et al. [14].

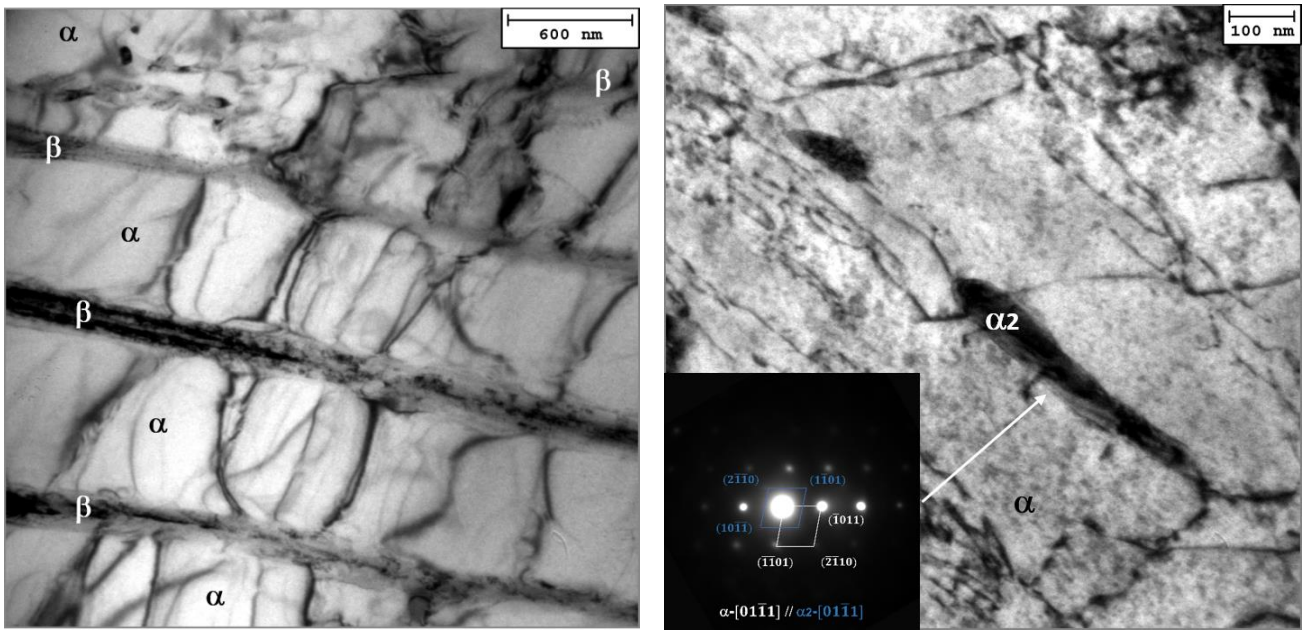

(a) (b)

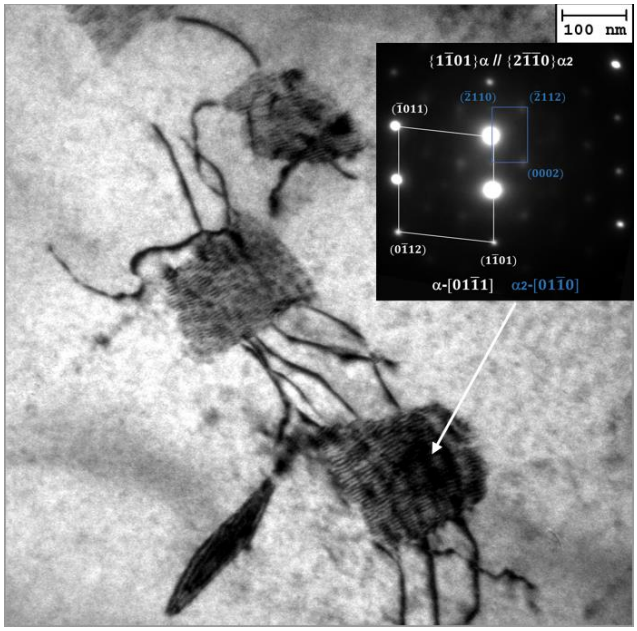

(c)

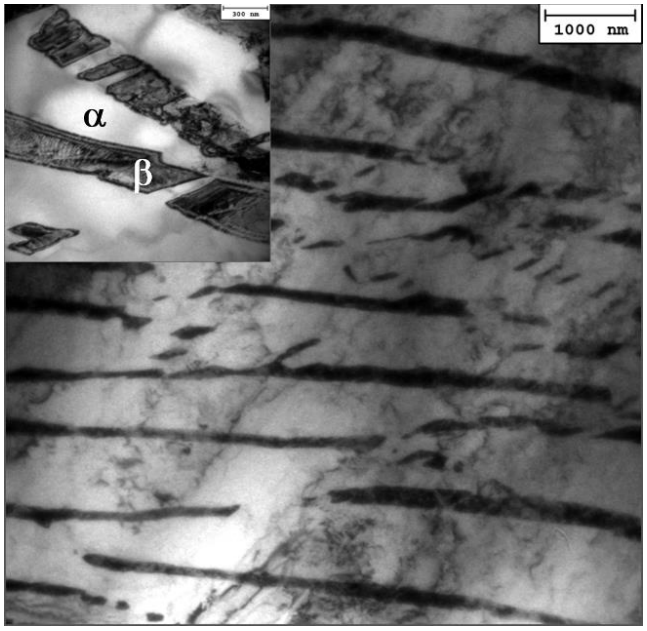

(d)

Figure 10. TEM micrographs of the VLE samples tested at 500 °C under an initial stress of 225 MPa crept sample showing (a) alloy α–β lamellar microstructure, α_2-Ti_3Al phase formation with long-thin morphology (b), and small particles with square morphology (c), and (d) β-lamellae fragmentation. Insets of (b) and (c) show SAEDPs of α_2-Ti_3Al; inset of (d) show details of some fragmented β-lamella.

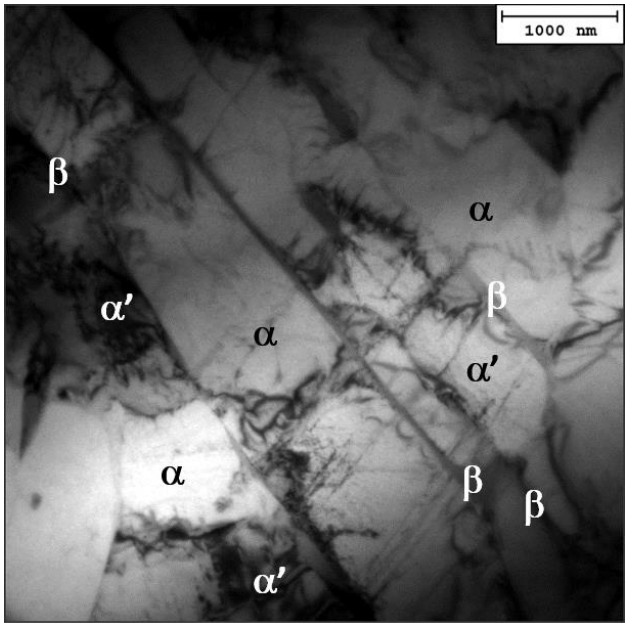

(a)

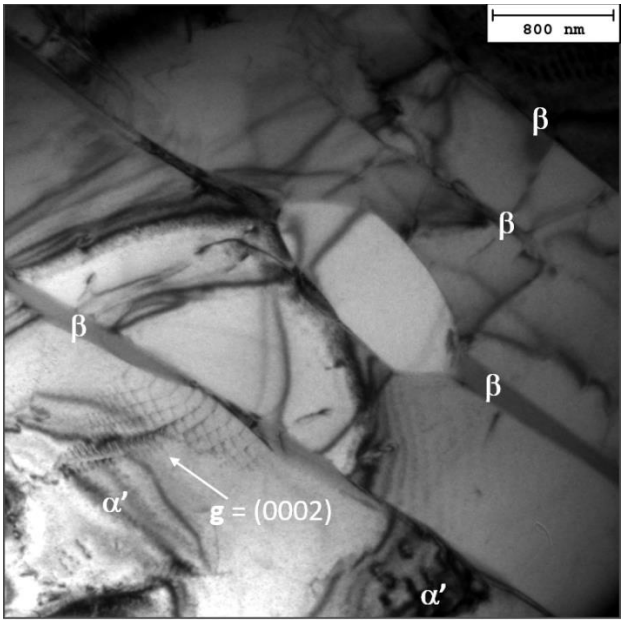

(b)

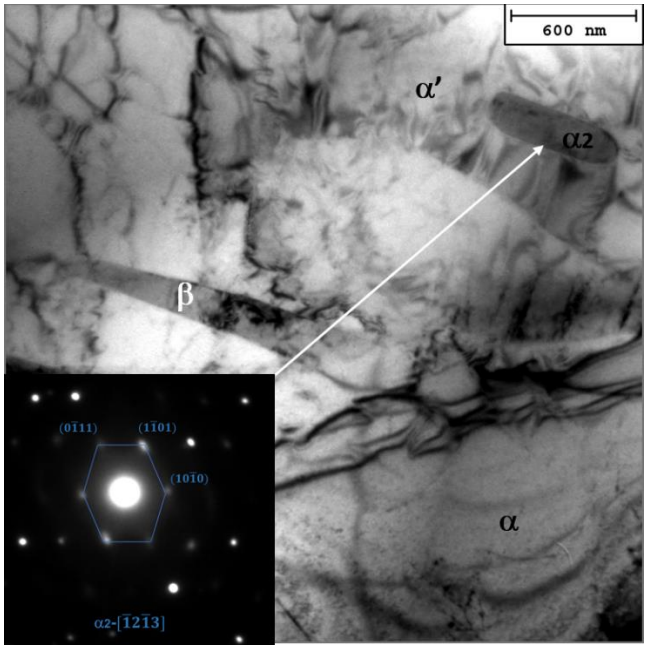

(c)

Figure 11. TEM micrographs of VLE sample tested at 650 °C under initial stress of 60 MPa, showing (a) α–β lamellar morphology, (b) tangled dislocations with wave-like sliding interactions, and (c) α_2-Ti_3Al phase and related indexed SAEDP (inset).

The presence of quite coarse α_2-Ti_3Al particles is also observed in the sample crept at 650 °C (Figure 11c). The Ti_3Al particles are ovoid in shape (120–150 nm in width and 600–800 nm in length). The crystallographic relationship between the α_2 and α phases was found to be α_2-$[2\bar{1}\bar{1}0]$ // α-$[2\bar{1}\bar{1}0]$ with α_2-$(0\bar{1}11)$ // α-(0001) crystallographic direction.

A quantitative evaluation of the β, α′, α_2, and α-phases in the samples annealed at 1050 °C and crept at 500 °C/60 MPa and 650 °C/225 MPa is reported in Table I.

Table I. Volume fractions (% vol.) of β, α′, α_2, and α-phases in VLE samples crept at 650 °C/60 MPa (initial stress) and 500 °C/225 MPa.

crept sample	β	α’	α_2	α
500 °C and 225/577/233/368 MPa	~12.0	~2	~0.15	bal.
650 °C and 60/373 MPa	~9.5	~1	~0.08	bal.

4. Discussion

4.1 Microstructural features of annealed Ti–6Al–4V produced by AM: context

Section 3 provides interesting information on the creep response of the AM Ti–6Al–4V alloy annealed at 1050 °C and the microstructures of the crept samples. The better creep response of the alloy annealed at 1050 °C than that of the alloy annealed at 740 °C is evident. Any rationalisation of this difference in the creep response should be based on a comparative analysis of the microstructural features.

It is widely known that the α–β phase transformation of a Ti–6Al–4V alloy strongly depends on the annealing temperature and the cooling rate. The equiaxed microstructure, obtained for example by a long annealing (6 h) at 850 °C followed by air cooling [3], consists primarily of α-grains surrounded by a much smaller volume fraction of finer β-grains. The duplex microstructure is characterised by the co-presence of equiaxed α- and lamellar α + β-grains. For example, colonies of α-lamellae, with an inter-lamellar small fraction of a retained vanadium-rich β-phase, form with equiaxed α-grains after annealing at 950 °C for 2 h, followed by air cooling to 700 °C [3]. Finally, annealing above the β-transus temperature followed by cooling at a relatively high cooling rate promotes the formation of a fine Widmanstätten structure.

The abovementioned microstructural evolution with thermal history is important as it considerably affects the mechanical properties, particularly at room temperature [15–17]. This is particularly for AM Ti–6Al–4V alloys [18]. During the additive manufacturing process, cooling rates can be as high as 10^6 °C/s [18]. Such cooling rates inhibit the complete α–β phase transition, and the bcc β-phase decomposes by martensitic diffusionless transformation, leading to the formation of α′-martensite in the as-synthesised condition. The α’-martensite forms as fine needles and has a high dislocation density. The co-presence of α-grains, α′-needles, and a possible small volume fraction of intergranular β-lamellae is the cause of the strong microstructural anisotropy. The size and morphology of the α′-martensite and its crystallographic orientation, which is closely related to the prior β-grain orientations, affect the

room-temperature mechanical properties of the AM alloy. The presence of α′-martensite in AM Ti–6Al–4V alloys results in high strength and poor ductility. Thus, post-processing heat treatments are needed to increase the ductility, inducing simultaneously a slight reduction in the alloy yield strength. To completely decompose α'-martensite to achieve a significant ductility improvement, the heating temperature should reach 800 °C for a typical minimum duration of 6 h [18–22].

4.2 Microstructure of Ti–6Al–4V during creep exposure: recalling effect of annealing at 740 °C

The findings obtained by TEM analysis of the sample crept after annealing at 740 °C in [2] are recalled for completeness. Additional micrographs are also discussed in this section to provide a sound basis for a reasonable interpretation of the material behaviour after annealing at 1050 °C.

Significant microstructural differences between the samples tested at 500 °C and 160/667 MPa (VLE) and those crept at 600 and 650 °C under 100 MPa (CLE) were observed in [2]. In particular, the microstructure of the sample tested at 500 °C after 476 h still showed a noticeable amount of α′-martensite in the α-grains. The volume fraction of the α-grains containing α′-martensite accounted for approximately 25 % volume. In fact, the α′-phase still present in these grains was only a small fraction of the grain volume; hence, the total amount of α′-martensite did not exceed 8–10 %. α′-martensite nucleated in the form of fine acicular structures at the prior β-grain boundaries, from which it grew within the α-grains being formed during rapid cooling by the SLM. The typical spatial configuration of different individual α′-colonies mostly consisted of chessboard structures. Both the α and α′-phases had the same hcp crystallographic structure with minimal lattice differences. In contrast, the chessboard structures were observed to have a fixed crystallographic orientation relationship with the hosting α phase, being approximately ±45° with respect to α. Crystallographic relationships between the different detected phases were determined using SAEDPs (Figure 12).

The material crept under a low load, e.g., σ = 100 MPa, and a high temperature, e.g., 600 and 650 °C, contained an extremely small fraction of α′-martensite colonies in the α-phase and a small fraction of the β-phase (Figure 12b). In contrast, some traces of the β-phase (3 % by volume) were also detected

in the sample tested at 500 °C. For clarity, the volume fractions of the β, α, and α′-phases in the three samples are listed in Table II.

Table II. Volume fractions (% vol.) of β, α, and α′ phases in VLE500, CLE600, and CLE650 samples.

Creep sample	β	α′	α
500 °C and 160/667 MPa	~3	~8	bal.
600 °C and 100 MPa	~4	<1	bal.
650 °C and 100 MPa	~8	<1	bal.

The reported amounts of the β-phase were not significantly different from those in the initial uncrept condition, being of a mean volume fraction of beta of 4 ± 1 %. The creep exposure did not considerably change the amount of the β-phase in the alloy. Regarding the size of the detected β-platelets, the typical lateral width (thickness) was 20 ± 4 nm, irrespective of the creep condition.

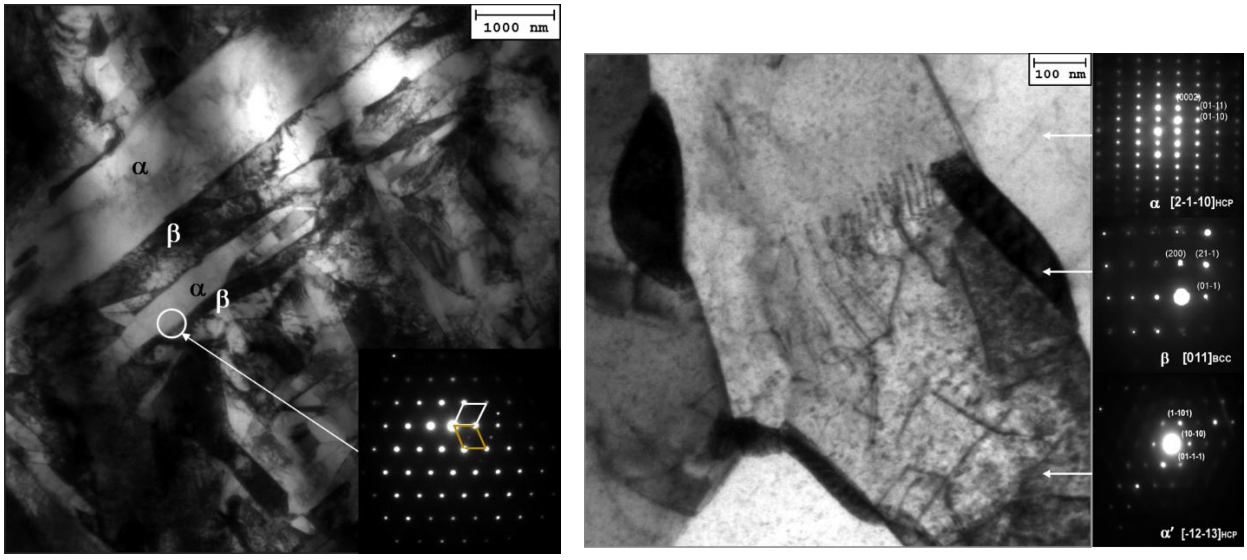

(a) (b)

Figure 12. Representative TEM microstructure of SLM-alloy after creep experiments: a) 500 °C and 160/667 MPa and b) 600 °C and 100 MPa. Insets of (b) show indexed SAEDPs of α, β, and α′ phases.

The experimental results showed that transformation of the retained α'-martensite occurred during creep exposure. Thus, it can be reasonably expected that higher exposure temperatures and longer

durations can induce a complete α′ to α-phase transformation [23]. Based on these observations, the minimum creep rate dependence on applied stress is primarily governed by the deformation of the α-phase, which accounts for approximately 90 % of the overall alloy structure.

4.3 Summary of possible roles of different phases in creep response

The results presented in this study allow to draw some important qualitative inferences on the possible roles of the different phases in the creep response of the studied Ti–6Al–4V alloy. These, as well as some of the conclusions obtained in the previous study on the material annealed at 740°C, are summarised as follows.

i. The creep responses of Ti–6Al–4V alloys with equiaxed and duplex microstructures can be described by the same set of constitutive relationships (Equations (1)–(4)), the only significant difference being the value of the UTS (see Appendix 3 for further details). For the former, the microstructure consists of equiaxed α-grains, with a relatively much lower volume fraction of β-grains decorating the α-grain boundaries. In contrast, the duplex structure consists of equiaxed α- and lamellar α–β grains. In both equiaxed and duplex materials, the α-phase is predominant, and they show similar creep responses. It is reasonable to conclude that the β-phase, present in remote grains or coarse lamellae, plays a minor role. When creep is controlled by the dislocation activity in the α-phase, the α–β interfaces could possibly act as a strengthening source; however, the distance between these interfaces is too long for this mechanism to be effective.

ii. The creep response of the AM alloy annealed at 740 °C was shown to obey to the same constitutive equations [2] Equations (1)–(4), provided that the correct value of the UTS was used. In this case, the microstructure comprised approximately 90 % α-phase and small amounts of the β and α′-phases. This picture is fully consistent with the conclusion that creep is controlled by the dislocation activity in the α-phase, and the presence of relatively sparse widely spaced β-particles plays virtually no role.

iii. The volume fraction of the β-phase in the material annealed at 1050 °C was higher than that in the alloy annealed at 740 °C. The β-phase volume fraction in the material annealed at 1050 °C was similar to that in the equiaxed and duplex alloys. A distinctive feature was the *bcc* phase, which here formed finely spaced lamellae. β-lamellae fragmentation occurred for long creep exposures at high temperatures following the initial annealing at 1050 °C. For the samples annealed at 740 °C, the β-phase did not form long lamellae as under the heat treatment at 1050 °C. The UTS after annealing was similar to those of the equiaxed and duplex microstructures; therefore, the use of Equations (1)–(4) yields the same curves. However, the observed minimum creep rates were significantly lower for the former. Thus, the two most important features of the microstructure that could play a role in this behaviour are the fine spacing (a few hundreds of nanometres) of the β-phase lamellae and the presence of α_2-particles.

The findings summarised in this section suggest that modifying Equation (1)–(4) is necessary to describe the creep response of the alloy annealed at 1050 °C. Accordingly, the approach proposed by Barboza et al. [7], who introduced a threshold stress σ_0 (slightly ambiguous in nature) in the traditional Norton power-law equation describing the minimum creep rate dependence on temperature and stress, was tentatively used in [9]. This procedure simply involves substituting Equation (3) with

$$\sigma = \sigma_\rho + \sigma_{ss} + \sigma_0 = \sigma_\rho + \delta(\sigma - \sigma_0) + \sigma_0 \qquad (5)$$

Understandably, this is an approach of a phenomenological nature; however, it seems reasonable. In a first instance, suppose that the effect of α_2-particles can be neglected. In this case, the α–β interfaces could act as effective barriers for dislocation motion, and the strengthening mechanism could be quantified by σ_0. The effectiveness of these barriers depends on their spacing L. This behaviour can be tentatively described by an equation in the form,

$$\sigma_0 \propto \left(\frac{MGb}{L}\right)^p, \qquad (6)$$

where p is a constant. Thus, $\sigma_0 \cong 0$ in the equiaxed microstructure, where spacing L between the interfaces equals the α-grain size. Similarly, $\sigma_0 \cong 0$ in all cases in which the spacing is large, i.e., measurable on the micron scale (e.g., in lamellar grains where the α-lamellae are coarse).

The above scenario is likely to differ when the alloy is annealed above the β-transus temperature. In the latter case, the β-phase appears in the form of more closely spaced lamellae. As long as the spacing of the β-particles remains low, fragmentation of the lamellae does not necessarily significantly impair the alloy strengthening effect. This strengthening effect can be described by a threshold stress $\sigma_0 \neq 0$. Additional α_2 precipitation, which introduces a typical particle-strengthening effect, also affects the magnitude of the threshold stress. This effect can compensate the softening effect, if any, due to the lamellae fragmentation.

Owing to the microstructural complexity described herein and limited physical models describing the strengthening effect of α–β interfaces and experimental information about the L-magnitude in crept materials, a quantitative correlation between microstructural features and σ_0 is presently impossible. Therefore, σ_0/G was calculated at a single temperature by fitting the experimental data. In particular, the preliminary results at 650 °C obtained in [9] were used as the basis for the analysis. In addition, first, it was arbitrarily assumed that σ_0/G did not change significantly with temperature. The other parameters for the calculation were the same as those used for the other Ti–6A–-4V alloy considered in [2]: Q_L = 303 kJ mol^{-1}, $D_0 = 1.4 \times 10^{-3}$ m^{2}s^{-1}, A = 40, and δ = 0.4. The UTS was assumed to be 1000 MPa, i.e., a value slightly higher than that obtained experimentally, to account for the strength reduction due to the surface being in the as-deposited state. In this regard, Figure 13 shows the experimental data for the alloys annealed at 740 °C and 1050 °C and the model curves obtained with the same parameters but σ_0/G = 0 and 1.19×10^{-3}, respectively. The correlation between the experimental and model results is good, except in the very high-strain rate region, where the model overestimates the strain rate. This deviation can be partly attributed to the underestimation of the UTS,

in particularly at 500 °C, where a limited precipitation of the α_2-particles slightly increases the tensile strength.

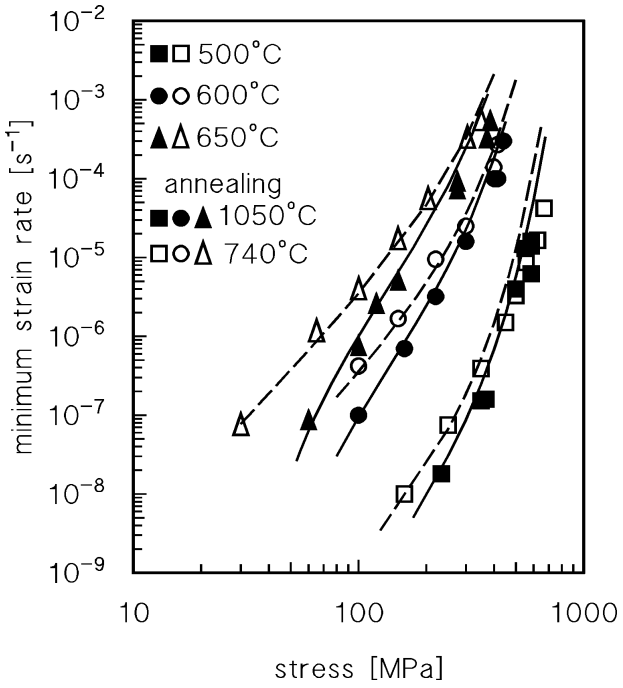

Figure 13. Experimental minimum creep rates for AM alloys annealed at 740 and 1050 °C and model curves with $\sigma_0/G = 0$ and 1.19×10^{-3}, respectively. Squares, circles and triangles represent tests carried out at 500, 600 or 650°C respectively. Open symbols represent creep results obtained by testing the alloy of the present study after annealing at 740°C.

Based on Figure 13, the original concept of Barboza et al., i.e., the difference in creep behaviour can be described by introducing a threshold stress, provides a good phenomenological description of the creep response of the alloy with a Widmanstätten structure. The model can also rationalise the abnormal scatter observed in the literature creep data for alloys with such microstructures. The finesse of the Widmanstätten structure, i.e., the distance between the α–β interfaces, directly depends on the heat-treatment parameters (temperature, duration of annealing, and cooling rate). The distance between the α–β interfaces, in turn, determines the magnitude of the threshold stress. Furthermore, different amounts of the α_2-phase could be present in each case owing to the different thermal histories. Thus, the scatter among the creep data obtained by testing various batches of alloys annealed above the β-

transus temperature, in this context, can be easily explained by simply introducing small differences in the β- and α_2-phase volume fractions and distributions. This is a result of the heat-treatment processing parameters.

Figure 14 shows a representative case study. The curves obtained by combining Equations (1), (2), (4) and (5) with the same parameters used for Figure 13 and $\sigma_0/G = 2.0 \times 10^{-3}$ are compared with the experimental data from [7]. For six out of eight data points, the description is excellent. A deviation is observed only for a long time of exposure at 500 °C, i.e., in conditions where additional precipitation of the α_2-phase can be problematic. The model curve correctly estimates the minimum strain rate under 291 MPa at 500 °C with $\sigma_0/G = 4.85 \times 10^{-3}$. Thus, the model is correct, i.e., the microstructure undergoes considerable strengthening due to a reduction in L, presumably due to α_2-precipitation, during creep exposure.

Figure 14 shows speculative results because of the lack of experimental data on important features such as β- and α_2-phase volume fractions and distributions (i.e., on L) of that material. However, the threshold stress calculation in most creep studies was conducted by similar fitting procedures (see two examples in [24, 25]), which were typically not calculated by physical models of the dislocation/particle interaction. Thus, if it Figure 14 needs to be validated by microstructural studies, it unambiguously demonstrates that the proposed model is, in principle, appropriate for describing the creep response of the alloy annealed above the β-transus temperature.

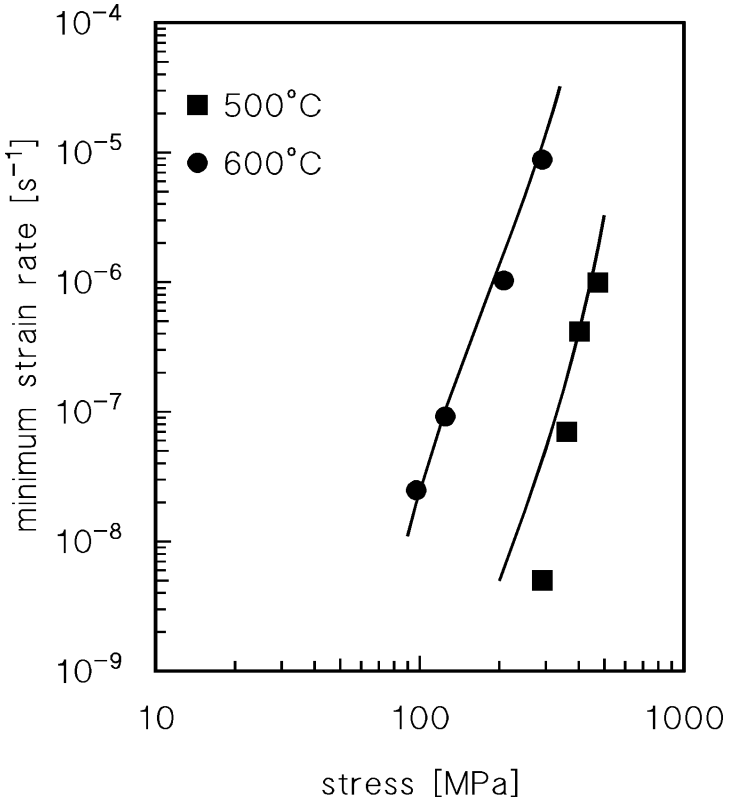

Figure 14. Model curves obtained with $\sigma_0/G = 2.0 \times 10^{-3}$ and experimental data from [7].

5. Conclusion

The creep responses of an AM Ti–6Al–4V alloy and annealed at 1050 °C were investigated at 500, 600, and 650 °C. The main findings of this study can be summarised as follows.

i. The alloy with a Widmanstätten microstructure typical of an alloy annealed above the β-transus temperature presented minimum creep rates lower than those of the same material annealed at lower temperatures.

ii. At a fine scale, the microstructure of the alloy annealed at 1050 °C, was characterised by the presence of finely spaced β-lamellae, which during creep exposure progressively underwent fragmentation. Nevertheless, at least for the relatively short durations investigated in the present study, the fragmented β-lamellae still formed a distribution of finely spaced particles.

iii. The presence of α_2-Ti_3Al particles was evident in all investigated microstructures, even at 650 °C, a temperature at which the presence of this phase is largely unexpected.

iv. The creep response of the alloy annealed at 1050 °C could be quantitatively described by introducing a threshold stress σ_0 in constitutive equations. These equations were previously used to analyse the creep responses of Ti–6Al–4V with equiaxed and duplex microstructures and the same alloy produced by additive manufacturing and annealed at 740 °C. This threshold stress can be considered as a quantification term for the strengthening role of both the α–β interfaces and α_2 particles. An excellent description could be obtained with a constant value of σ_0/G at the different temperatures, which suggests that the same hardening effect dominates between 500 and 650 °C.

v. For equiaxed, duplex, and annealed SLM-alloys, $\sigma_0/G = 0$ possibly suggests that the distance between the α–β interfaces is extremely long to be effective. This conclusion was supported by the experimental evidence obtained by studying the microstructure of the SLM-alloy annealed at 740 °C.

Appendix 1

The model discussed in this paper was originally developed for cfc metals. The starting point was the formulation of the evolution of the dislocation density (ρ) during straining expressed in simplified form, as [26,27]

$$\frac{d\rho}{d\varepsilon} = \frac{m}{bL^*} - \frac{2}{\dot{\varepsilon}} M\tau_l \rho^2 \quad \text{(A1)}$$

where τ_l is the dislocation line tension (τ_l=0.5Gb^2), M is the dislocation mobility and L^* is the dislocation mean free path (distance travelled by a dislocation before it undergoes a reaction) expressed, as

$$L^* = \frac{C_L}{\sqrt{\rho}} \quad \text{(A2)}$$

Combination of Eqns. (A1) and (A2) gives

$$\frac{d\rho}{d\varepsilon} = \frac{m\sqrt{\rho}}{bC_L} - \frac{2}{\dot{\varepsilon}} M \tau_l \rho^2 \quad \text{(A3)}$$

The second term of the right-hand part of Eqn.(A3) is strongly temperature-dependent through the dislocation mobility term *M*, which can be written as [28-30]

$$M = \frac{D_0 b}{kT} exp\left(\frac{\sigma_\rho b^3}{kT}\right) exp\left\{-\frac{Q_L}{RT}\left[1 - \left(\frac{\sigma_\rho}{R_{max}}\right)^2\right]\right\} \quad \text{(A4)}$$

where R_{max} is the maximum strength of the material. Equation (A4), at steady state, when dislocation density is constant, combined with Eqn. (A1), gives

$$\dot{\varepsilon}_m = \frac{2\tau_l D_0 b^2 C_L}{mkT}\left(\frac{\sigma_\rho}{\alpha m G b}\right)^3 exp\left(\frac{\sigma_\rho b^3}{kT}\right) exp\left\{-\frac{Q_L}{RT}\left[1 - \left(\frac{\sigma_\rho}{R_{max}}\right)^2\right]\right\} \quad \text{(A5)}$$

or

$$\dot{\varepsilon}_m = A\frac{D_0 G b}{kT}\left(\frac{\sigma_\rho}{G}\right)^3 exp\left(\frac{\sigma_\rho b^3}{kT}\right) exp\left\{-\frac{Q_L}{RT}\left[1 - \left(\frac{\sigma_\rho}{R_{max}}\right)^2\right]\right\} \quad \text{(A6)}$$

being

$$A = \frac{C_L}{\alpha^3 m^4} \quad \text{(A7)}$$

Interestingly enough, for pure Al, where C_L=85, α=0.3 and m=3.06 [31], A=35.9. This value is very close to A=40 here used for Ti (m values close to 3 have been indeed predicted [32]).

Appendix 2

Combination of Eqns.(1) - (4) can be used to obtain the model curves describing the minimum creep rate as a function of stress and temperature, by using as input datum only the value of the UTS. This procedure was described in detail in [2]. This appendix just presents few examples of the resulting description. For all these curves, Q_L = 303 kJ mol^{-1}, D_0 = 1.4 × 10^{-3} m^{2}s^{-1}, A = 40, and δ = 0.4. UTS

values from [3]. The typical scatter of the available experimental data can be easily appreciated in b). As a whole, if one takes into account that no fitting was required, the description is excellent, except than for the alloys with fully lamellar structure, characterized by an enormous dispersion of the data.

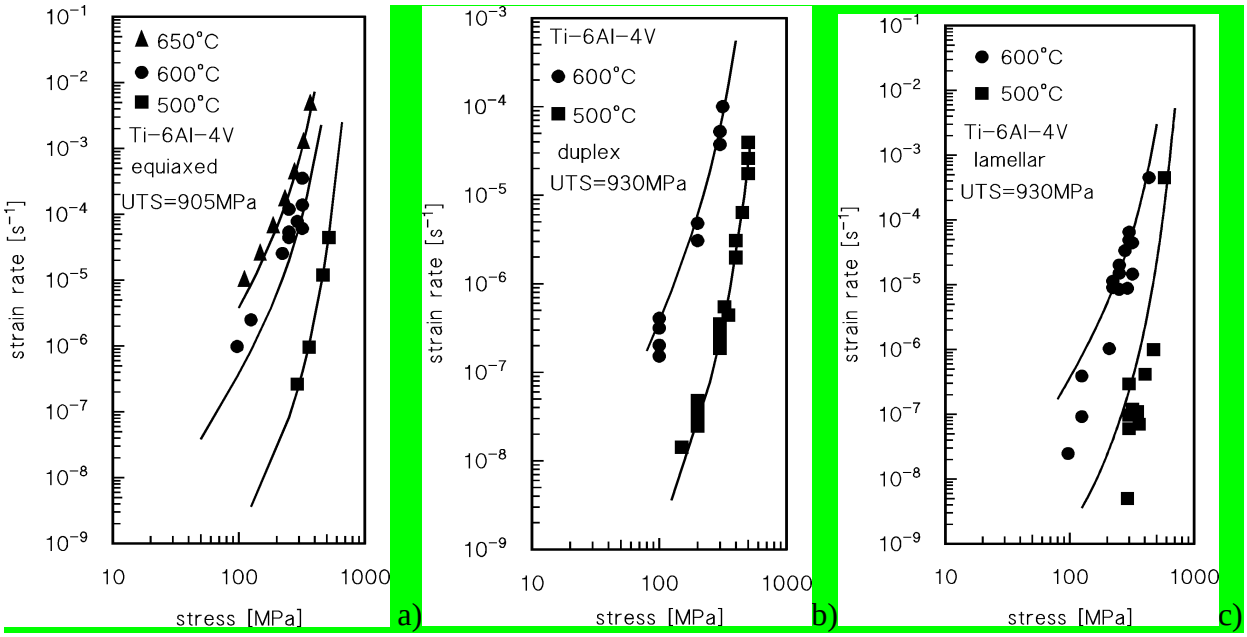

Figure A2.1. Model curves from Eqns.(1) - (4). The equations did not contain free-parameters, the only required input being the UTS. The Figures illustrates: a) alloys with fully equiaxed α-grains, data from [33-37]; b) alloys with duplex microstructure (equiaxed and lamellar grains), data from [38,39]; c) data for alloys with lamellar (Widmanstätten) microstructure, data from [3-8].

Acknowledgements

This research was partially funded by the Grant of Excellence Departments, MIUR-Italy (ARTICOLO 1, COMMI 314–337 LEGGE 232/2016).

Data availability

The raw/processed data required to reproduce these findings cannot be shared at this time as the data also forms part of an ongoing study.

References

1. S. Liu, Y.C. Shin, Additive manufacturing of Ti6Al4V alloy: A review, Mater. Des. 164 (2019) 107552. https://doi.org/10.1016/j.matdes.2018.107552.

2. S. Spigarelli, C. Paoletti, M. Cabibbo, E. Cerri, E. Santecchia. On the creep performance of the Ti-6Al-4V alloy processed by additive manufacturing. Additive Manufacturing 49 (2022) 102520https://doi.org/10.1016/j.addma.2021.102520

3. S. Nishino, K. Shiozawa, Y. Aikawa, Effect of microstructure on creep and creep-fatigue behavior in Ti-6Al-4V alloy at elevated temperature, Mater. Sci. Sci. Res. Int. 4 (1997) 206–211. https://doi.org/10.2472/jsms.46.512.

4. G.F.C. Almeida, A.A. Couto, D.A.P. Reis, M. Massi, A.S. da Silva Sobrinho, N.B. de Lima, Effect of plasma nitriding on the creep and tensile properties of the Ti-6Al-4V alloy, Metals (Basel). 8 (2018) 0618. https://doi.org/10.3390/met8080618.

5. V.M.C.A. De Oliveira, M.C.L. Da Silva, C.G. Pinto, P.A. Suzuki, J.P.B. Machado, V.M. Chad, M.J.R. Barboza, Short-term creep properties of Ti-6Al-4V alloy subjected to surface plasma carburizing process, J. Mater. Res. Technol. 4 (2015) 359–366. https://doi.org/10.1016/j.jmrt.2015.05.006.

6. T. Sugahara, D.A.P. Reis, C. Moura Neto, M.J.R. Barboza, E.A.C. Perez, F. Piorino Neto, A.C.O. Hirschmann, The effect of Widmanstätten and equiaxed microstructures of Ti-6Al-4V on the oxidation rate and creep behavior, in: Mater. Sci. Forum, 2010: pp. 636-637 657-662. https://doi.org/10.4028/www.scientific.net/MSF.636-637.657.

7. M.J.R. Barboza, E.A.C. Perez, M.M. Medeiros, D.A.P. Reis, M.C.A. Nono, F.P. Neto, C.R.M. Silva, Creep behavior of Ti-6Al-4V and a comparison with titanium matrix composites, Mater. Sci. Eng. A. A428 (2006) 319–326. https://doi.org/10.1016/j.msea.2006.05.089.

8. V.M.C.A. Oliveira, A.M. Vazquez, C. Aguiar, A. Robin, M.J.R. Barboza, Nitride coatings improve Ti-6Al-4V alloy behavior in creep tests, Mater. Sci. Eng. A670 (2016) 357–368. https://doi.org/10.1016/j.msea.2016.06.041.

9. C. Paoletti, M. Cabibbo, E. Santecchia, E. Cerri, S. Spigarelli, Effect of Post-Processing Heat Treatments on Short-Term Creep Response at 650 °C for a Ti-6Al-4V Alloy Produced by Additive Manufacturing, Metals 12 (2022) 1084.
https://doi.org/10.3390/met12071084

10. A. Nespoli, N. Bennato, E. Villa, F. Passaretti. Study of anisotropy through microscopy, internal friction and electrical resistivity measurements of Ti-6Al-4V samples fabricated by selective laser melting, Rapid Prototyping Journal (2022) 28.
https://doi.org/1060–1075. 10.1108/RPJ-06-2021-0151.

11. Xiao Li, Tian Sugui, Bao Xianyu, Chen Liqing, Creep properties and effect factors of hot continuous rolled Ti–6Al–4V alloy, Mater. Sci. Eng., A529 (2011) 452-458, ISSN 0921-5093, https://doi.org/10.1016/j.msea.2011.09.061.

12. M. Paghandeh, A. Zarei-Hanzaki, H.R. Abedi, Y. Vahidshad, On the warm temperature strain accommodation mechanisms of Ti–6Al–4V alloy holding different starting microstructures, J. Mater. Res. Technol., 14 (2021) 496-506.
https://doi.org/10.1016/j.jmrt.2021.06.077.

13. Ying Zhang, Dongsheng Li, Xiaoqiang Li, Xiaochun Liu, Shiteng Zhao, Yong Li, Creep deformation and strength evolution mechanisms of a Ti-6Al-4V alloy during stress relaxation at elevated temperatures from elastic to plastic loading, J. Mater. Sci. Technol 126 (2022) 93-105, https://doi.org/10.1016/j.jmst.2022.02.042.

14. Jinlong Su, Xiankun Ji, Jin Liu, Jie Teng, Fulin Jiang, Dingfa Fu, Hui Zhang, Revealing the decomposition mechanisms of dislocations and metastable α' phase and their effects on mechanical properties in a Ti-6Al-4V alloy, Journal of Materials Science & Technology, 107 (2022) 136-148, https://doi.org/10.1016/j.jmst.2021.07.048.

15. D.G. Lee, S. Kim, S. Lee, Chong Soo Lee, Effects of microstructural morphology on quasi-1static and dynamic deformation behavior of Ti-6AI-4V alloy, Metall. Mater. Trans. A Phys. Metall. Mater. Sci. 32A (2001) 315–324. https://doi.org/10.1007/s11661-001-0263-y.

16. J. Tiley, T. Searles, E. Lee, S. Kar, R. Banerjee, J.C. Russ, H.L. Fraser, Quantification of microstructural features in α/β titanium alloys, Mater. Sci. Eng. A. A372 (2004) 191–198. https://doi.org/10.1016/j.msea.2003.12.008.

17. R. Sahoo, B.B. Jha, T.K. Sahoo, Effect of Microstructure on the Creep Properties of Ti–6Al–4V Alloys: An Analysis, Trans. Indian Inst. Met. Met 71 (2018) 1573–1582. https://doi.org/10.1007/s12666-018-1292-1.

18. J. Yu, M. Rombouts, G. Maes, F. Motmans, Material Properties of Ti6Al4V Parts Produced by Laser Metal Deposition, Phys. Procedia. 39 (2012) 416–424. https://doi.org/https://doi.org/10.1016/j.phpro.2012.10.056.

19. B. Vrancken, L. Thijs, J.P. Kruth, J. Van Humbeeck, Heat treatment of Ti6Al4V produced by Selective Laser Melting: Microstructure and mechanical properties, J. Alloys Compd. (2012) 177–185. https://doi.org/10.1016/j.jallcom.2012.07.022.

20.C. Qiu, N.J.E. Adkins, M.M. Attallah, Microstructure and tensile properties of selectively laser-melted and of HIPed laser-melted Ti-6Al-4V, Mater. Sci. Eng. A. A578 (2013) 230–239. https://doi.org/10.1016/j.msea.2013.04.099.

21.T.M. Mower, M.J. Long, Mechanical behavior of additive manufactured, powder-bed laser-fused materials, Mater. Sci. Eng. A. A651 (2016) 198–213. https://doi.org/10.1016/j.msea.2015.10.068.

22.S. Liu, Y.C. Shin, Additive manufacturing of Ti6Al4V alloy: A review, Mater. Des. 164 (2019) 107552. https://doi.org/10.1016/j.matdes.2018.107552.

23. S. Cao, R. Chu, X. Zhou, K. Yang, Q. Jia, C.V.S. Lim, A. Huang, X. Wu, Role of martensite decomposition in tensile properties of selective laser melted Ti-6Al-4V, J. Alloys Compd. 744 (2018) 357–363.
https://doi.org/10.1016/j.jallcom.2018.02.111.

24. Y.Li, T.G.Langdon, A simple procedure for estimating threshold stresses in the creep of metal matrix composites, Scripta Mater 36 (1997) 1457-1460.
https://doi.org/10.1016/S1359-6462(97)00041-9

25.J.K. Benz, L.J. Carroll, J.K. Wright, R.N. Wright, T.M. Lillo. Threshold Stress Creep Behavior of Alloy 617 at Intermediate Temperatures, Metall Mater Trans 45A (2014) 3010-3022.
https://doi.org/10.1007/s11661-014-2244-y

26. R. Sandström, J. Hallgren, The role of creep in stress strain curves for copper, J Nucl Mater, 422 (2012) 51-57.
https://doi.org/10.1016/j.jnucmat.2011.12.012

27. R. Sandström, The role of cell structure during creep of cold worked copper, Mater. Sci. Eng. A. A, 674 (2016) 318-327.
https://doi.org/10.1016/j.msea.2016.08.004

28. J.P. Hirth, J. Lothe, Theory of Dislocations, Krieger, Malabar, Florida, 1982.

29. U.F.Kocks, A.S.Argon, M.F.Ashby, Thermodinamics and kinetics of slip, Prog.Mater.Sci 15 (1979) 1

30. R. Sandström, H.C.M. Andersson, Creep in phosphorus alloyed copper during power-law breakdown, J.Nucl. Mater. 372 (2008) 76-88.
https://doi.org/10.1016/j.jnucmat.2007.02.005

31. S. Spigarelli, R. Sandström. Basic creep modelling of Aluminum. Mater Sci Eng A, 711 (2018) 343-349.
https://doi.org/10.1016/j.msea.2017.11.053

32. S. Panda, S.K. Sahoo, A. Dash, M. Bagwan, G. Kumar, S.C. Mishra, S. Suwas. Orientation dependent mechanical properties of commercially pure (cp) titanium. Materials Characterization 98 (2014) 93–101.
http://dx.doi.org/10.1016/j.matchar.2014.10.011
33. E. Alabort, P. Kontis, D. Barba, K. Dragnevski, R.C. Reed, On the mechanisms of superplasticity in Ti-6Al-4V, Acta Mater. 105 (2016) 449–463.
https://doi.org/10.1016/j.actamat.2015.12.003.
34. D.A.P. Reis, C.R.M. Silva, M.C.A. Nono, M.J.R. Barboza, F. Piorino Neto, E.A.C. Perez, Effect of environment on the creep behavior of the Ti-6Al-4V alloy, Mater. Sci. Eng. A. A399 (2005) 276–280.
https://doi.org/10.1016/j.msea.2005.03.073.
35. A.G. dos Reis, D.A.P. Reis, C. de Moura Neto, M.J.R. Barboza, J. Oñoro, Creep behavior and surface characterization of a laser surface nitrided Ti-6Al-4V alloy, Mater. Sci. Eng. A. A577 (2013) 48–53.
https://doi.org/10.1016/j.msea.2013.04.042.
36. L.A.N.S. Briguente, A.A. Couto, N.M. Guimarães, D.A.P. Reis, C. Moura Neto, M.J.R. Barboza, Determination of creep parameters of Ti-6Al-4V with bimodal and equiaxed microstructure, in: Defect Diffus. Forum, 2012: pp. 326-328 520-524.
https://doi.org/10.4028/www.scientific.net/DDF.326-328.520.
37. M.J.R. Barboza, C. Moura Neto, C.R.M. Silva, Creep mechanisms and physical modeling for Ti-6Al-4V, Mater. Sci. Eng. A. A369 (2004) 201–209. https://doi.org/10.1016/j.msea.2003.11.016.
38. V.B. Badea Lavina, Surand Martin, Ruau Jacques, Creep behavior of Ti-6Al-4V from 450°C to 600°C., Univ. Polytech. Bucharest Sci. Bull. Ser. B. 76 (2014) 185–196. hal-01186469.
39. M.T. Whittaker, W.J. Harrison, R.J. Lancaster, S. Williams, An analysis of modern creep lifing methodologies in the titanium alloy Ti6-4, Mater. Sci. Eng. A. A577 (2013) 114–119.
https://doi.org/10.1016/j.msea.2013.03.030.

Creep response of Ti–6Al–4V alloy produced by additive manufacturing: effect of annealing at 1050 °C

S. Spigarelli[1], C. Paoletti[2], E. Cerri[3], E. Santecchia[1,*], M. Cabibbo[1]

1. DIISM, Università Politecnica delle Marche, via Brecce Bianche, 60131 Ancona, Italy

2. Faculty of Engineering, Università degli Studi eCampus, Via Isimbardi 10, 22060 Novedrate, Italy

3. DIA Università di Parma, V.le G. Usberti 181/A, 43124, Parma, Italy

*E. Santecchia: corresponding author

Abstract

The present study mainly aims at investigating the creep response of a Ti–6Al–4V alloy produced by additive manufacturing and annealed above the β-transus, and at rationalizing the differences observed when comparing its behaviour to that of the same alloy annealed at lower temperatures. Herein, the creep response of this alloy produced by additive manufacturing and subsequently annealed at 1050 °C is investigated at temperatures ranging from 500 to 650 °C. The heat treatment produces the typical Widmanstätten microstructure with thin β-lamellae interposed between coarse α-lamellae. The minimum creep rate dependence on the applied stress and temperature is compared with literature data of tests of alloys with Widmanstätten microstructures produced by traditional technologies. A modified form of an equation, successfully used to describe the creep responses of the Ti–6Al–4V alloy with different initial microstructures, was here proposed. The suggested modification introduces a threshold stress, which is related to the presence of finely spaced α–β interfaces and α_2-Ti_3Al particles. This threshold stress is considered to be negligible when the distance between the α–β interfaces is long and the α_2-Ti_3Al particles are absent or excessively spaced. In contrast, in the materials with Widmanstätten microstructures, even minor differences in the heat treatment conditions and/or the processing history cause considerable variations in the distance between the α–β interfaces. This coupled with the occasional precipitation of α_2-Ti_3Al particles results in different threshold stress values.

Keywords: Additive manufacturing; Phase Transitions; Creep; Microstructure; Titanium alloys

1. Introduction

Ti–6Al–4V alloy is a commercial material well suited for processing by additive manufacturing. In particular, selective laser melting (SLM), also known as laser-beam powder-bed fusion, is an excellent candidate for industrial-scale production of Ti–6Al–4V components. Consequently, several recent studies, accurately reviewed by Liu and Shin [1], thoroughly investigated the microstructural features and mechanical properties of the additively manufactured (AM) alloy. Notably, the creep response of the AM alloy has not received equal attention. Thus, in a previous study all recently available data on the creep behaviour of Ti–6Al–4V produced by different technologies and having different initial microstructures were collected [2]. Moreover, they were compared with new experimental results obtained by testing a Ti–6Al–4V alloy produced by SLM and subsequently annealed at 740 °C for 130 min. Furthermore, an additional effort was made to rationalise the creep responses of the alloys produced by traditional technologies and AM, respectively. This analysis demonstrated that the same equation can be successfully used to describe the creep response of Ti–6Al–4V alloy, irrespective of the initial microstructure and the production technique. The minimum strain rate ($\dot{\varepsilon}_m$) dependences on the stress (σ) and temperature (T) of "traditional" materials with both equiaxed and duplex microstructures and annealed or as-deposited AM alloys were expressed by

$$\dot{\varepsilon}_m = A\frac{D_0 G b}{kT}\left(\frac{\sigma_\rho}{G}\right)^3 exp\left(\frac{\sigma_\rho b^3}{kT}\right) exp\left\{-\frac{Q_L}{RT}\left[1-\left(\frac{\sigma_\rho}{R_{max}}\right)^2\right]\right\}, \quad (1)$$

where b was the Burgers vector; G was the shear modulus; k was Boltzmann's constant; A was a constant, and D was the self-diffusion coefficient, which was expressed as:

$$D = D_0 exp\left(-\frac{Q_L}{RT}\right), \quad (2)$$

where D_0 was a material parameter and Q_L was the activation energy (for lattice self-diffusion in pure metals). The σ_ρ term (dislocation hardening) was calculated by handling the equation:

$$\sigma = \sigma_\rho + \sigma_{ss} = \sigma_\rho + \delta\sigma \quad (3)$$

where σ_{ss} was the solid solution strengthening term and δ is a constant (= 0.4) introduced to represent its effect.

The R_{max} parameter (maximum strength) was expressed as

$$R_{max} = 1.5UTS\frac{G_T}{G_{RT}}, \quad (4)$$

where G_{RT} and G_T were the shear moduli at room temperature and the testing T, respectively.

For any interested reader, Equations (1)–(4) are described in detail in [2], although Appendix 1 provides a synthetic description of the genesis of their formulation. This set of constitutive equations provided an excellent description of the minimum creep rate dependence on applied stress for equiaxed and duplex microstructures, the input parameter being the UTS (see Appendix II for few non-exhaustive examples of the findings reported in [2]). However, an important issue was the extremely large scatter of the minimum creep rate data observed when comparing different lots of Ti–6Al–4V alloys having Widmanstätten structures [3–8]. This peculiar microstructure forms after annealing the alloy above the β-transus temperature and subsequently cooling at a relatively high cooling rate. Equations (1)–(4) provide curves that bisect the 'clouds' of experimental data; however, the scatter is extremely large to conclude that the model is perfectly adequate for describing the creep response. This discrepancy suggests broadening the study on the creep response of AM Ti–6Al–4V by also annealing the alloy at 1050 °C, which is well above the β-transus temperature, to obtain a Widmanstätten structure. A few creep results at 650 °C, a temperature above the predictable range of α_2-Ti_3Al precipitation, have recently been reported by the authors of the present study [9]. The aim of that preliminary investigation was limited to comparing the creep responses of the alloy with a Widmanstätten structure before and after annealing below the β-transus temperature. The experimental results proved that at this temperature, the alloy with a Widmanstätten microstructure exhibited lower creep rates than after annealing at 704 or 740 °C. This behaviour cannot be explained by Equations (1)–(4), in particular, owing to the ultimate tensile strength (UTS) of the alloy annealed above the β-transus temperature being slightly lower than that of the material annealed at 704–740 °C. These observations indicated the need to enlarge the range of the experimental conditions to be investigated to cover the full temperature

range considered in [2]. Thus, the aim of the present study was twofold: i) present a much more extensive set of experimental data obtained by testing the AM alloy annealed at 1050 °C at different temperatures by both constant-load and variable-load creep experiments (CLEs and VLE, respectively) and ii) provide a model on a wider scale applicable to alloys produced by traditional technologies and able to describe the creep response of Ti–6Al–4V with a Widmanstätten structure. Therefore, the present study reports new data on the creep responses at 500 and 600 °C of the AM Ti–6Al–Ti-6Al-4V annealed at 1050 °C.

2. Material and Experimental procedures

2.1 Material and sample production

In this study, commercial gas-atomised Ti–6Al–4V grade 23 extra-low-interstitial powders (5.5–6.5 % Al, 3.5–4.5 % V, 0.25 % F, 0.1 % O, 0.05 % maximum N, 0.08 % maximum C, 0.011 % maximum H, and Ti balance wt.%) were used. The powder particles had sizes ranging from 15 μm to 45 μm. An SLM280 machine (SLM Solutions AG, Lübeck, Germany) equipped with a 400 W IPG fibre laser was used for the production of dog-bone creep samples, with a square section of area A_0 = 3 mm × 3 mm and a 25 mm gauge length (Figure 1).

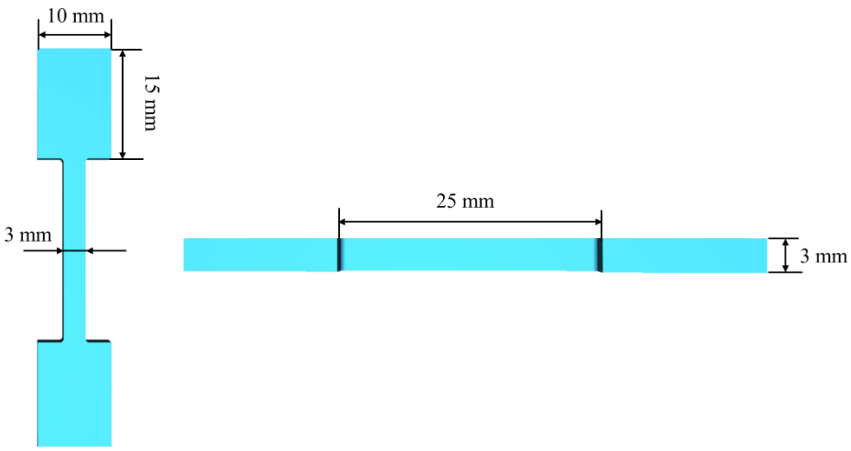

Figure 1. Geometry of the creep sample.

A powder bed was preheated at 80 °C, and deposition was performed in argon (Ar) to reduce oxygen concentration to 0.05 %. The building direction was parallel to the gauge length of the specimen. The deposition was conducted to a thickness of 60 μm at a scanning speed of 1250 mm/s, with hatch spacing of 120 μm, and laser power of 340 W. The post-processing treatment consisted of annealing at 1050 °C, which is sufficiently above the β-transus temperature to ensure the full transformation of the microstructure, for 1 h, followed by cooling in Ar at 0.4 °C/s. This relatively slow cooling was expected to lead to the formation of a Widmanstätten structure with reduced internal stress [10]. Both sample production and post-processing heat treatment were performed by BEAMIT (https://www.beam-it.eu/, Fornovo di Taro 43045, Italy).

2.2 Creep experiments

CLEs and VLEs were conducted at 500, 600, and 650 °C in air on samples whose surfaces were in the as-deposited state. In a CLE, a load *P* was applied immediately after a short soaking time at the testing temperature and maintained until rupture or test interruption in the tertiary stage. In a VLE, a sample was loaded similarly to in a CLE under a given initial stress; however, after the minimum creep rate range was presumably attained, the load was abruptly changed.

The soaking time at temperature before loading was typically 0.5–1 h, except before a CLE test, in which the soaking time was 145 h.

The test temperature was measured using four thermocouples, and the elongation was continuously measured using a linear variable displacement transducer.

2.3 Room-temperature mechanical properties

To evaluate the UTS, tensile tests at room temperature were performed on samples having the geometry of a creep experiment specimen. The surfaces of the samples used for the tensile tests were in the as-deposited state. The test strain rate was 3×10^{-2} s^{-1}. The UTS after heat treatment at 1050 °C was 922 ± 2 MPa.

Rockwell hardness (HRC) tests were performed on as-heat treated and crept sample heads. Because these tests were merely aimed at assessing the age-hardening responses of the alloy, the hardness was measured in these (almost) unstressed portions of the samples. The dislocation substructures introduced by loading and straining considerably influenced the hardness of the gauge lengths, thus masking the possibly considerably limited effects of age hardening. The HRC value after heat treatment was 38.1 ± 0.5 for the alloy after annealing.

2.4 Microscopy

Samples for light microscopy analyses were mechanically ground and polished with a colloidal suspension and subsequently etched using Kroll's reagent (100 mL H_2O + 2 mL HF + 4 mL HNO_3). Following this, the samples were observed under a Leica DMi8 optical microscope (Germany).

Scanning electron microscopy (SEM) observations were conducted using a Tescan Vega 3 scanning electron microscope (Brno, Czech Republic) at an accelerating voltage of 30 keV.

For transmission electron microscopy (TEM) analyses, thin foils were obtained from untested and crept sample heads. The samples were prepared by mechanical grinding and polishing to a thickness of 150 µm. This was followed by twin-jet electro-polishing to reach 60 µm thickness using a Struers™ Tenupol-5® device (Struers Inc., Westlake, Cleveland, OH, USA) with a solution consisting of 5 % perchloric acid, 35 % butanol, and 60 % methanol at −35 °C and voltage V = 24 V. The discs were dimpled to a reach a thickness of 20–25 µm and ion-milled to electron transparency using a Gatan© precision ion polishing system (Gatan Inc., Pleasanton, CA, USA) operating at 8 keV (incident beam angle progressively reduced to 8°, 6°, and 4°). The TEM analyses were performed using a Philips™ CM-20 microscope (Philips It, Milano, Italy) working at 200 kV and equipped with a double-tilt liquid nitrogen cooling specimen holder. Selected area diffraction patterns (SAEDPs) were recorded using a converged beam. Based on the SAEDPs, The crystallographic structures of the α, α′, and α_2-phases were found to have α-[0001] or α-[$2\bar{1}\bar{1}0$] directions parallel to the beam direction. Converged-beam electron diffraction (CBED) was used to identify the different detected phases, using a nominal electron

beam of 5-6 nm. Volume fraction of detected phases (namely, α′, α_2, and β) was evaluated by the Schwartz–Saltykov method. The method, was adapted to the TEM thin foil analyses by consider the bias introduced by the TEM thin foil and the precipitate morphology, i.e., lamellae (α), thin ribbon-like structures (β), and coarser lenticular morphological phase (α', α_2).

3. Results

3.1 Initial Microstructure

Figure 2 shows the initial microstructure of an annealed SLM-manufactured-alloy (referred as SLM-alloy) (light microscopy and SEM images). A Widmanstätten microstructure is noticeable as thin layers of light α-phase-decorating prior β-grains.

Figure 3 shows a representative TEM micrograph of the annealed SLM-alloy. The microstructure consists of thin and long β-lamellae interposed between much thicker α-lamellae. The thicknesses of the β and α-lamellae are in the ranges of 110–140 and 390–460 nm, respectively. In addition, remote α'-martensite colonies having essentially the same thickness as the α-lamellae are uniformly distributed in the α-phase of the Widmanstätten microstructure.

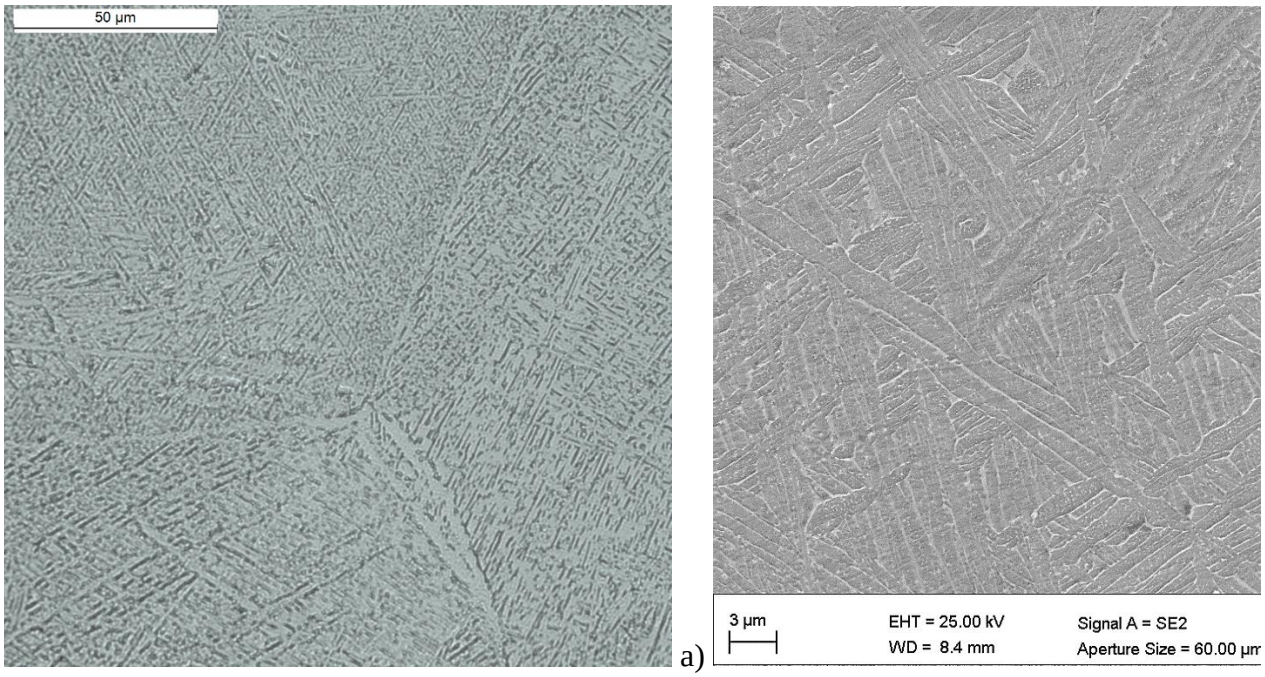

Figure 2. Microstructure of SLM-alloy after annealing at 1050 °C observed by a) optical microscopy and b) SEM; the α-phase is bright in Figure 2a, and dark-grey in Figure 2b; β-phase is dark-grey in a), and light-grey in b).

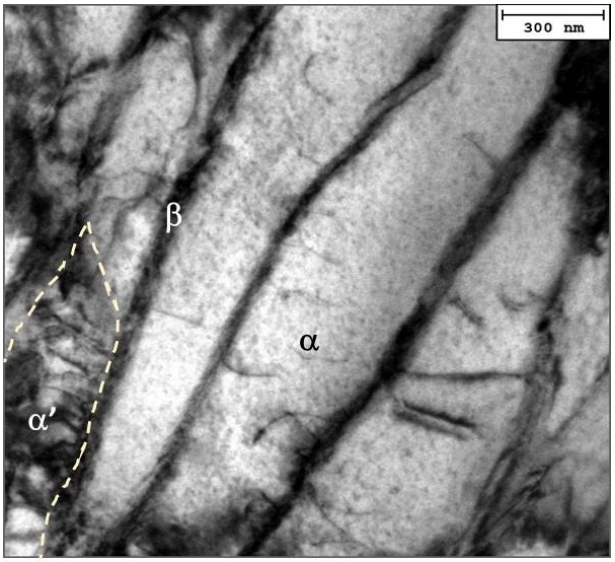

Figure 3. Microstructure of SLM-alloy after annealing at 1050 °C observed by TEM, showing α (the broad lenticular region), β (the long narrow features in-between), and α' (region included in the dashed line).

3.2 Creep response

Figure 4 shows the strain rate versus strain creep curves obtained in the present study at 500 and 600 °C (from CLEs and VLEs). Figure 5 displays the creep curves at 650 °C from [9] and supplemented by one additional VLE curve obtained in this study at this temperature. Figure 5 compares the curves obtained after short (0.5 h) and very long (145 h) soaking times at the testing temperature before loading.

In general, the shapes of the creep curves are similar to that observed when testing the alloy after annealing at 740 °C [2], and consist of a well-defined primary stage, a minimum creep rate range, and an extended tertiary stage. Figure 5 clearly shows that a long permanence at 650 °C before loading only results in a slight increase in the creep rates and a reduction in the strain to fracture.

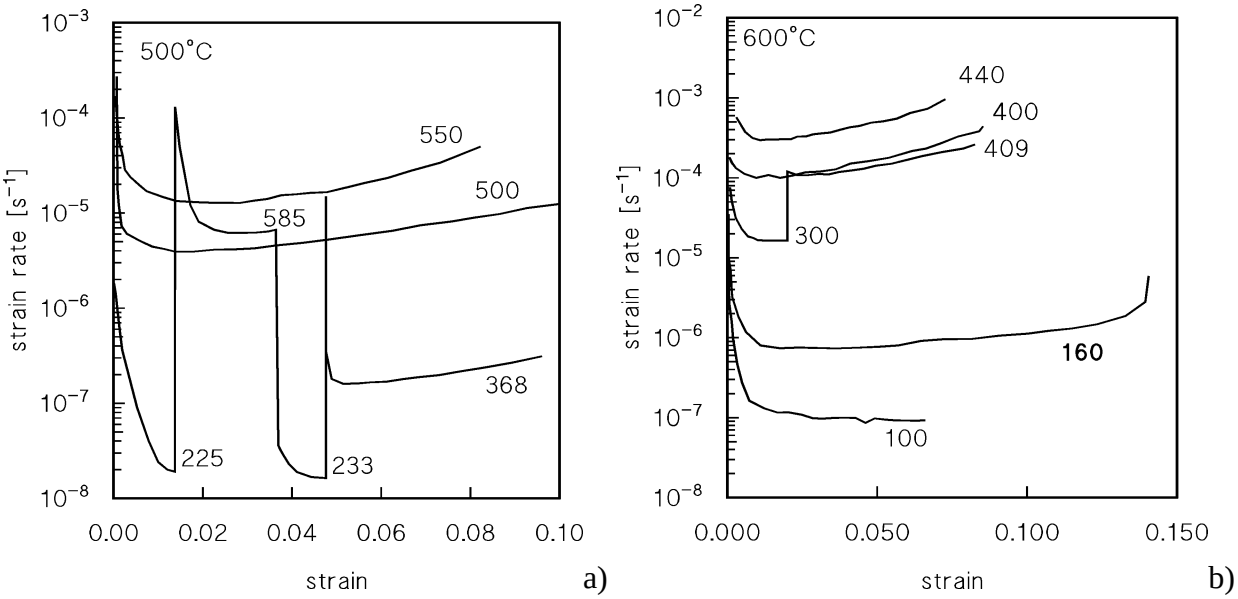

Figure 4. Strain rate versus strain creep curves from CLEs and VLEs at 500 and 600 °C of AM alloy annealed at 1050 °C. Numbers are nominal stresses in MPa. Test conducted under 100 MPa is interrupted.

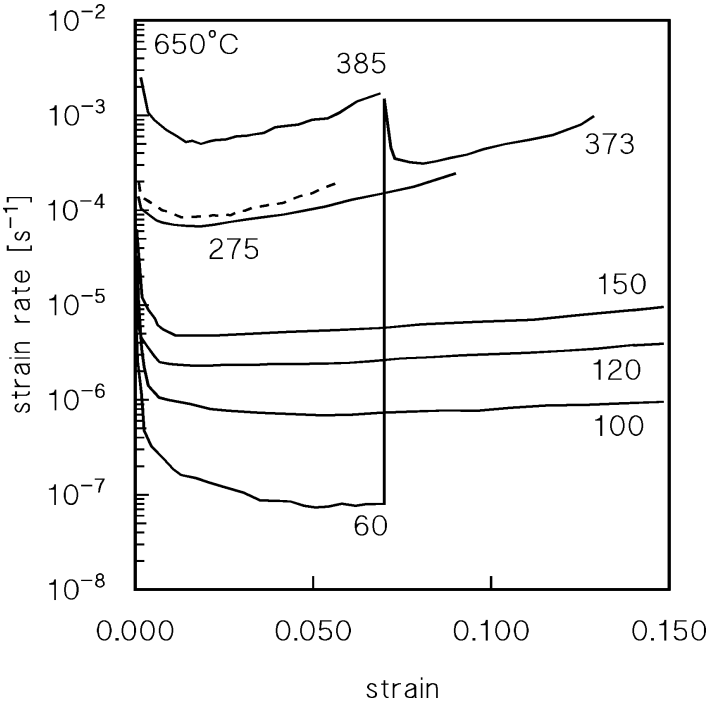

Figure 5. Representative strain rate verses strain creep curves from CLEs and VLEs at 650 °C of AM alloy annealed at 1050 °C [9]. Numbers are nominal stresses in MPa. Broken line corresponds to test conducted under 275 MPa after 145 h annealing prior to loading.

Figure 6 shows the minimum strain rate as a function of the applied stress obtained from experimental curves; the data approximately align on straight lines with slopes 7, 5.2, and 4.8 at 500, 600, and 650 °C, respectively. The datum for the VLE at 500°C, under 225 MPa was omitted, since presumably the

minimum creep rate range was not reached. The other data from VLE experiments (open symbols) roughly align with CLE results, except in the case of the test at 500°C. As illustrated in Figure 4a, long exposure at high temperature under a low stress, seems to result in a moderate hardening of the alloy, possibly due to a limited Ti_3Al precipitation. Yet, this effect will be here neglected, since the deviation between CLE and VLE data is fairly negligible. The data displayed in Figure 6 cover over three orders of magnitude of strain rates, and do not present a large scatter; therefore, they present an excellent basis for the search of a reliable constitutive model.

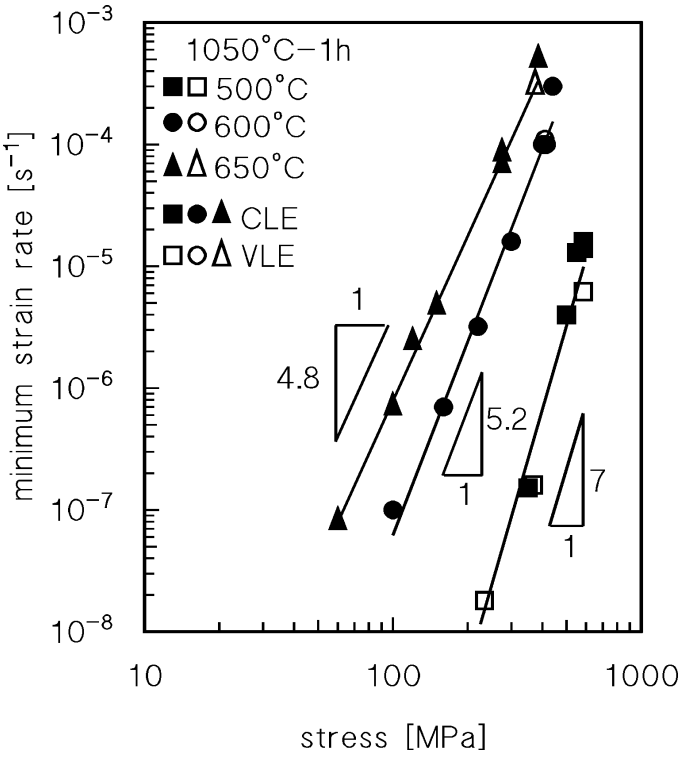

Figure 6. Minimum creep rate as function of applied (nominal) stress.

Figure 7a shows the data obtained in the present study and the literature data on alloys with Widmanstätten structures [3–8] produced by traditional technologies. The data obtained in this study cross the ‘cloud’ of the literature data. The drastic scatter of the latter causes occasionally a substantial deviation between the solid (this study) and open (literature) data points.

Figure 7b presents a comparison of the minimum creep rate measured in this study and those reported for the AM alloy annealed at 740 °C in [2]. As already noted in [9], compared to annealing at 740 °C,

annealing at 1050 °C results in lower creep rates in the entire investigated stress and temperature ranges; however, the difference progressively vanishes in the high-stress regime.

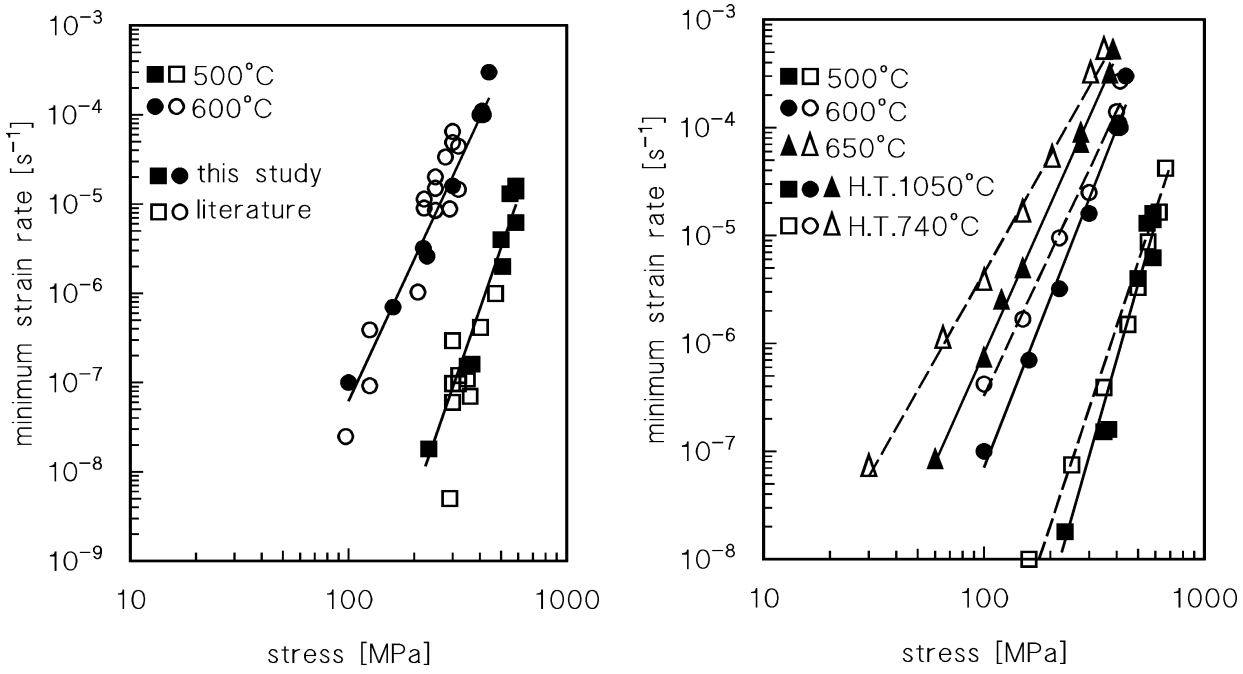

Figure 7. Comparison of data obtained in present study by testing AM alloy annealed at 1050 °C with a) literature data of traditionally processed Ti–6Al–4V with Widmanstätten microstructure [3–8] and b) data of same alloy produced by additive manufacturing and annealed at 740 °C [2]. Squares, circles and triangles represent tests carried out at 500, 600 or 650°C respectively. Open symbols represent literature data in a), and creep results obtained by testing the alloy of the present study after annealing at 740°C in b).

3.3 Hardness after high-temperature exposure

Figure 8 shows the HRC measurement results of the heads of crept samples. The data approximately present curves typical of age-hardening materials. Although this behaviour does not necessarily fully represent the phenomena occurring in the gauge lengths, where the dislocation activity significantly affects the microstructural evolution, it can be considered of interest for the description of the present model. At 500 °C, the hardness increases above 200 h of exposure, a possible indication of α_2-Ti_3Al precipitation. At 600 and 650 °C, the hardness decreases for the sample heads after a long time of exposure. At 650 °C, the hardness continuously reduces with the time of creep exposure. Because the dislocation activity considerably alters the microstructural evolution in the gauge length, the hardness trend showed in Figure 8 cannot be used to qualitatively predict the creep response of the alloy.

However, the results in Figure 8 remain significant as they show that the alloy is unstable at high temperatures. Permanence at high temperatures causes a moderate variation in the properties of the alloy.

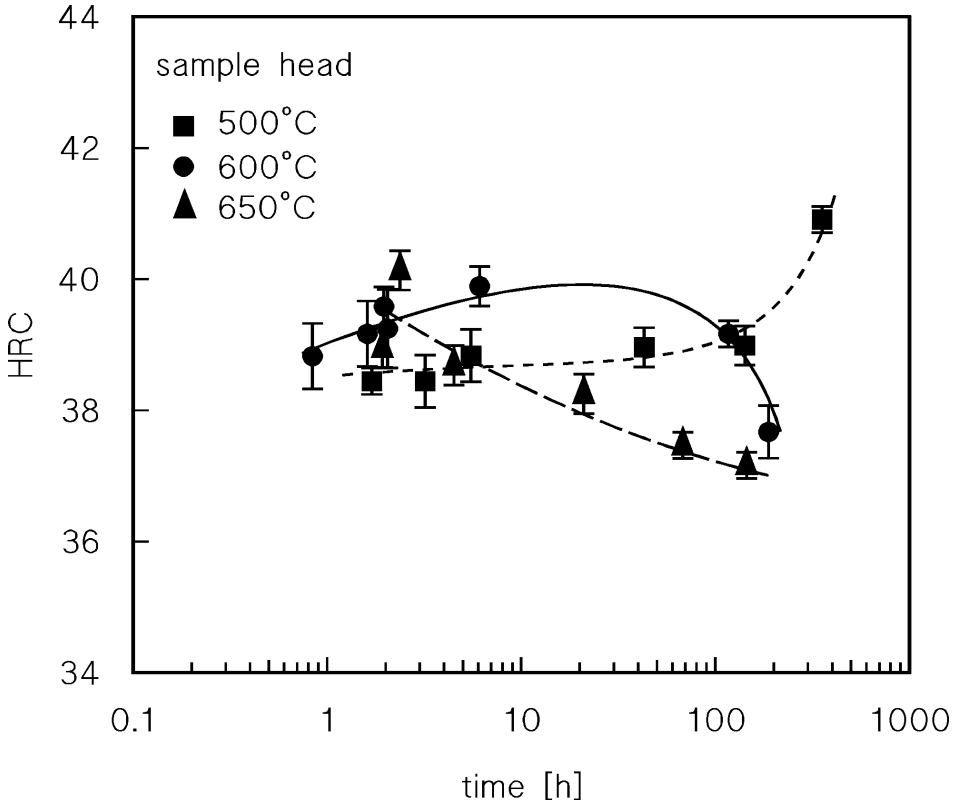

Figure 8. HRC hardness measured on crept sample heads.

3.4 Microstructure after creep experiments

Figures 9–11 show the microstructures of the crept samples observed using SEM and TEM. The most straightforward finding of the analysis shown in Figure 9 is the fragmentation of the β-lamellae at 650 °C. The micrographs obtained by TEM are more relatively interesting (Figures 10 and 11). They reveal that the microstructure of the alloy crept at 500 °C under an initial stress of 225 MPa (VLE in Figure 4a, at high-temperature exposure for 355 h) is still characterised by diffused long and thin β-lamellae (Figure 10a). Their thickness is approximately four times lower than those of the α-lamellae. Within the α-phase, the precipitation of α_2-Ti_3Al is evident (Figure 10b). This precipitated phase exists in the form of both long precipitates and much smaller cube-shaped particles, as presented in Figures 10b and

10c, respectively. The long particles have an average length of 450–480 nm and an average width of 55–60 nm, whereas the square-shaped particles are 180 nm in size. The dislocations bow around these particles, indicating a remarkable strengthening effect due to the dislocation–particle interactions (Orowan bowing and/or climbing above the particles). The formation of the α_2-Ti_3Al phase, as also reported by other studies (see [11]), is expected, because the testing temperature is in the range where its precipitation is probable. The crystallographic relationship between the α_2 and α-phases is found to be was α_2-$[01\bar{1}1] \parallel \alpha$-$[01\bar{1}1]$, as shown in the insets of Figures 10b and c.

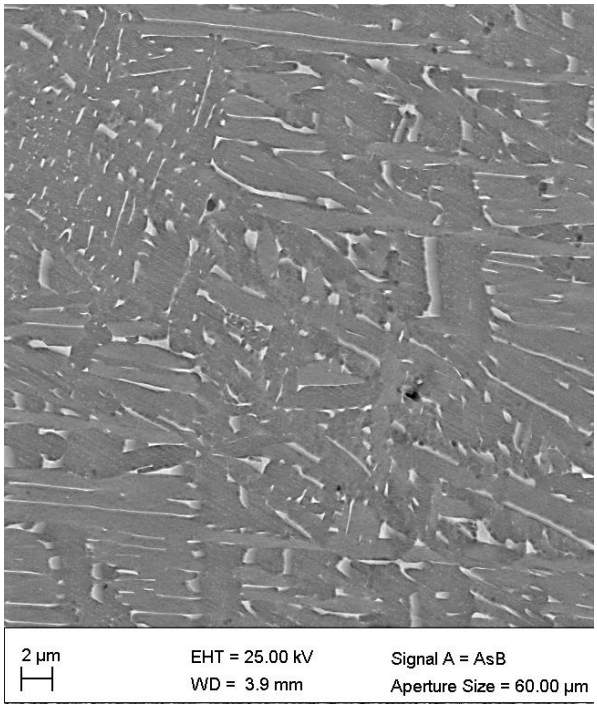

Figure 9. SEM micrograph of the sample tested at 650 °C/275 MPa, where α is the darker region and β the bright needle-like structure.

The distinctive microstructural feature is the β-lamellae fragmentation phenomenon, as shown in Figure 10d. It is activated by long holding times at high temperatures, as noticeable in Figures 9 and 10d, and has been described in other studies [10]. The dislocation activity due to creep straining is ultimately responsible for the progressive β-lamellae fragmentation.

The lamellar microstructure of the alloy crept at 650 °C under an initial stress of 60 MPa (VLE in Figure 5, total exposure time of 187 h) is shown in Figure 11. In particular, in the α-phase, dislocation sliding primarily occurs along $\boldsymbol{g}$ = *(0002*) and $\boldsymbol{g}$ = $(0\bar{1}10)$ [13], as shown in Figure 11b. These two sliding directions form a local network of dislocations. Similar results have been reported by Li *et al.* [11].

Occasionally, α'-martensite colonies are still observed. Dislocation accumulation occurs in the α′ to α lath interfacial region owing to local strain accommodation followed by both β to α and β to α′-phase transformations. Stacking faults (SFs) are formed in the α-lamellar structures, which was also reported by Li et al. [11] and Su et al. [14].

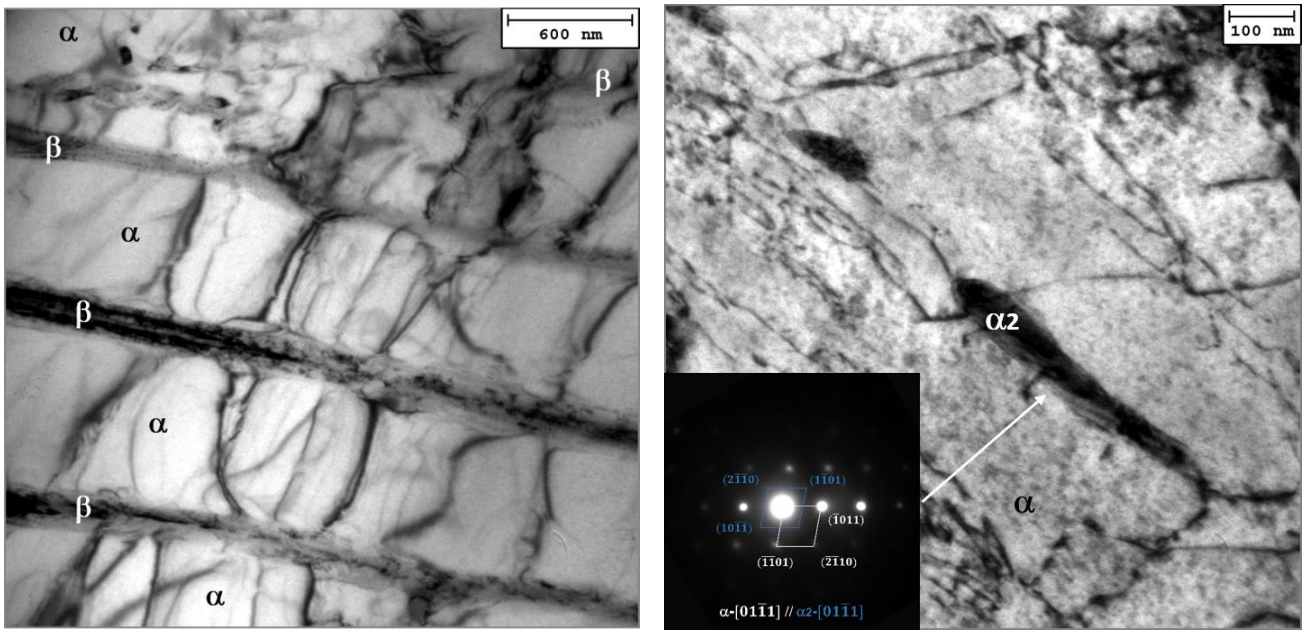

(a) (b)

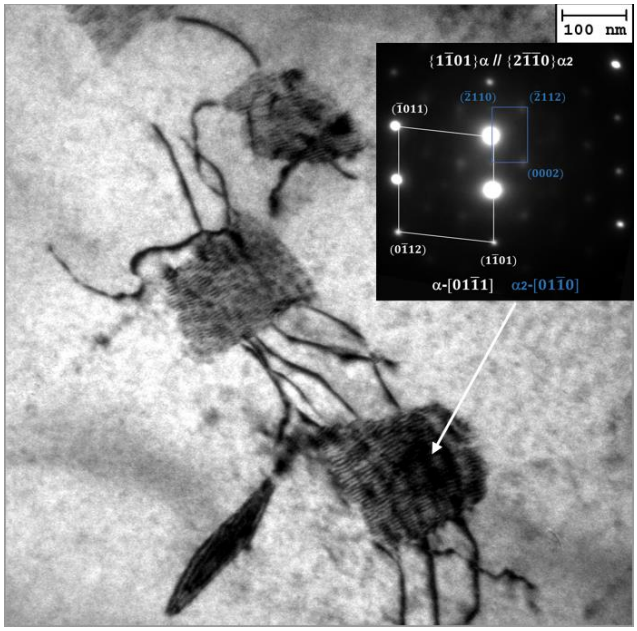

(c)

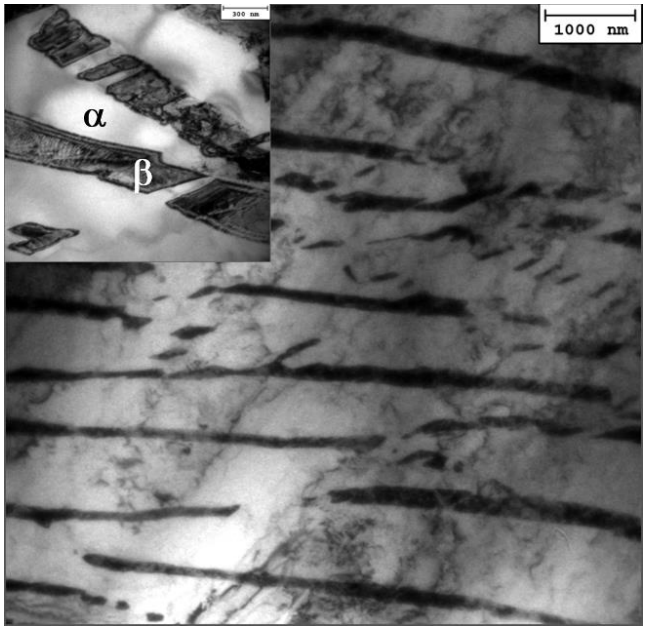

(d)

Figure 10. TEM micrographs of the VLE samples tested at 500 °C under an initial stress of 225 MPa crept sample showing (a) alloy α–β lamellar microstructure, α_2-Ti_3Al phase formation with long-thin morphology (b), and small particles with square morphology (c), and (d) β-lamellae fragmentation. Insets of (b) and (c) show SAEDPs of α_2-Ti_3Al; inset of (d) show details of some fragmented β-lamella.

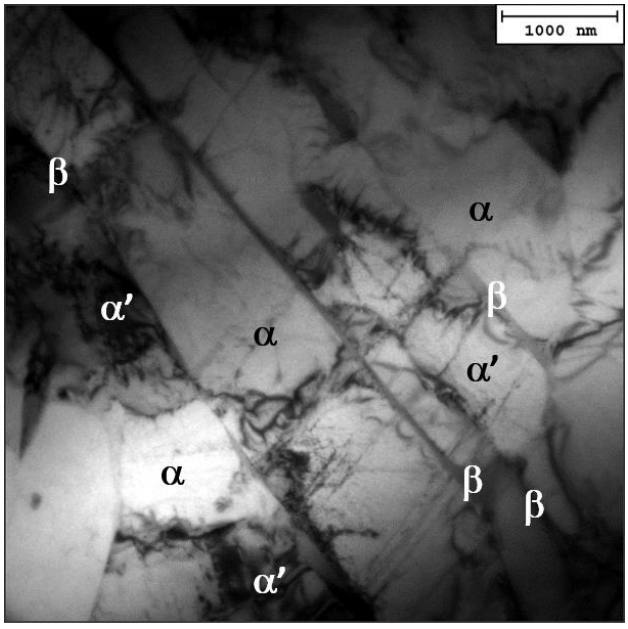

(a)

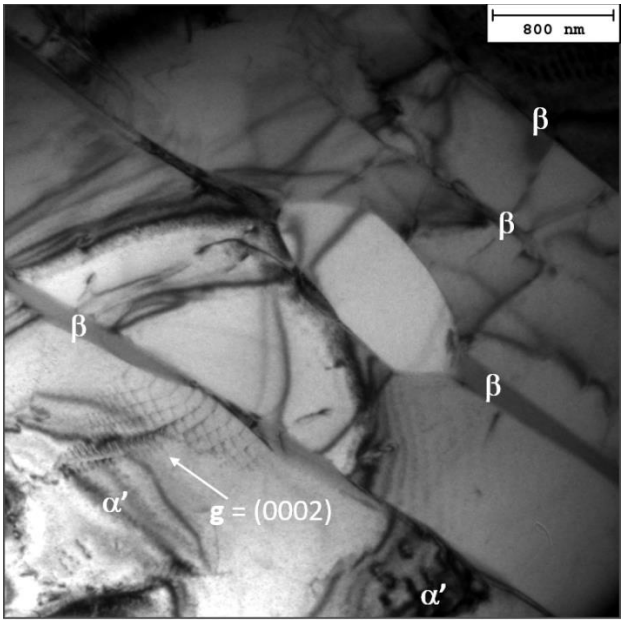

(b)

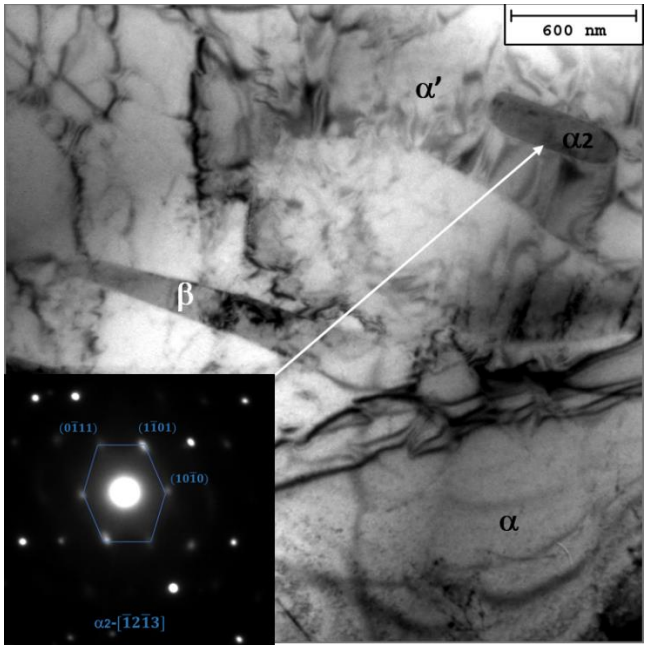

(c)

Figure 11. TEM micrographs of VLE sample tested at 650 °C under initial stress of 60 MPa, showing (a) α–β lamellar morphology, (b) tangled dislocations with wave-like sliding interactions, and (c) α_2-Ti_3Al phase and related indexed SAEDP (inset).

The presence of quite coarse α_2-Ti_3Al particles is also observed in the sample crept at 650 °C (Figure 11c). The Ti_3Al particles are ovoid in shape (120–150 nm in width and 600–800 nm in length). The crystallographic relationship between the α_2 and α phases was found to be α_2-$[2\bar{1}\bar{1}0]$ // α-$[2\bar{1}\bar{1}0]$ with α_2-$(0\bar{1}11)$ // α-(0001) crystallographic direction.

A quantitative evaluation of the β, α′, α_2, and α-phases in the samples annealed at 1050 °C and crept at 500 °C/60 MPa and 650 °C/225 MPa is reported in Table I.

Table I. Volume fractions (% vol.) of β, α′, α_2, and α-phases in VLE samples crept at 650 °C/60 MPa (initial stress) and 500 °C/225 MPa.

crept sample	β	α’	α_2	α
500 °C and 225/577/233/368 MPa	~12.0	~2	~0.15	bal.
650 °C and 60/373 MPa	~9.5	~1	~0.08	bal.

4. Discussion

4.1 Microstructural features of annealed Ti–6Al–4V produced by AM: context

Section 3 provides interesting information on the creep response of the AM Ti–6Al–4V alloy annealed at 1050 °C and the microstructures of the crept samples. The better creep response of the alloy annealed at 1050 °C than that of the alloy annealed at 740 °C is evident. Any rationalisation of this difference in the creep response should be based on a comparative analysis of the microstructural features.

It is widely known that the α–β phase transformation of a Ti–6Al–4V alloy strongly depends on the annealing temperature and the cooling rate. The equiaxed microstructure, obtained for example by a long annealing (6 h) at 850 °C followed by air cooling [3], consists primarily of α-grains surrounded by a much smaller volume fraction of finer β-grains. The duplex microstructure is characterised by the co-presence of equiaxed α- and lamellar α + β-grains. For example, colonies of α-lamellae, with an inter-lamellar small fraction of a retained vanadium-rich β-phase, form with equiaxed α-grains after annealing at 950 °C for 2 h, followed by air cooling to 700 °C [3]. Finally, annealing above the β-transus temperature followed by cooling at a relatively high cooling rate promotes the formation of a fine Widmanstätten structure.

The abovementioned microstructural evolution with thermal history is important as it considerably affects the mechanical properties, particularly at room temperature [15–17]. This is particularly for AM Ti–6Al–4V alloys [18]. During the additive manufacturing process, cooling rates can be as high as 10^6 °C/s [18]. Such cooling rates inhibit the complete α–β phase transition, and the bcc β-phase decomposes by martensitic diffusionless transformation, leading to the formation of α′-martensite in the as-synthesised condition. The α’-martensite forms as fine needles and has a high dislocation density. The co-presence of α-grains, α′-needles, and a possible small volume fraction of intergranular β-lamellae is the cause of the strong microstructural anisotropy. The size and morphology of the α′-martensite and its crystallographic orientation, which is closely related to the prior β-grain orientations, affect the

room-temperature mechanical properties of the AM alloy. The presence of α′-martensite in AM Ti–6Al–4V alloys results in high strength and poor ductility. Thus, post-processing heat treatments are needed to increase the ductility, inducing simultaneously a slight reduction in the alloy yield strength. To completely decompose α'-martensite to achieve a significant ductility improvement, the heating temperature should reach 800 °C for a typical minimum duration of 6 h [18–22].

4.2 Microstructure of Ti–6Al–4V during creep exposure: recalling effect of annealing at 740 °C

The findings obtained by TEM analysis of the sample crept after annealing at 740 °C in [2] are recalled for completeness. Additional micrographs are also discussed in this section to provide a sound basis for a reasonable interpretation of the material behaviour after annealing at 1050 °C.

Significant microstructural differences between the samples tested at 500 °C and 160/667 MPa (VLE) and those crept at 600 and 650 °C under 100 MPa (CLE) were observed in [2]. In particular, the microstructure of the sample tested at 500 °C after 476 h still showed a noticeable amount of α′-martensite in the α-grains. The volume fraction of the α-grains containing α′-martensite accounted for approximately 25 % volume. In fact, the α′-phase still present in these grains was only a small fraction of the grain volume; hence, the total amount of α′-martensite did not exceed 8–10 %. α′-martensite nucleated in the form of fine acicular structures at the prior β-grain boundaries, from which it grew within the α-grains being formed during rapid cooling by the SLM. The typical spatial configuration of different individual α′-colonies mostly consisted of chessboard structures. Both the α and α′-phases had the same hcp crystallographic structure with minimal lattice differences. In contrast, the chessboard structures were observed to have a fixed crystallographic orientation relationship with the hosting α phase, being approximately ±45° with respect to α. Crystallographic relationships between the different detected phases were determined using SAEDPs (Figure 12).

The material crept under a low load, e.g., σ = 100 MPa, and a high temperature, e.g., 600 and 650 °C, contained an extremely small fraction of α′-martensite colonies in the α-phase and a small fraction of the β-phase (Figure 12b). In contrast, some traces of the β-phase (3 % by volume) were also detected

in the sample tested at 500 °C. For clarity, the volume fractions of the β, α, and α′-phases in the three samples are listed in Table II.

Table II. Volume fractions (% vol.) of β, α, and α′ phases in VLE500, CLE600, and CLE650 samples.

Creep sample	β	α′	α
500 °C and 160/667 MPa	~3	~8	bal.
600 °C and 100 MPa	~4	<1	bal.
650 °C and 100 MPa	~8	<1	bal.

The reported amounts of the β-phase were not significantly different from those in the initial uncrept condition, being of a mean volume fraction of beta of 4 ± 1 %. The creep exposure did not considerably change the amount of the β-phase in the alloy. Regarding the size of the detected β-platelets, the typical lateral width (thickness) was 20 ± 4 nm, irrespective of the creep condition.

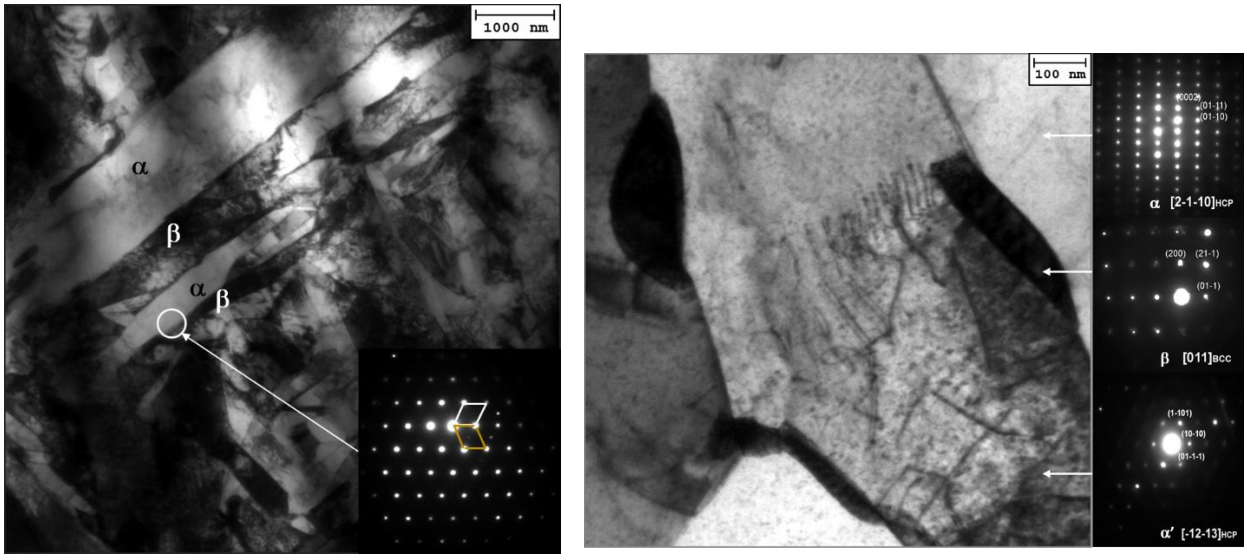

(a) (b)

Figure 12. Representative TEM microstructure of SLM-alloy after creep experiments: a) 500 °C and 160/667 MPa and b) 600 °C and 100 MPa. Insets of (b) show indexed SAEDPs of α, β, and α′ phases.

The experimental results showed that transformation of the retained α'-martensite occurred during creep exposure. Thus, it can be reasonably expected that higher exposure temperatures and longer

durations can induce a complete α′ to α-phase transformation [23]. Based on these observations, the minimum creep rate dependence on applied stress is primarily governed by the deformation of the α-phase, which accounts for approximately 90 % of the overall alloy structure.

4.3 Summary of possible roles of different phases in creep response

The results presented in this study allow to draw some important qualitative inferences on the possible roles of the different phases in the creep response of the studied Ti–6Al–4V alloy. These, as well as some of the conclusions obtained in the previous study on the material annealed at 740°C, are summarised as follows.

i. The creep responses of Ti–6Al–4V alloys with equiaxed and duplex microstructures can be described by the same set of constitutive relationships (Equations (1)–(4)), the only significant difference being the value of the UTS (see Appendix 3 for further details). For the former, the microstructure consists of equiaxed α-grains, with a relatively much lower volume fraction of β-grains decorating the α-grain boundaries. In contrast, the duplex structure consists of equiaxed α- and lamellar α–β grains. In both equiaxed and duplex materials, the α-phase is predominant, and they show similar creep responses. It is reasonable to conclude that the β-phase, present in remote grains or coarse lamellae, plays a minor role. When creep is controlled by the dislocation activity in the α-phase, the α–β interfaces could possibly act as a strengthening source; however, the distance between these interfaces is too long for this mechanism to be effective.

ii. The creep response of the AM alloy annealed at 740 °C was shown to obey to the same constitutive equations [2] Equations (1)–(4), provided that the correct value of the UTS was used. In this case, the microstructure comprised approximately 90 % α-phase and small amounts of the β and α′-phases. This picture is fully consistent with the conclusion that creep is controlled by the dislocation activity in the α-phase, and the presence of relatively sparse widely spaced β-particles plays virtually no role.

iii. The volume fraction of the β-phase in the material annealed at 1050 °C was higher than that in the alloy annealed at 740 °C. The β-phase volume fraction in the material annealed at 1050 °C was similar to that in the equiaxed and duplex alloys. A distinctive feature was the *bcc* phase, which here formed finely spaced lamellae. β-lamellae fragmentation occurred for long creep exposures at high temperatures following the initial annealing at 1050 °C. For the samples annealed at 740 °C, the β-phase did not form long lamellae as under the heat treatment at 1050 °C. The UTS after annealing was similar to those of the equiaxed and duplex microstructures; therefore, the use of Equations (1)–(4) yields the same curves. However, the observed minimum creep rates were significantly lower for the former. Thus, the two most important features of the microstructure that could play a role in this behaviour are the fine spacing (a few hundreds of nanometres) of the β-phase lamellae and the presence of α_2-particles.

The findings summarised in this section suggest that modifying Equation (1)–(4) is necessary to describe the creep response of the alloy annealed at 1050 °C. Accordingly, the approach proposed by Barboza et al. [7], who introduced a threshold stress σ_0 (slightly ambiguous in nature) in the traditional Norton power-law equation describing the minimum creep rate dependence on temperature and stress, was tentatively used in [9]. This procedure simply involves substituting Equation (3) with

$$\sigma = \sigma_\rho + \sigma_{ss} + \sigma_0 = \sigma_\rho + \delta(\sigma - \sigma_0) + \sigma_0 \qquad (5)$$

Understandably, this is an approach of a phenomenological nature; however, it seems reasonable. In a first instance, suppose that the effect of α_2-particles can be neglected. In this case, the α–β interfaces could act as effective barriers for dislocation motion, and the strengthening mechanism could be quantified by σ_0. The effectiveness of these barriers depends on their spacing L. This behaviour can be tentatively described by an equation in the form,

$$\sigma_0 \propto \left(\frac{MGb}{L}\right)^p, \qquad (6)$$

where p is a constant. Thus, $\sigma_0 \cong 0$ in the equiaxed microstructure, where spacing L between the interfaces equals the α-grain size. Similarly, $\sigma_0 \cong 0$ in all cases in which the spacing is large, i.e., measurable on the micron scale (e.g., in lamellar grains where the α-lamellae are coarse).

The above scenario is likely to differ when the alloy is annealed above the β-transus temperature. In the latter case, the β-phase appears in the form of more closely spaced lamellae. As long as the spacing of the β-particles remains low, fragmentation of the lamellae does not necessarily significantly impair the alloy strengthening effect. This strengthening effect can be described by a threshold stress $\sigma_0 \neq 0$. Additional α_2 precipitation, which introduces a typical particle-strengthening effect, also affects the magnitude of the threshold stress. This effect can compensate the softening effect, if any, due to the lamellae fragmentation.

Owing to the microstructural complexity described herein and limited physical models describing the strengthening effect of α–β interfaces and experimental information about the L-magnitude in crept materials, a quantitative correlation between microstructural features and σ_0 is presently impossible. Therefore, σ_0/G was calculated at a single temperature by fitting the experimental data. In particular, the preliminary results at 650 °C obtained in [9] were used as the basis for the analysis. In addition, first, it was arbitrarily assumed that σ_0/G did not change significantly with temperature. The other parameters for the calculation were the same as those used for the other Ti–6A–-4V alloy considered in [2]: Q_L = 303 kJ mol^{-1}, $D_0 = 1.4 \times 10^{-3}$ m^{2}s^{-1}, A = 40, and δ = 0.4. The UTS was assumed to be 1000 MPa, i.e., a value slightly higher than that obtained experimentally, to account for the strength reduction due to the surface being in the as-deposited state. In this regard, Figure 13 shows the experimental data for the alloys annealed at 740 °C and 1050 °C and the model curves obtained with the same parameters but σ_0/G = 0 and 1.19×10^{-3}, respectively. The correlation between the experimental and model results is good, except in the very high-strain rate region, where the model overestimates the strain rate. This deviation can be partly attributed to the underestimation of the UTS,

in particularly at 500 °C, where a limited precipitation of the α_2-particles slightly increases the tensile strength.

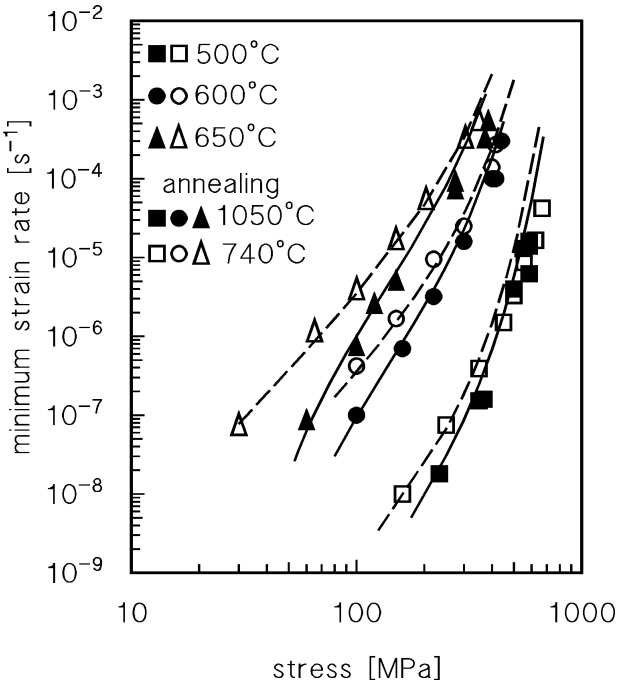

Figure 13. Experimental minimum creep rates for AM alloys annealed at 740 and 1050 °C and model curves with $\sigma_0/G = 0$ and 1.19×10^{-3}, respectively. Squares, circles and triangles represent tests carried out at 500, 600 or 650°C respectively. Open symbols represent creep results obtained by testing the alloy of the present study after annealing at 740°C.

Based on Figure 13, the original concept of Barboza et al., i.e., the difference in creep behaviour can be described by introducing a threshold stress, provides a good phenomenological description of the creep response of the alloy with a Widmanstätten structure. The model can also rationalise the abnormal scatter observed in the literature creep data for alloys with such microstructures. The finesse of the Widmanstätten structure, i.e., the distance between the α–β interfaces, directly depends on the heat-treatment parameters (temperature, duration of annealing, and cooling rate). The distance between the α–β interfaces, in turn, determines the magnitude of the threshold stress. Furthermore, different amounts of the α_2-phase could be present in each case owing to the different thermal histories. Thus, the scatter among the creep data obtained by testing various batches of alloys annealed above the β-

transus temperature, in this context, can be easily explained by simply introducing small differences in the β- and α_2-phase volume fractions and distributions. This is a result of the heat-treatment processing parameters.

Figure 14 shows a representative case study. The curves obtained by combining Equations (1), (2), (4) and (5) with the same parameters used for Figure 13 and $\sigma_0/G = 2.0 \times 10^{-3}$ are compared with the experimental data from [7]. For six out of eight data points, the description is excellent. A deviation is observed only for a long time of exposure at 500 °C, i.e., in conditions where additional precipitation of the α_2-phase can be problematic. The model curve correctly estimates the minimum strain rate under 291 MPa at 500 °C with $\sigma_0/G = 4.85 \times 10^{-3}$. Thus, the model is correct, i.e., the microstructure undergoes considerable strengthening due to a reduction in L, presumably due to α_2-precipitation, during creep exposure.

Figure 14 shows speculative results because of the lack of experimental data on important features such as β- and α_2-phase volume fractions and distributions (i.e., on L) of that material. However, the threshold stress calculation in most creep studies was conducted by similar fitting procedures (see two examples in [24, 25]), which were typically not calculated by physical models of the dislocation/particle interaction. Thus, if it Figure 14 needs to be validated by microstructural studies, it unambiguously demonstrates that the proposed model is, in principle, appropriate for describing the creep response of the alloy annealed above the β-transus temperature.

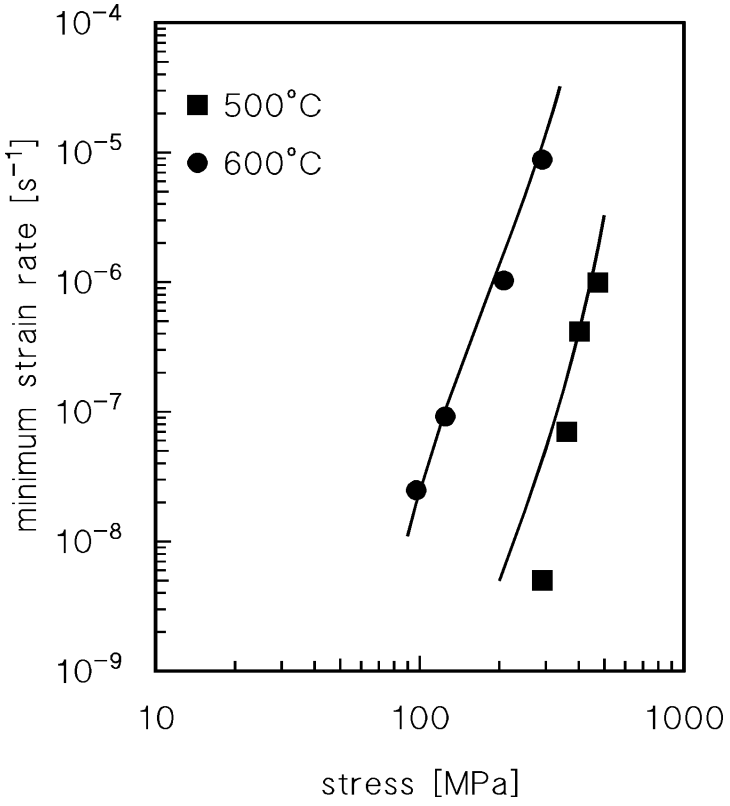

Figure 14. Model curves obtained with $\sigma_0/G = 2.0 \times 10^{-3}$ and experimental data from [7].

5. Conclusion

The creep responses of an AM Ti–6Al–4V alloy and annealed at 1050 °C were investigated at 500, 600, and 650 °C. The main findings of this study can be summarised as follows.

i. The alloy with a Widmanstätten microstructure typical of an alloy annealed above the β-transus temperature presented minimum creep rates lower than those of the same material annealed at lower temperatures.

ii. At a fine scale, the microstructure of the alloy annealed at 1050 °C, was characterised by the presence of finely spaced β-lamellae, which during creep exposure progressively underwent fragmentation. Nevertheless, at least for the relatively short durations investigated in the present study, the fragmented β-lamellae still formed a distribution of finely spaced particles.

iii. The presence of α_2-Ti_3Al particles was evident in all investigated microstructures, even at 650 °C, a temperature at which the presence of this phase is largely unexpected.

iv. The creep response of the alloy annealed at 1050 °C could be quantitatively described by introducing a threshold stress σ_0 in constitutive equations. These equations were previously used to analyse the creep responses of Ti–6Al–4V with equiaxed and duplex microstructures and the same alloy produced by additive manufacturing and annealed at 740 °C. This threshold stress can be considered as a quantification term for the strengthening role of both the α–β interfaces and α_2 particles. An excellent description could be obtained with a constant value of σ_0/G at the different temperatures, which suggests that the same hardening effect dominates between 500 and 650 °C.

v. For equiaxed, duplex, and annealed SLM-alloys, $\sigma_0/G = 0$ possibly suggests that the distance between the α–β interfaces is extremely long to be effective. This conclusion was supported by the experimental evidence obtained by studying the microstructure of the SLM-alloy annealed at 740 °C.

Appendix 1

The model discussed in this paper was originally developed for cfc metals. The starting point was the formulation of the evolution of the dislocation density (ρ) during straining expressed in simplified form, as [26,27]

$$\frac{d\rho}{d\varepsilon} = \frac{m}{bL^*} - \frac{2}{\dot{\varepsilon}} M\tau_l \rho^2 \qquad \text{(A1)}$$

where τ_l is the dislocation line tension (τ_l=0.5Gb^2), M is the dislocation mobility and L^* is the dislocation mean free path (distance travelled by a dislocation before it undergoes a reaction) expressed, as

$$L^* = \frac{C_L}{\sqrt{\rho}} \qquad \text{(A2)}$$

Combination of Eqns. (A1) and (A2) gives

$$\frac{d\rho}{d\varepsilon} = \frac{m\sqrt{\rho}}{bC_L} - \frac{2}{\dot{\varepsilon}} M\tau_l \rho^2 \quad \text{(A3)}$$

The second term of the right-hand part of Eqn.(A3) is strongly temperature-dependent through the dislocation mobility term *M*, which can be written as [28-30]

$$M = \frac{D_0 b}{kT} exp\left(\frac{\sigma_\rho b^3}{kT}\right) exp\left\{-\frac{Q_L}{RT}\left[1 - \left(\frac{\sigma_\rho}{R_{max}}\right)^2\right]\right\} \quad \text{(A4)}$$

where R_{max} is the maximum strength of the material. Equation (A4), at steady state, when dislocation density is constant, combined with Eqn. (A1), gives

$$\dot{\varepsilon}_m = \frac{2\tau_l D_0 b^2 C_L}{mkT}\left(\frac{\sigma_\rho}{\alpha m G b}\right)^3 exp\left(\frac{\sigma_\rho b^3}{kT}\right) exp\left\{-\frac{Q_L}{RT}\left[1 - \left(\frac{\sigma_\rho}{R_{max}}\right)^2\right]\right\} \quad \text{(A5)}$$

or

$$\dot{\varepsilon}_m = A\frac{D_0 G b}{kT}\left(\frac{\sigma_\rho}{G}\right)^3 exp\left(\frac{\sigma_\rho b^3}{kT}\right) exp\left\{-\frac{Q_L}{RT}\left[1 - \left(\frac{\sigma_\rho}{R_{max}}\right)^2\right]\right\} \quad \text{(A6)}$$

being

$$A = \frac{C_L}{\alpha^3 m^4} \quad \text{(A7)}$$

Interestingly enough, for pure Al, where C_L=85, α=0.3 and m=3.06 [31], A=35.9. This value is very close to A=40 here used for Ti (m values close to 3 have been indeed predicted [32]).

Appendix 2

Combination of Eqns.(1) - (4) can be used to obtain the model curves describing the minimum creep rate as a function of stress and temperature, by using as input datum only the value of the UTS. This procedure was described in detail in [2]. This appendix just presents few examples of the resulting description. For all these curves, Q_L = 303 kJ mol^{-1}, D_0 = 1.4 × 10^{-3} m^{2}s^{-1}, A = 40, and δ = 0.4. UTS

values from [3]. The typical scatter of the available experimental data can be easily appreciated in b). As a whole, if one takes into account that no fitting was required, the description is excellent, except than for the alloys with fully lamellar structure, characterized by an enormous dispersion of the data.

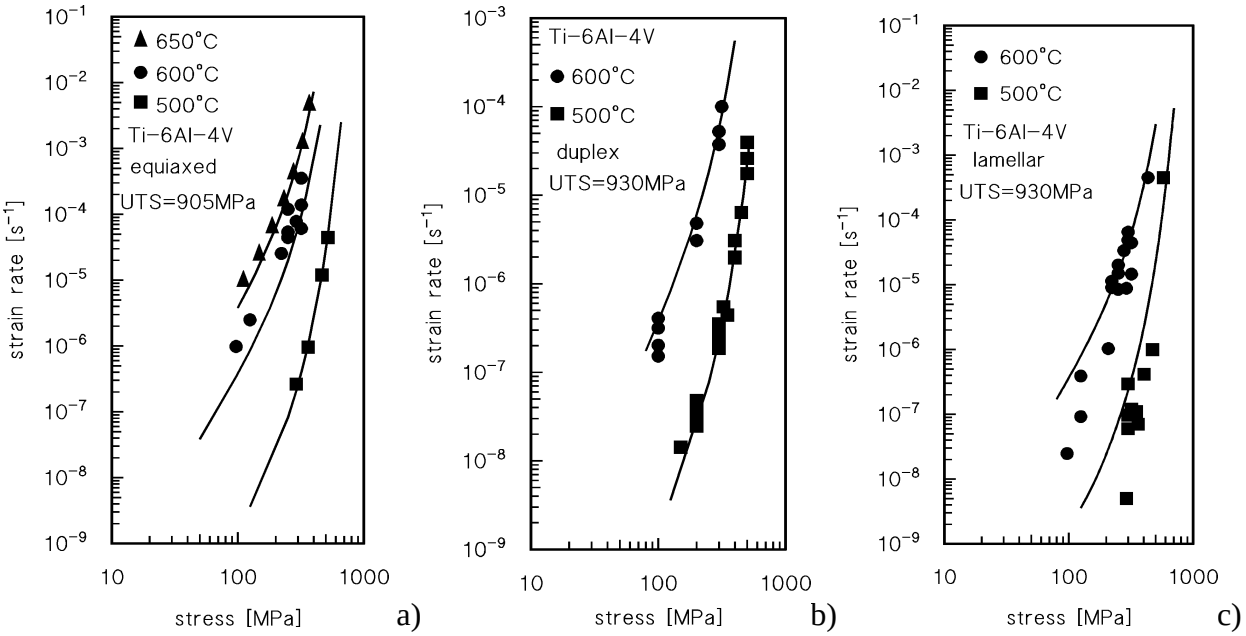

Figure A2.1. Model curves from Eqns.(1) - (4). The equations did not contain free-parameters, the only required input being the UTS. The Figures illustrates: a) alloys with fully equiaxed α-grains, data from [33-37]; b) alloys with duplex microstructure (equiaxed and lamellar grains), data from [38,39]; c) data for alloys with lamellar (Widmanstätten) microstructure, data from [3-8].

Acknowledgements

This research was partially funded by the Grant of Excellence Departments, MIUR-Italy (ARTICOLO 1, COMMI 314–337 LEGGE 232/2016).

Data availability

The raw/processed data required to reproduce these findings cannot be shared at this time as the data also forms part of an ongoing study.

References

1. S. Liu, Y.C. Shin, Additive manufacturing of Ti6Al4V alloy: A review, Mater. Des. 164 (2019) 107552. https://doi.org/10.1016/j.matdes.2018.107552.

2. S. Spigarelli, C. Paoletti, M. Cabibbo, E. Cerri, E. Santecchia. On the creep performance of the Ti-6Al-4V alloy processed by additive manufacturing. Additive Manufacturing 49 (2022) 102520https://doi.org/10.1016/j.addma.2021.102520

3. S. Nishino, K. Shiozawa, Y. Aikawa, Effect of microstructure on creep and creep-fatigue behavior in Ti-6Al-4V alloy at elevated temperature, Mater. Sci. Sci. Res. Int. 4 (1997) 206–211. https://doi.org/10.2472/jsms.46.512.

4. G.F.C. Almeida, A.A. Couto, D.A.P. Reis, M. Massi, A.S. da Silva Sobrinho, N.B. de Lima, Effect of plasma nitriding on the creep and tensile properties of the Ti-6Al-4V alloy, Metals (Basel). 8 (2018) 0618. https://doi.org/10.3390/met8080618.

5. V.M.C.A. De Oliveira, M.C.L. Da Silva, C.G. Pinto, P.A. Suzuki, J.P.B. Machado, V.M. Chad, M.J.R. Barboza, Short-term creep properties of Ti-6Al-4V alloy subjected to surface plasma carburizing process, J. Mater. Res. Technol. 4 (2015) 359–366. https://doi.org/10.1016/j.jmrt.2015.05.006.

6. T. Sugahara, D.A.P. Reis, C. Moura Neto, M.J.R. Barboza, E.A.C. Perez, F. Piorino Neto, A.C.O. Hirschmann, The effect of Widmanstätten and equiaxed microstructures of Ti-6Al-4V on the oxidation rate and creep behavior, in: Mater. Sci. Forum, 2010: pp. 636-637 657-662. https://doi.org/10.4028/www.scientific.net/MSF.636-637.657.

7. M.J.R. Barboza, E.A.C. Perez, M.M. Medeiros, D.A.P. Reis, M.C.A. Nono, F.P. Neto, C.R.M. Silva, Creep behavior of Ti-6Al-4V and a comparison with titanium matrix composites, Mater. Sci. Eng. A. A428 (2006) 319–326. https://doi.org/10.1016/j.msea.2006.05.089.

8. V.M.C.A. Oliveira, A.M. Vazquez, C. Aguiar, A. Robin, M.J.R. Barboza, Nitride coatings improve Ti-6Al-4V alloy behavior in creep tests, Mater. Sci. Eng. A670 (2016) 357–368. https://doi.org/10.1016/j.msea.2016.06.041.

9. C. Paoletti, M. Cabibbo, E. Santecchia, E. Cerri, S. Spigarelli, Effect of Post-Processing Heat Treatments on Short-Term Creep Response at 650 °C for a Ti-6Al-4V Alloy Produced by Additive Manufacturing, Metals 12 (2022) 1084.
https://doi.org/10.3390/met12071084

10. A. Nespoli, N. Bennato, E. Villa, F. Passaretti. Study of anisotropy through microscopy, internal friction and electrical resistivity measurements of Ti-6Al-4V samples fabricated by selective laser melting, Rapid Prototyping Journal (2022) 28.
https://doi.org/1060–1075. 10.1108/RPJ-06-2021-0151.

11. Xiao Li, Tian Sugui, Bao Xianyu, Chen Liqing, Creep properties and effect factors of hot continuous rolled Ti–6Al–4V alloy, Mater. Sci. Eng., A529 (2011) 452-458, ISSN 0921-5093, https://doi.org/10.1016/j.msea.2011.09.061.

12. M. Paghandeh, A. Zarei-Hanzaki, H.R. Abedi, Y. Vahidshad, On the warm temperature strain accommodation mechanisms of Ti–6Al–4V alloy holding different starting microstructures, J. Mater. Res. Technol., 14 (2021) 496-506.
https://doi.org/10.1016/j.jmrt.2021.06.077.

13. Ying Zhang, Dongsheng Li, Xiaoqiang Li, Xiaochun Liu, Shiteng Zhao, Yong Li, Creep deformation and strength evolution mechanisms of a Ti-6Al-4V alloy during stress relaxation at elevated temperatures from elastic to plastic loading, J. Mater. Sci. Technol 126 (2022) 93-105, https://doi.org/10.1016/j.jmst.2022.02.042.

14. Jinlong Su, Xiankun Ji, Jin Liu, Jie Teng, Fulin Jiang, Dingfa Fu, Hui Zhang, Revealing the decomposition mechanisms of dislocations and metastable α' phase and their effects on mechanical properties in a Ti-6Al-4V alloy, Journal of Materials Science & Technology, 107 (2022) 136-148, https://doi.org/10.1016/j.jmst.2021.07.048.

15. D.G. Lee, S. Kim, S. Lee, Chong Soo Lee, Effects of microstructural morphology on quasi-1static and dynamic deformation behavior of Ti-6AI-4V alloy, Metall. Mater. Trans. A Phys. Metall. Mater. Sci. 32A (2001) 315–324. https://doi.org/10.1007/s11661-001-0263-y.

16. J. Tiley, T. Searles, E. Lee, S. Kar, R. Banerjee, J.C. Russ, H.L. Fraser, Quantification of microstructural features in α/β titanium alloys, Mater. Sci. Eng. A. A372 (2004) 191–198. https://doi.org/10.1016/j.msea.2003.12.008.

17. R. Sahoo, B.B. Jha, T.K. Sahoo, Effect of Microstructure on the Creep Properties of Ti–6Al–4V Alloys: An Analysis, Trans. Indian Inst. Met. Met 71 (2018) 1573–1582. https://doi.org/10.1007/s12666-018-1292-1.

18. J. Yu, M. Rombouts, G. Maes, F. Motmans, Material Properties of Ti6Al4V Parts Produced by Laser Metal Deposition, Phys. Procedia. 39 (2012) 416–424. https://doi.org/https://doi.org/10.1016/j.phpro.2012.10.056.

19. B. Vrancken, L. Thijs, J.P. Kruth, J. Van Humbeeck, Heat treatment of Ti6Al4V produced by Selective Laser Melting: Microstructure and mechanical properties, J. Alloys Compd. (2012) 177–185. https://doi.org/10.1016/j.jallcom.2012.07.022.

20.C. Qiu, N.J.E. Adkins, M.M. Attallah, Microstructure and tensile properties of selectively laser-melted and of HIPed laser-melted Ti-6Al-4V, Mater. Sci. Eng. A. A578 (2013) 230–239. https://doi.org/10.1016/j.msea.2013.04.099.

21.T.M. Mower, M.J. Long, Mechanical behavior of additive manufactured, powder-bed laser-fused materials, Mater. Sci. Eng. A. A651 (2016) 198–213. https://doi.org/10.1016/j.msea.2015.10.068.

22.S. Liu, Y.C. Shin, Additive manufacturing of Ti6Al4V alloy: A review, Mater. Des. 164 (2019) 107552. https://doi.org/10.1016/j.matdes.2018.107552.

23. S. Cao, R. Chu, X. Zhou, K. Yang, Q. Jia, C.V.S. Lim, A. Huang, X. Wu, Role of martensite decomposition in tensile properties of selective laser melted Ti-6Al-4V, J. Alloys Compd. 744 (2018) 357–363.
https://doi.org/10.1016/j.jallcom.2018.02.111.

24. Y.Li, T.G.Langdon, A simple procedure for estimating threshold stresses in the creep of metal matrix composites, Scripta Mater 36 (1997) 1457-1460.
https://doi.org/10.1016/S1359-6462(97)00041-9

25.J.K. Benz, L.J. Carroll, J.K. Wright, R.N. Wright, T.M. Lillo. Threshold Stress Creep Behavior of Alloy 617 at Intermediate Temperatures, Metall Mater Trans 45A (2014) 3010-3022.
https://doi.org/10.1007/s11661-014-2244-y

26. R. Sandström, J. Hallgren, The role of creep in stress strain curves for copper, J Nucl Mater, 422 (2012) 51-57.
https://doi.org/10.1016/j.jnucmat.2011.12.012

27. R. Sandström, The role of cell structure during creep of cold worked copper, Mater. Sci. Eng. A. A, 674 (2016) 318-327.
https://doi.org/10.1016/j.msea.2016.08.004

28. J.P. Hirth, J. Lothe, Theory of Dislocations, Krieger, Malabar, Florida, 1982.

29. U.F.Kocks, A.S.Argon, M.F.Ashby, Thermodinamics and kinetics of slip, Prog.Mater.Sci 15 (1979) 1

30. R. Sandström, H.C.M. Andersson, Creep in phosphorus alloyed copper during power-law breakdown, J.Nucl. Mater. 372 (2008) 76-88.
https://doi.org/10.1016/j.jnucmat.2007.02.005

31. S. Spigarelli, R. Sandström. Basic creep modelling of Aluminum. Mater Sci Eng A, 711 (2018) 343-349.
https://doi.org/10.1016/j.msea.2017.11.053

32. S. Panda, S.K. Sahoo, A. Dash, M. Bagwan, G. Kumar, S.C. Mishra, S. Suwas. Orientation dependent mechanical properties of commercially pure (cp) titanium. Materials Characterization 98 (2014) 93–101.
http://dx.doi.org/10.1016/j.matchar.2014.10.011
33. E. Alabort, P. Kontis, D. Barba, K. Dragnevski, R.C. Reed, On the mechanisms of superplasticity in Ti-6Al-4V, Acta Mater. 105 (2016) 449–463.
https://doi.org/10.1016/j.actamat.2015.12.003.
34. D.A.P. Reis, C.R.M. Silva, M.C.A. Nono, M.J.R. Barboza, F. Piorino Neto, E.A.C. Perez, Effect of environment on the creep behavior of the Ti-6Al-4V alloy, Mater. Sci. Eng. A. A399 (2005) 276–280.
https://doi.org/10.1016/j.msea.2005.03.073.
35. A.G. dos Reis, D.A.P. Reis, C. de Moura Neto, M.J.R. Barboza, J. Oñoro, Creep behavior and surface characterization of a laser surface nitrided Ti-6Al-4V alloy, Mater. Sci. Eng. A. A577 (2013) 48–53.
https://doi.org/10.1016/j.msea.2013.04.042.
36. L.A.N.S. Briguente, A.A. Couto, N.M. Guimarães, D.A.P. Reis, C. Moura Neto, M.J.R. Barboza, Determination of creep parameters of Ti-6Al-4V with bimodal and equiaxed microstructure, in: Defect Diffus. Forum, 2012: pp. 326-328 520-524.
https://doi.org/10.4028/www.scientific.net/DDF.326-328.520.
37. M.J.R. Barboza, C. Moura Neto, C.R.M. Silva, Creep mechanisms and physical modeling for Ti-6Al-4V, Mater. Sci. Eng. A. A369 (2004) 201–209. https://doi.org/10.1016/j.msea.2003.11.016.
38. V.B. Badea Lavina, Surand Martin, Ruau Jacques, Creep behavior of Ti-6Al-4V from 450°C to 600°C., Univ. Polytech. Bucharest Sci. Bull. Ser. B. 76 (2014) 185–196. hal-01186469.
39. M.T. Whittaker, W.J. Harrison, R.J. Lancaster, S. Williams, An analysis of modern creep lifing methodologies in the titanium alloy Ti6-4, Mater. Sci. Eng. A. A577 (2013) 114–119.
https://doi.org/10.1016/j.msea.2013.03.030.

Figure 1

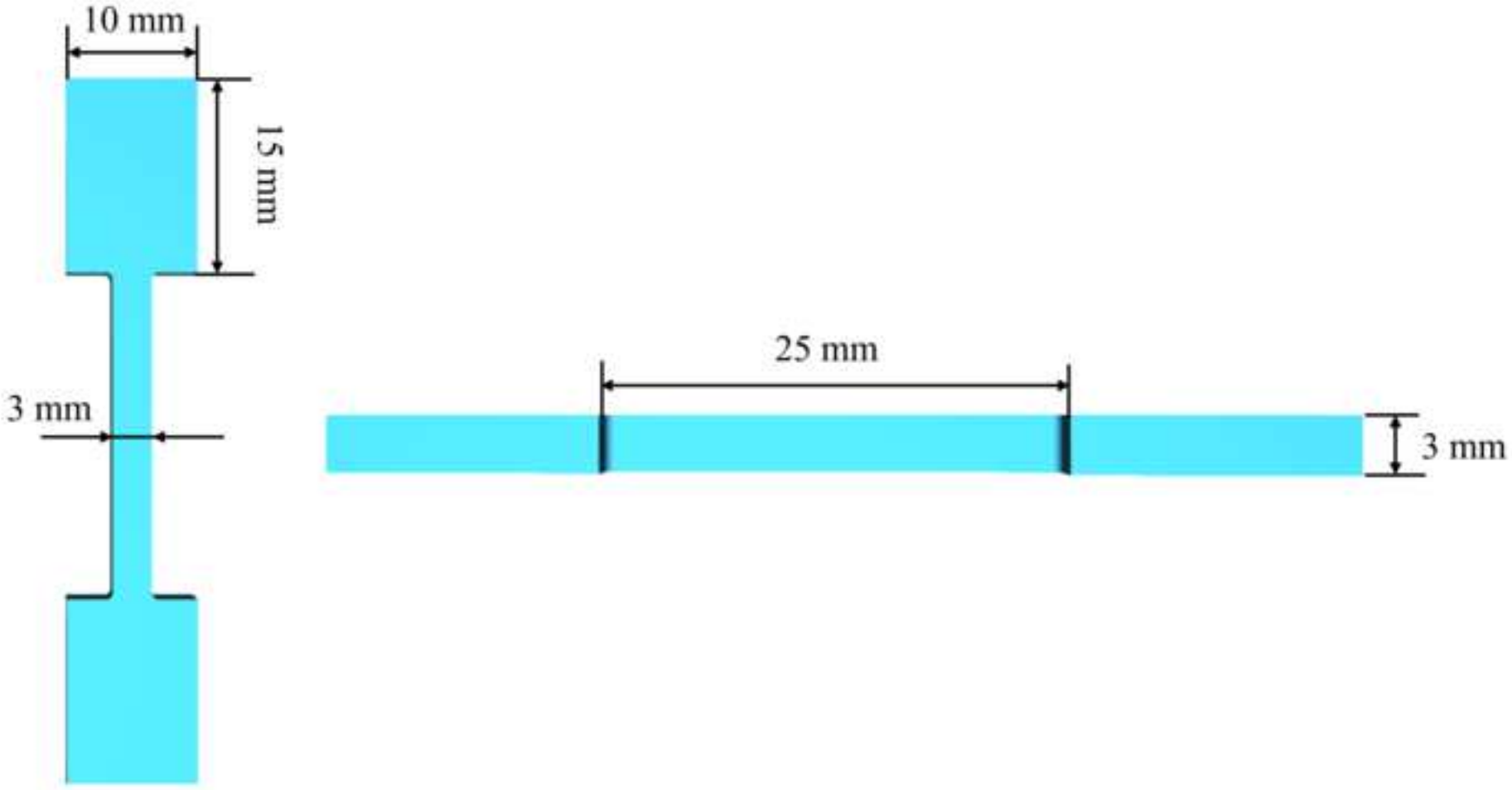

Figure 2a

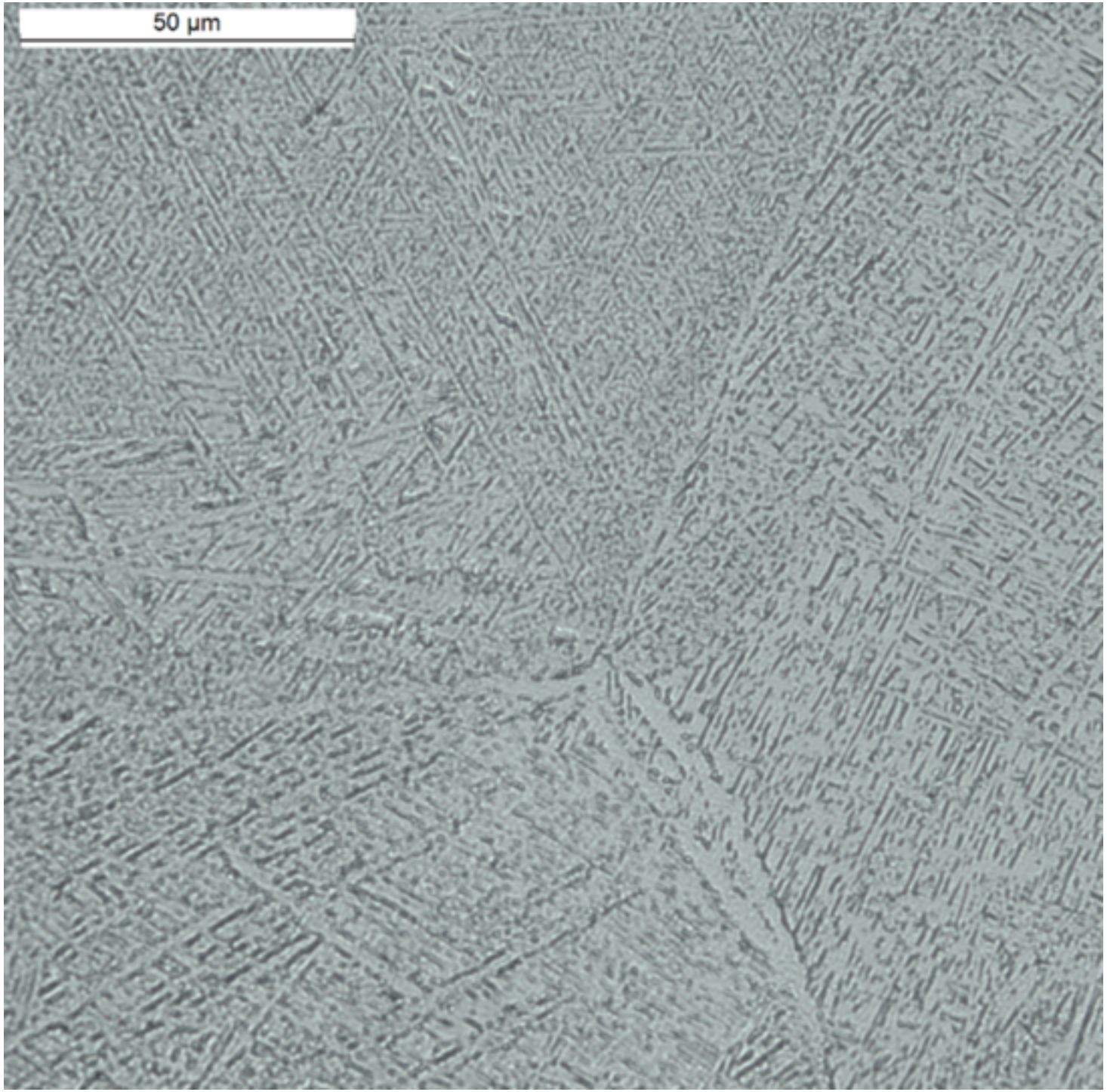

Figure 2b

Click here to access/download;Figure(s);Fig 2b.tif

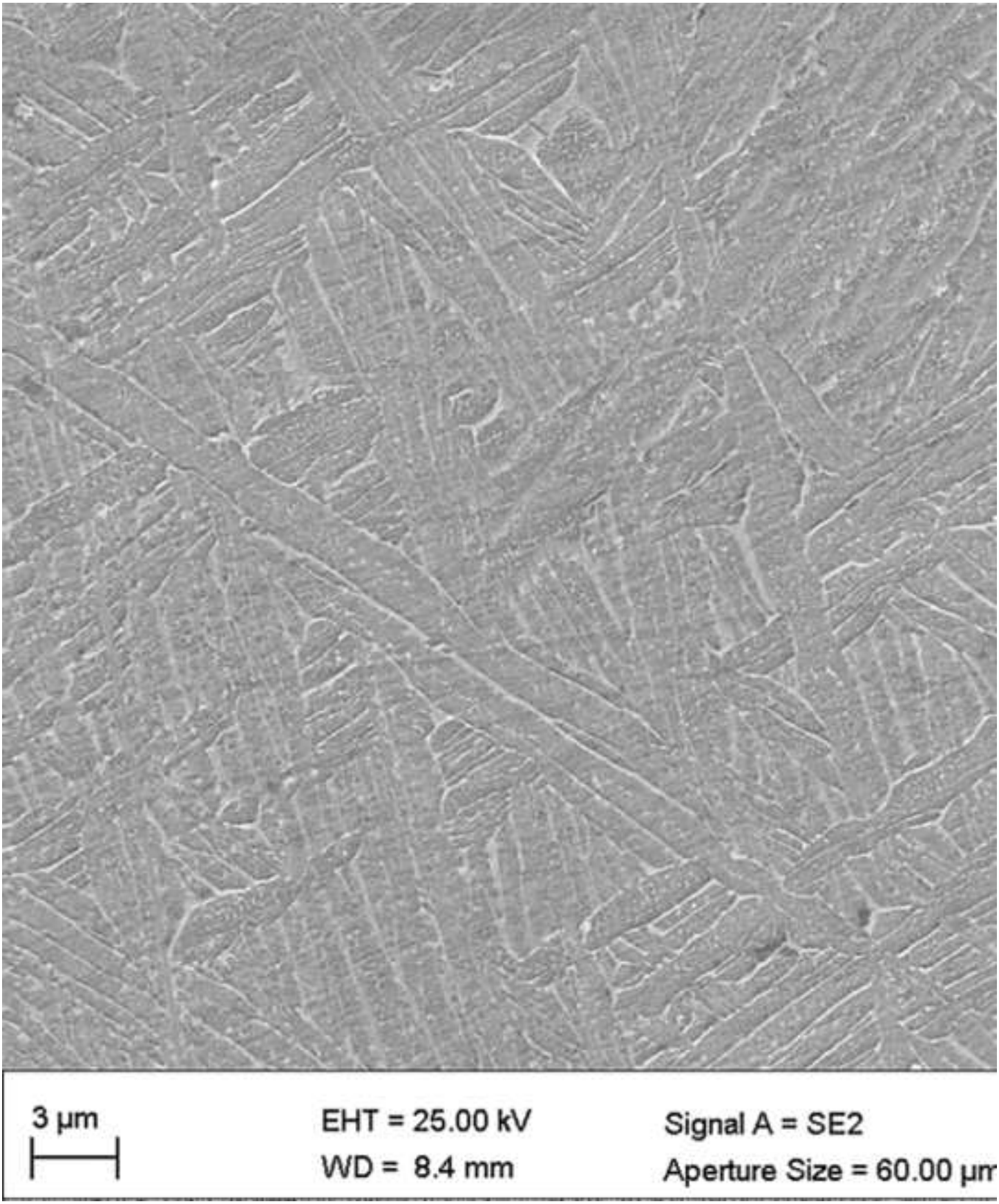

Figure 3

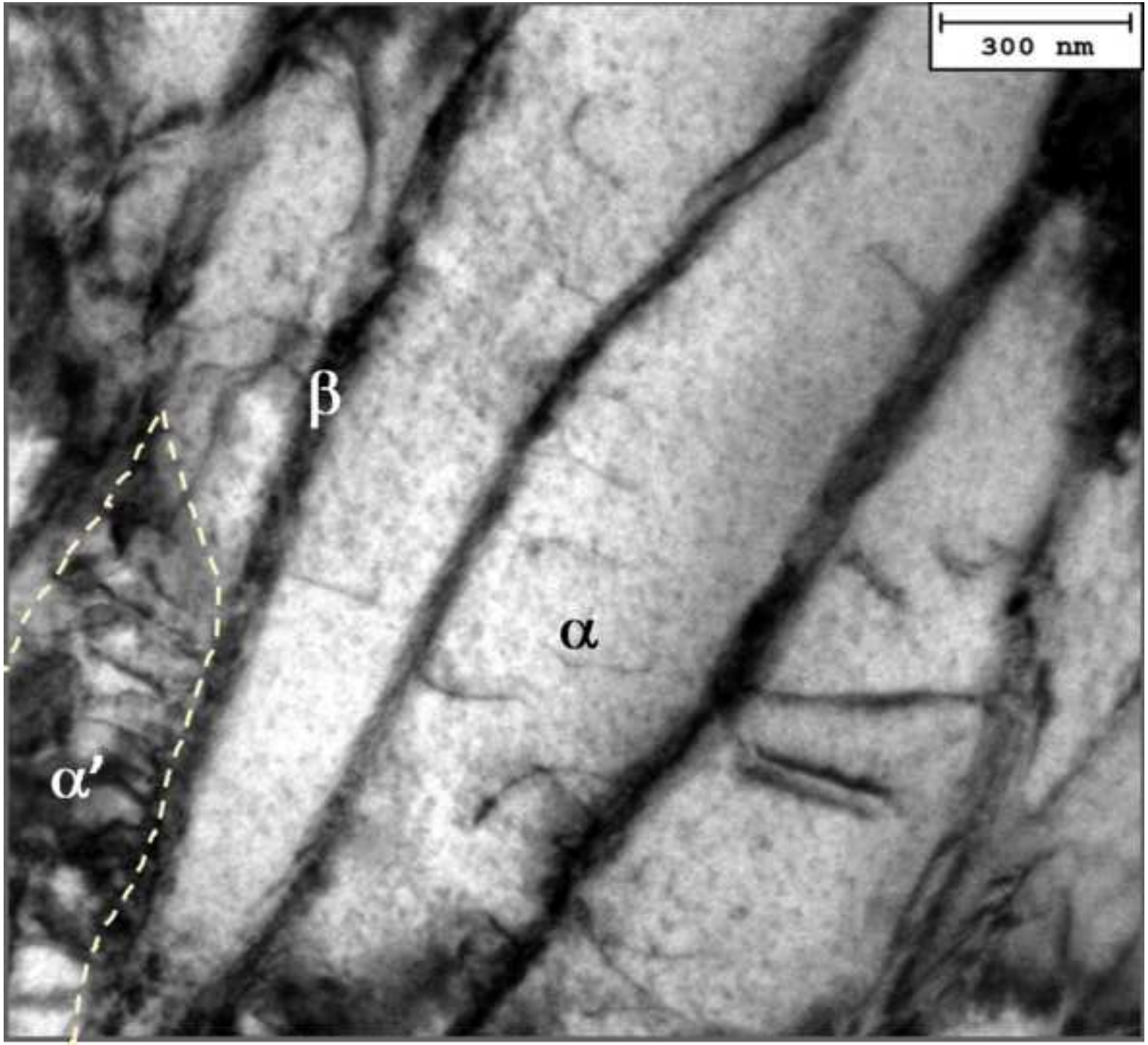

Figure 4a

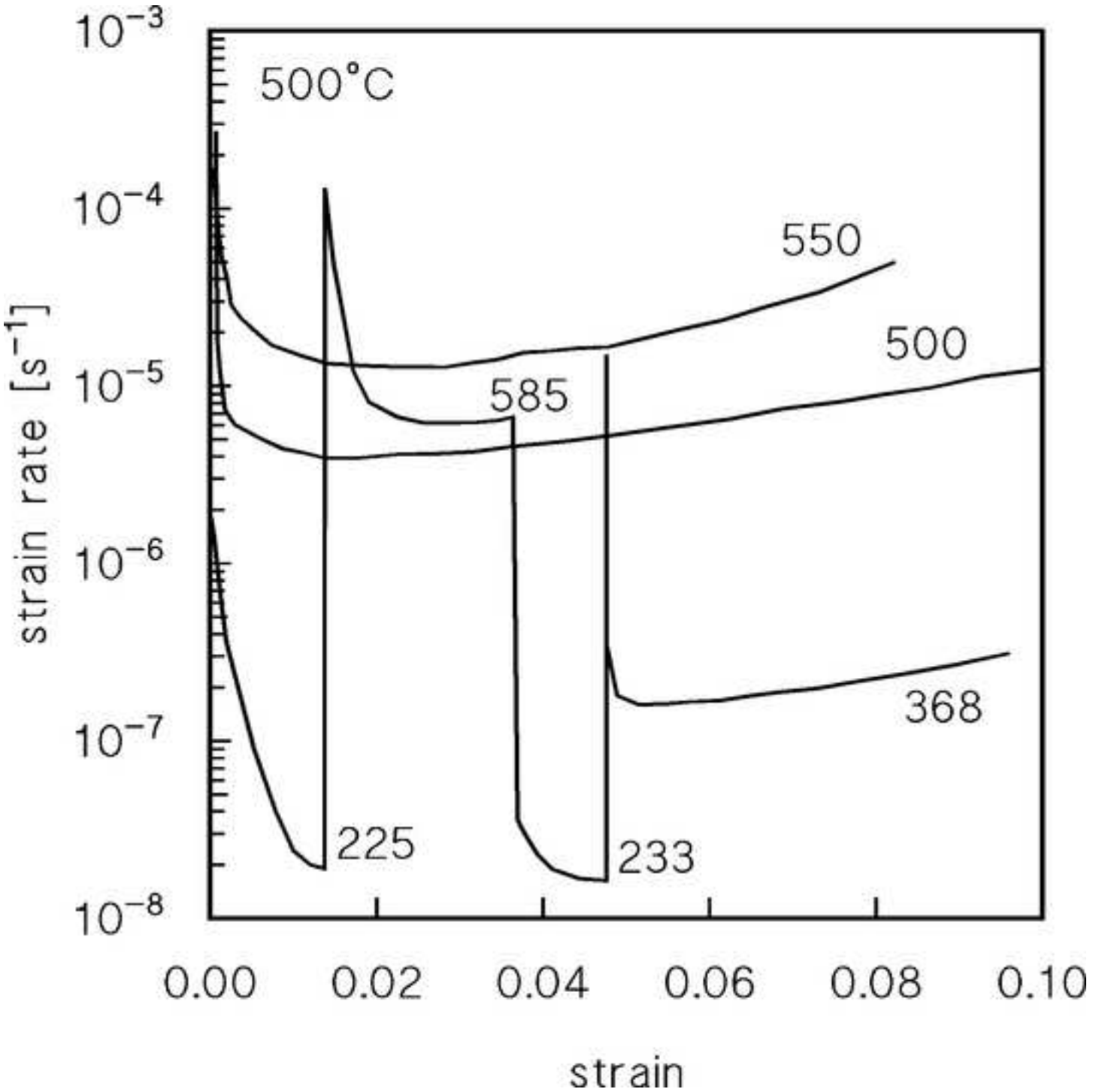

Figure 4b

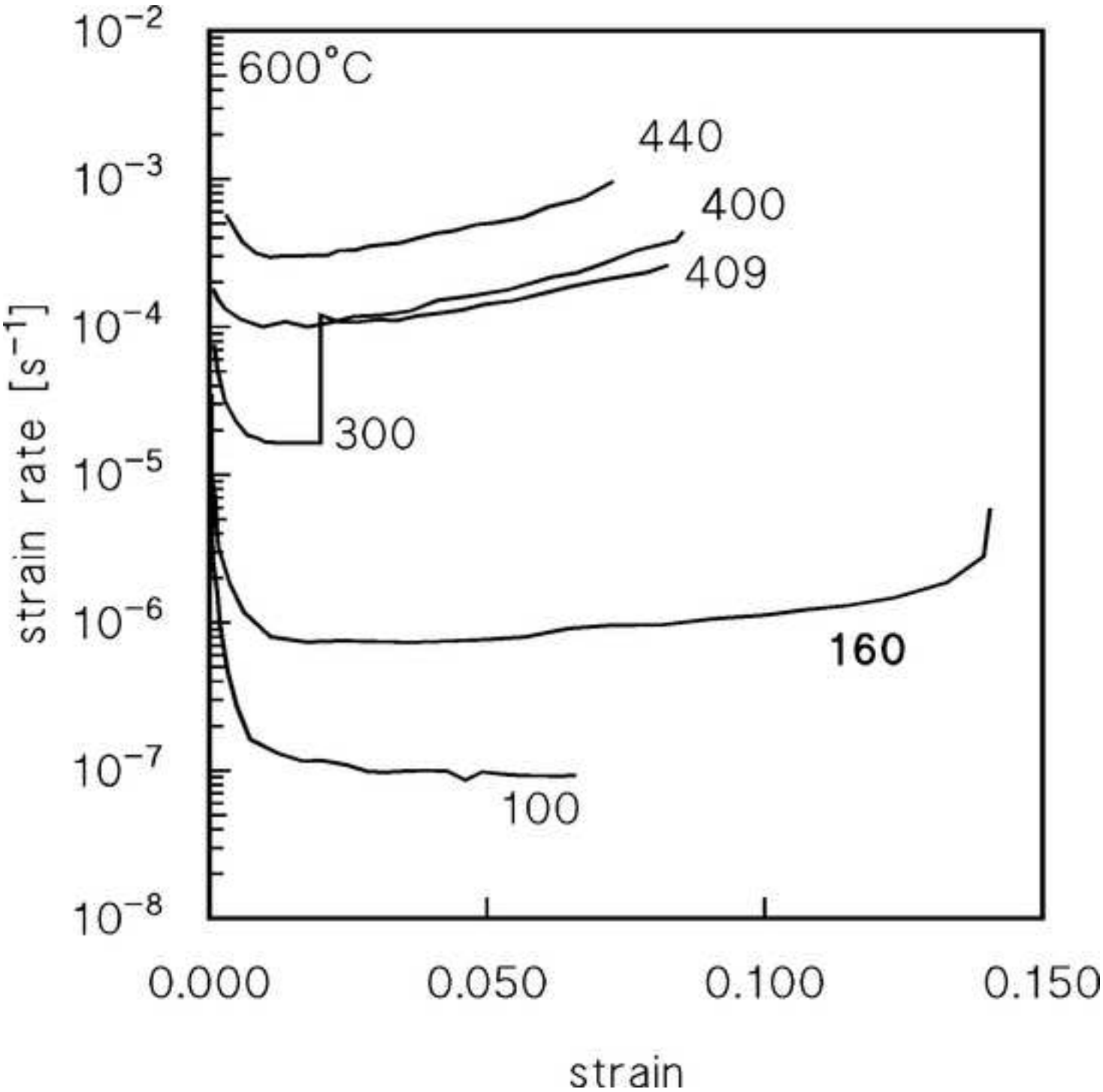

Figure 5

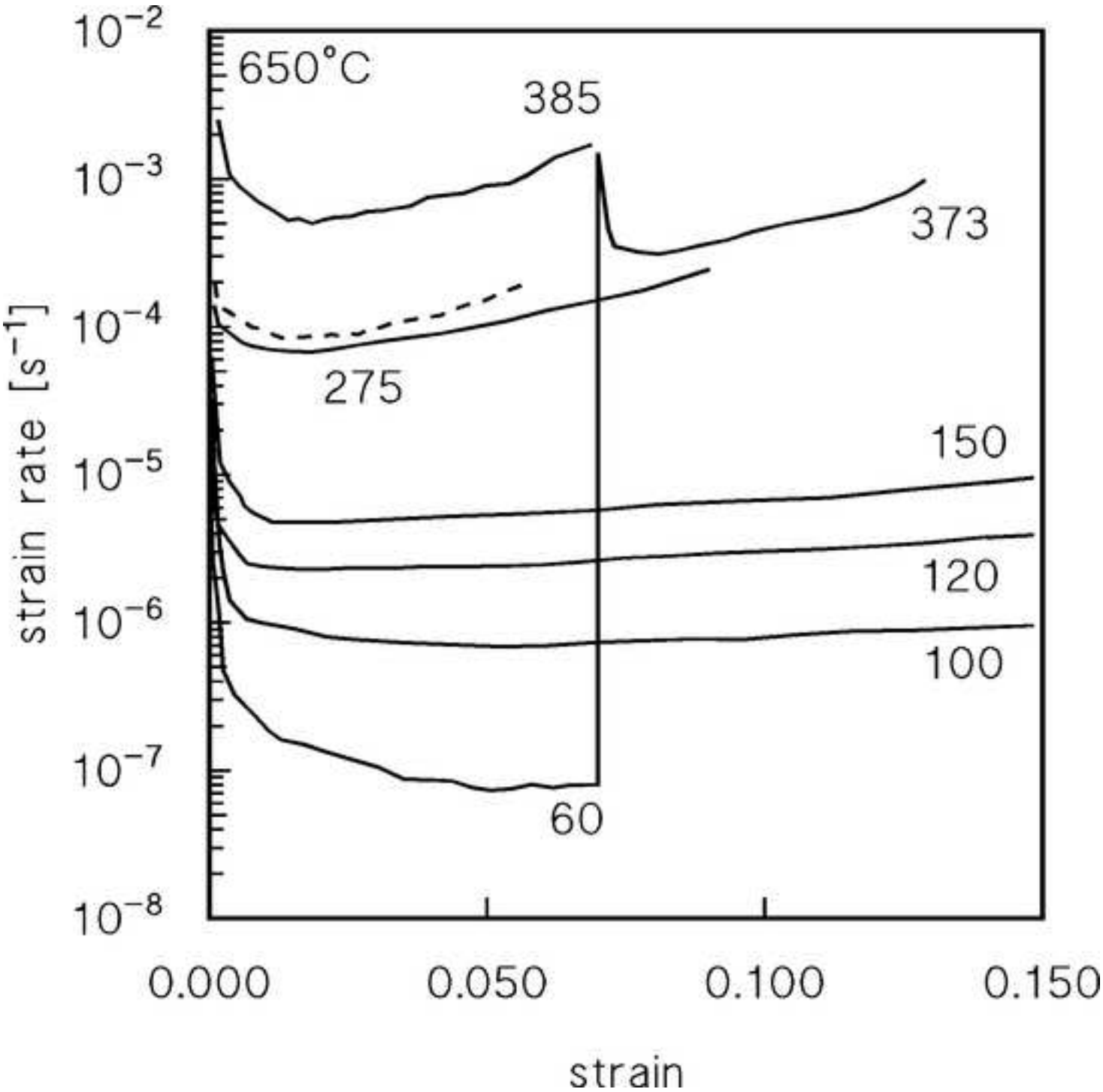

Figure 6

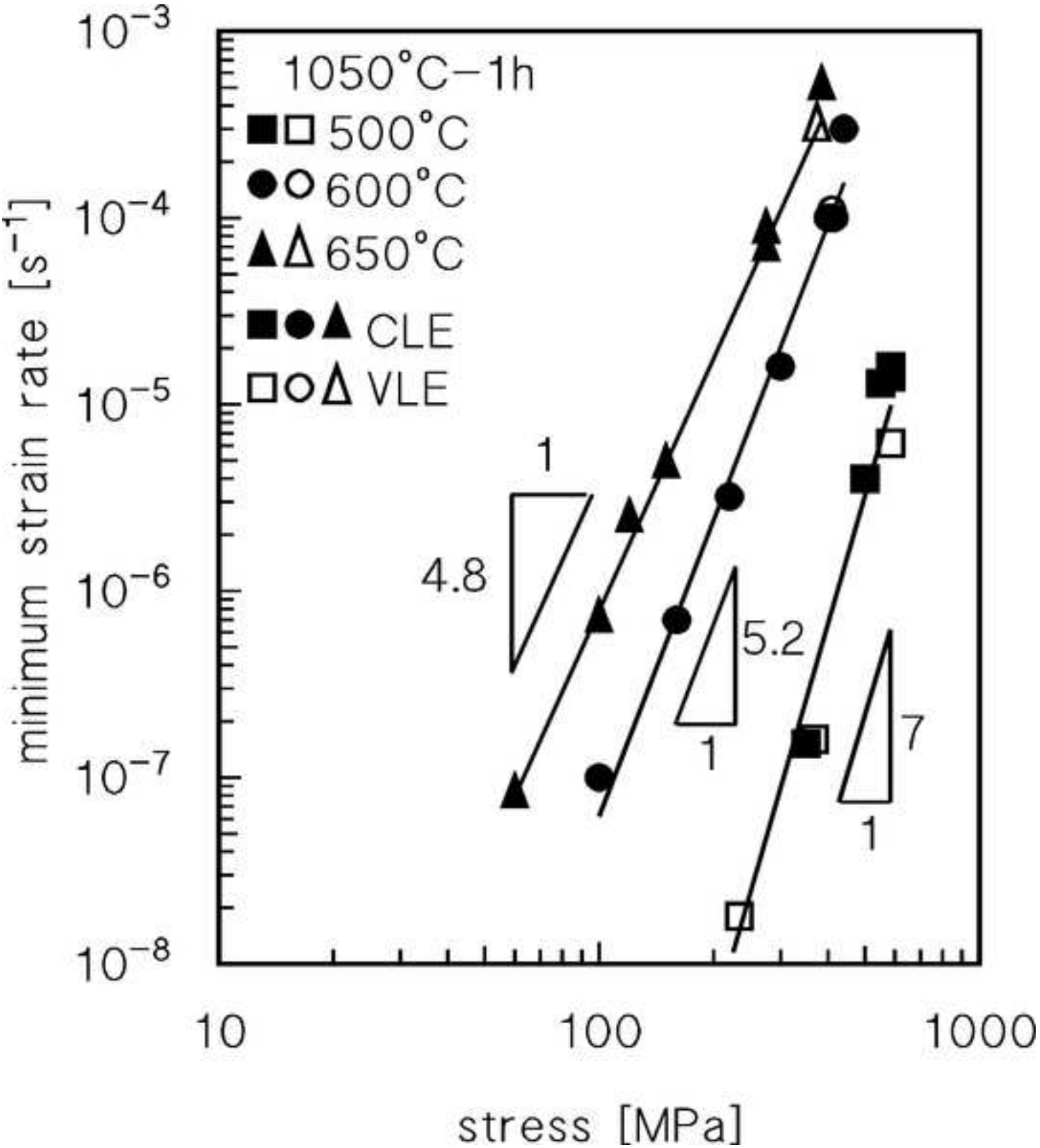

Figure 7a

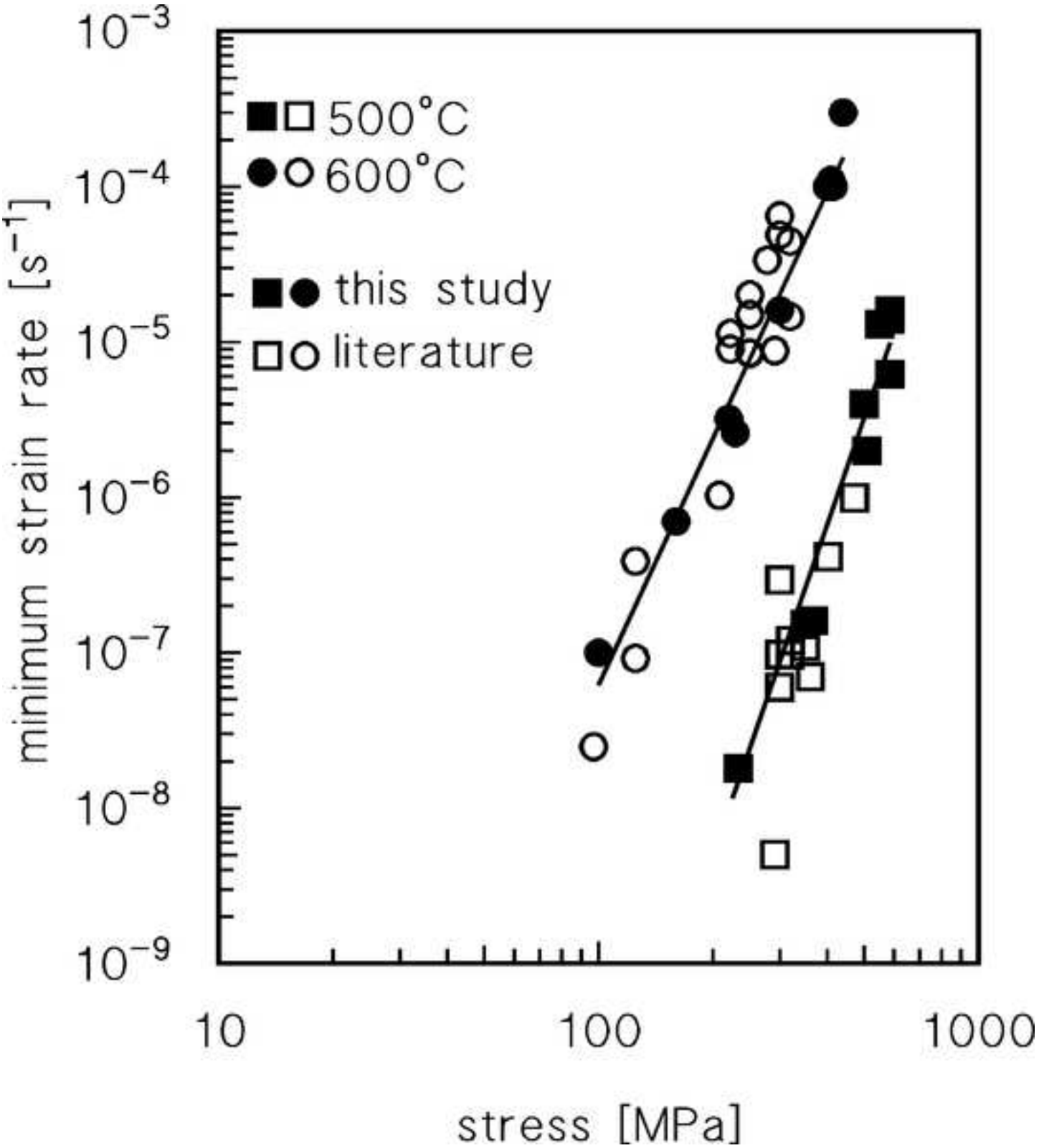

Figure 7b

Click here to access/download;Figure(s);Fig 7BN.TIF

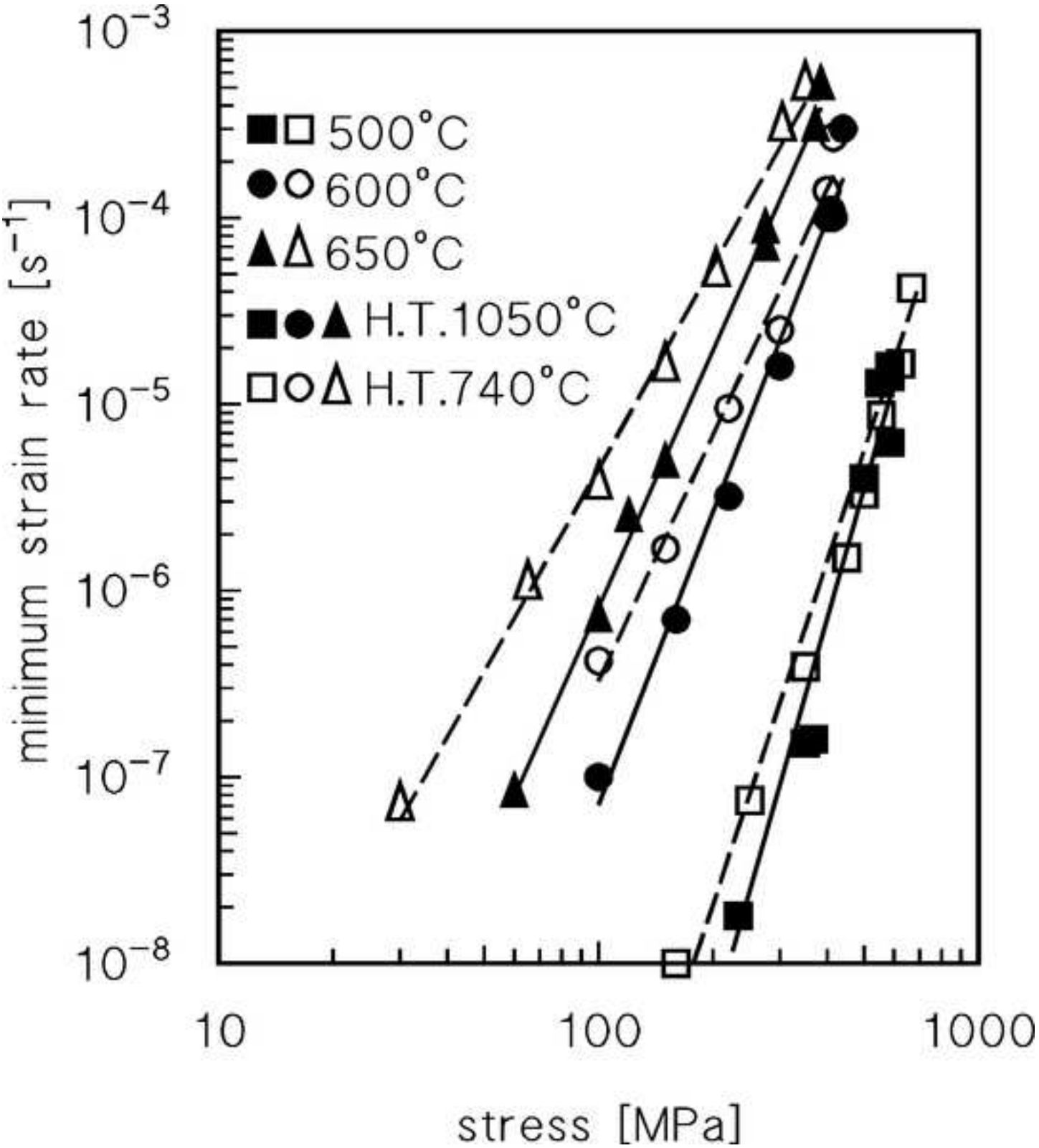

Figure 8

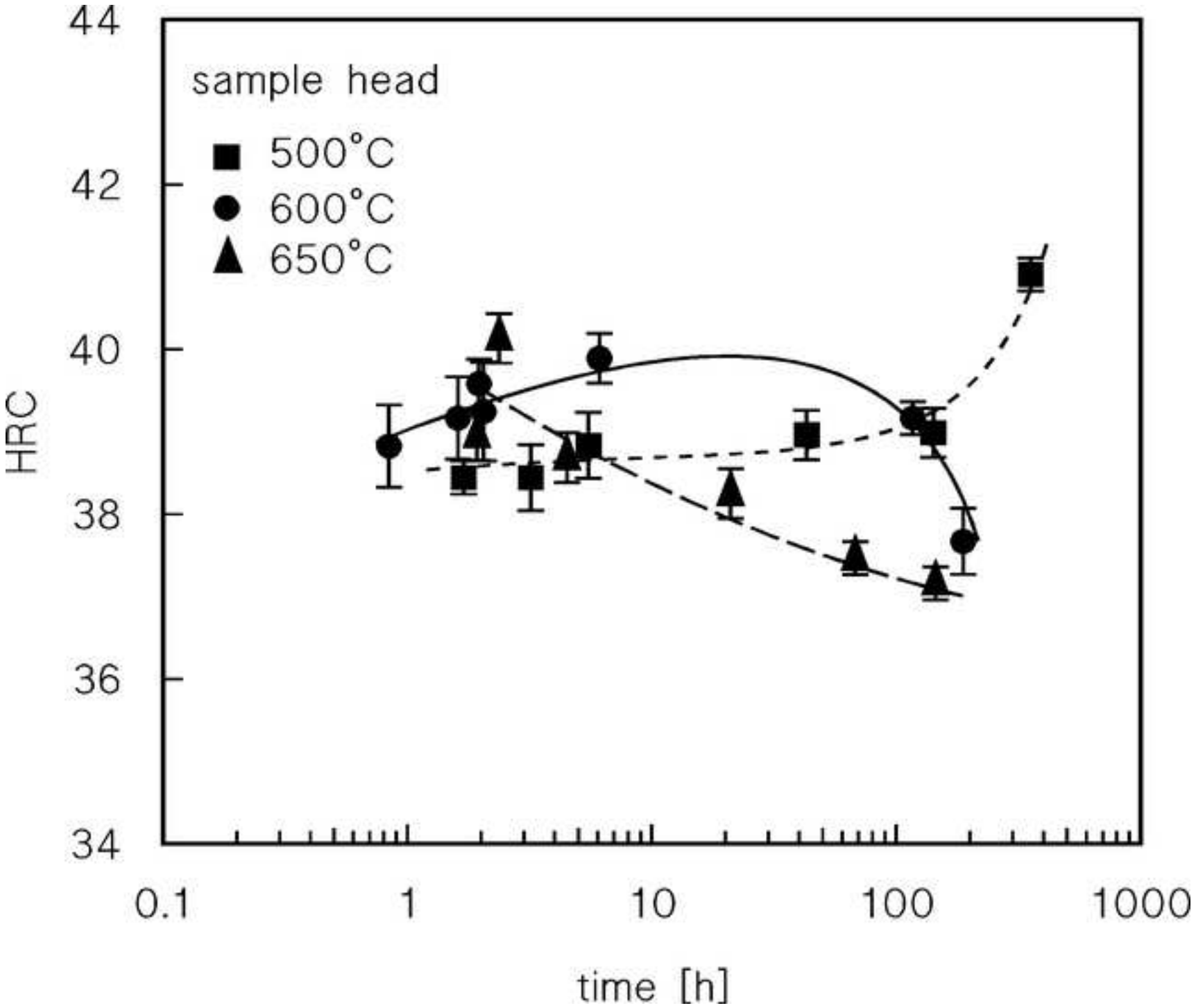

Figure 9

Click here to access/download;Figure(s);Fig 9.tif

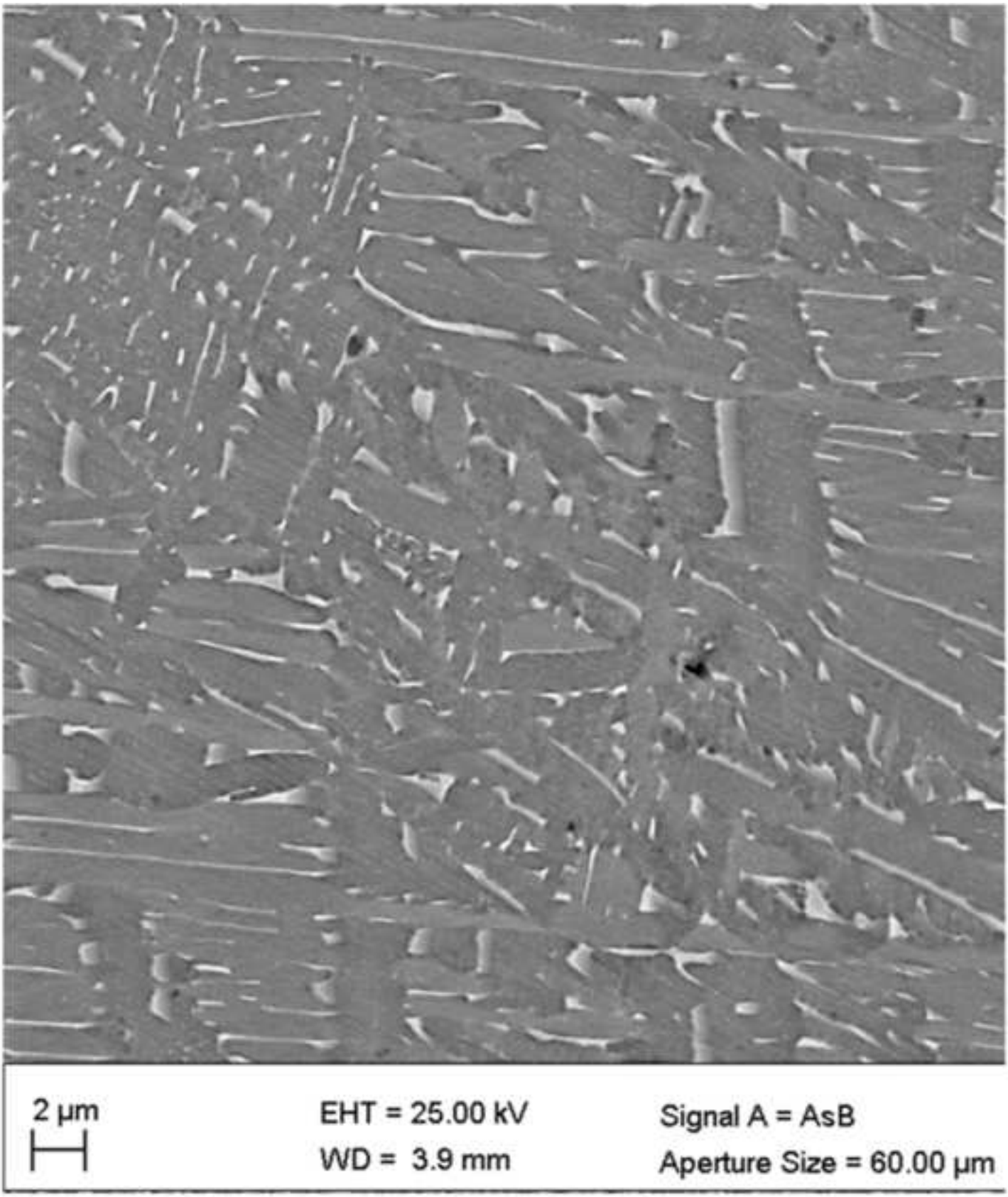

Figure 10a

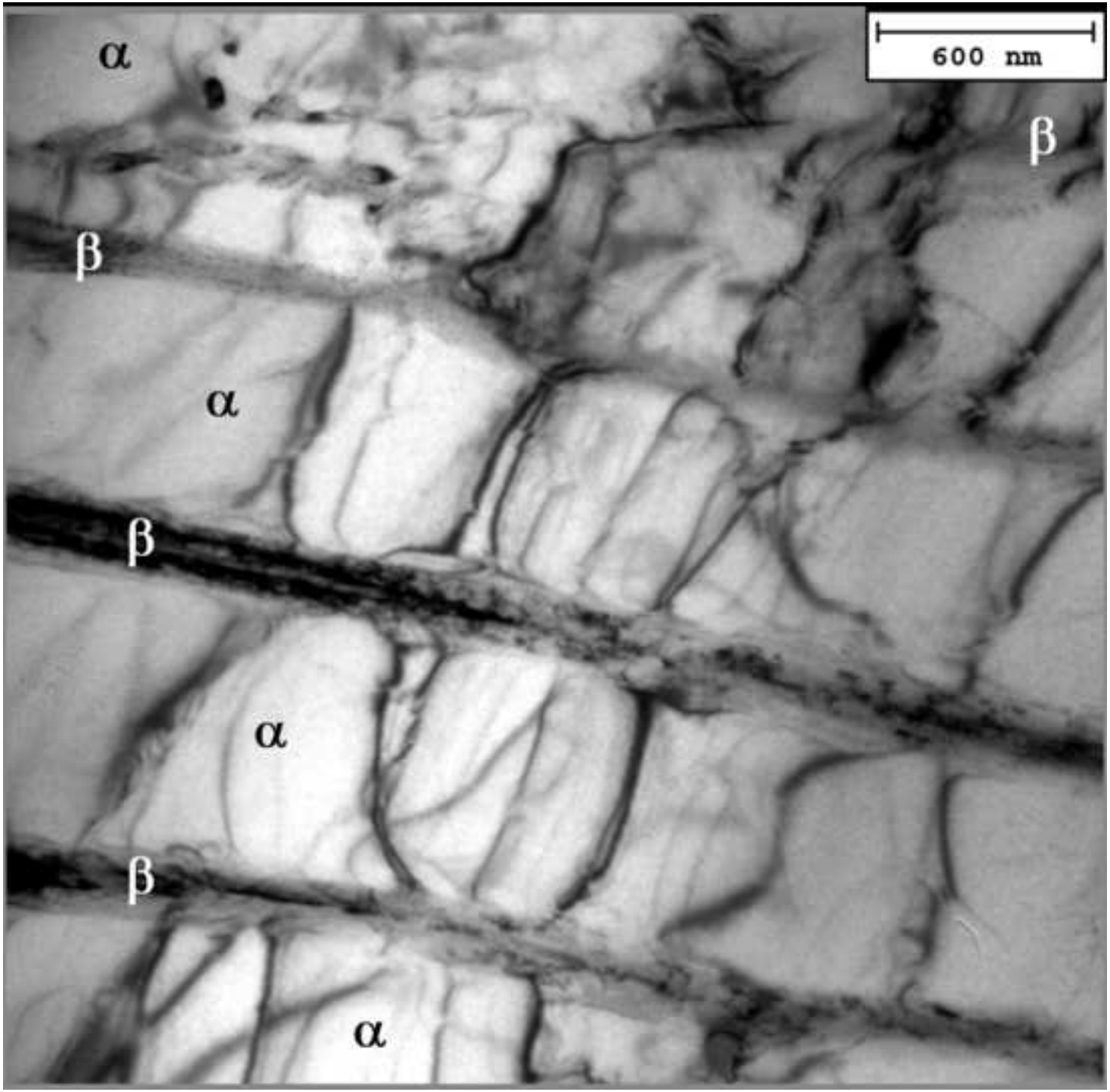

Figure 10b

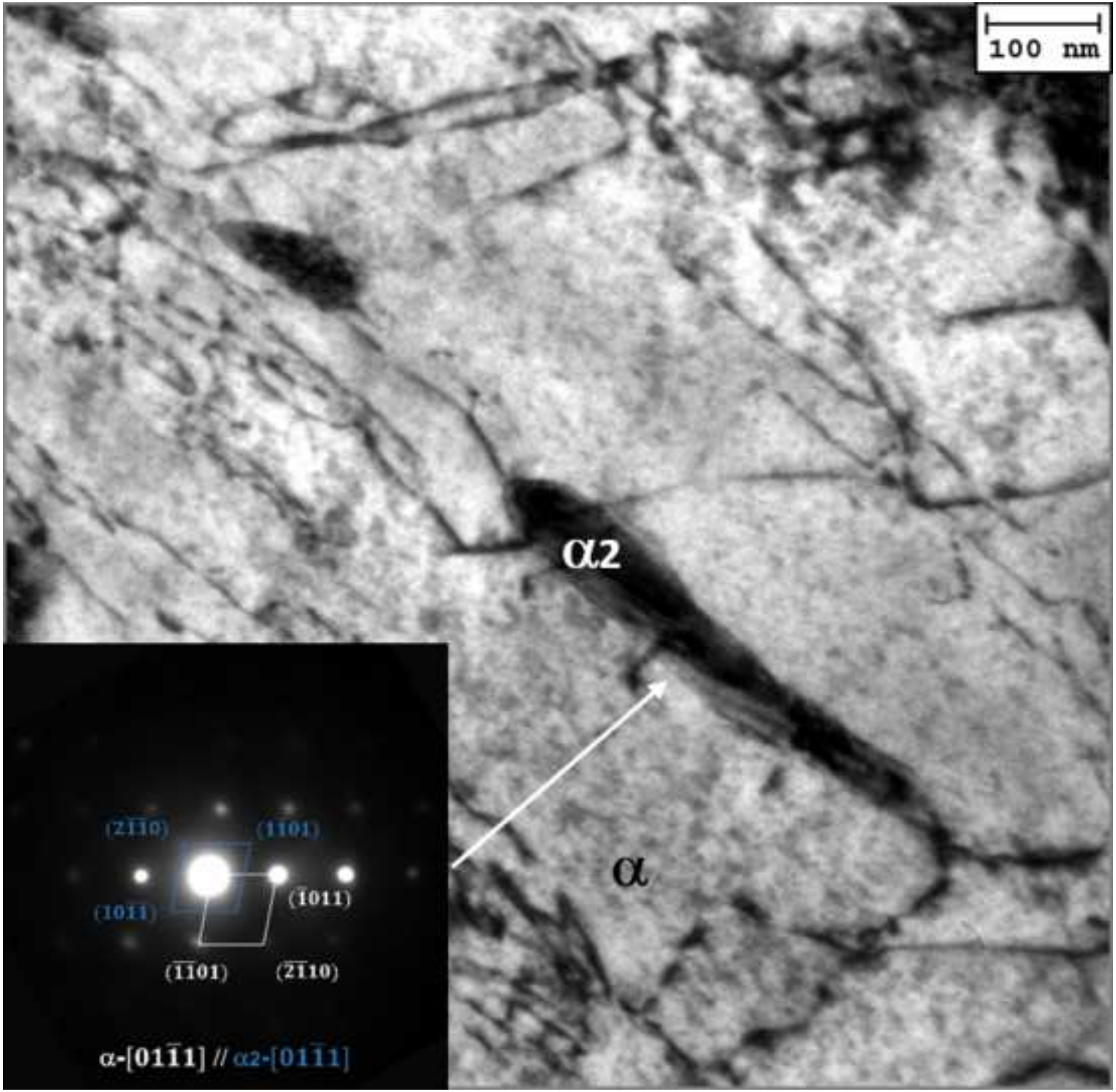

Figure 10c

Click here to access/download;Figure(s);Fig 10c.tif

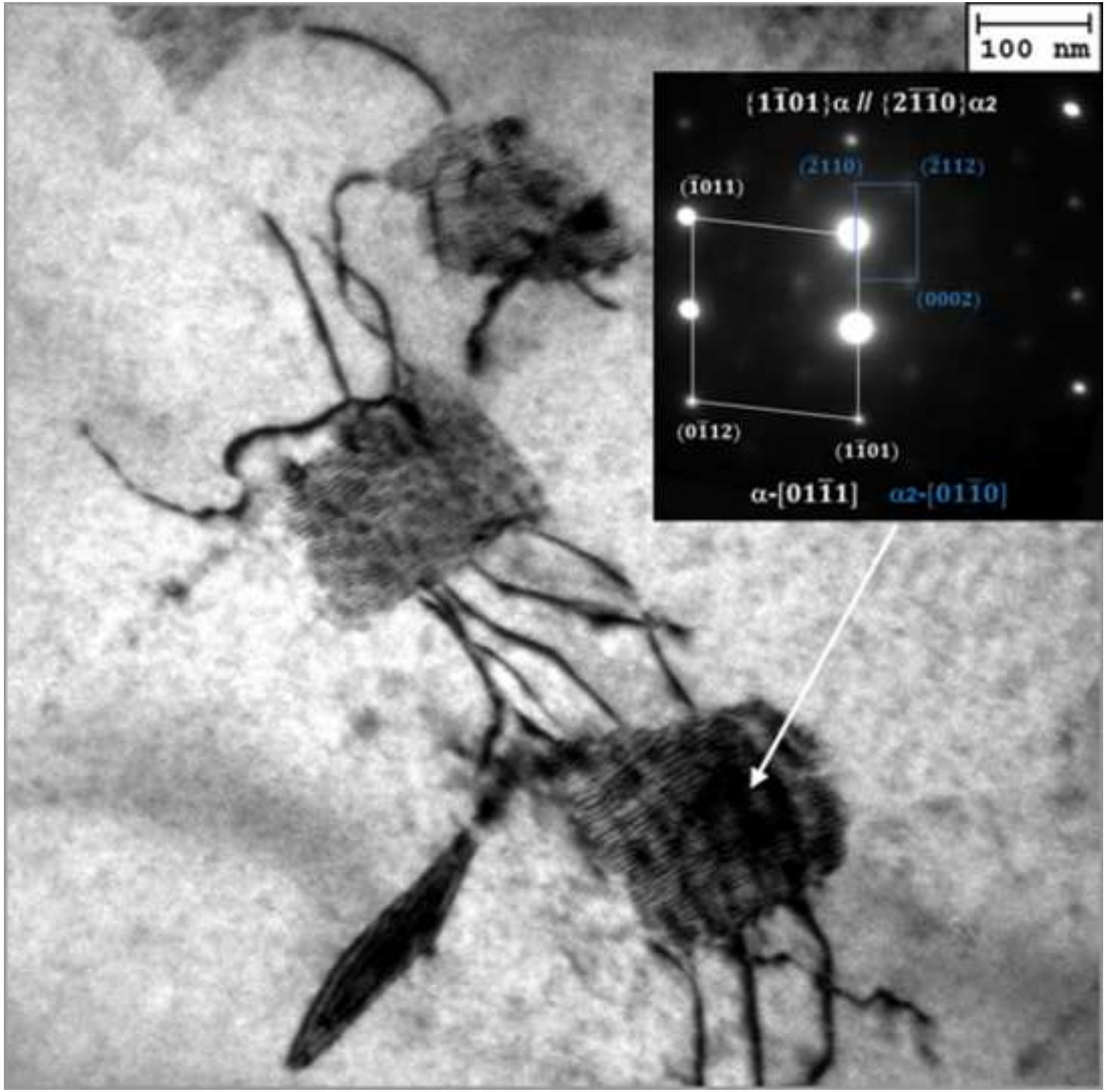

Figure 10d

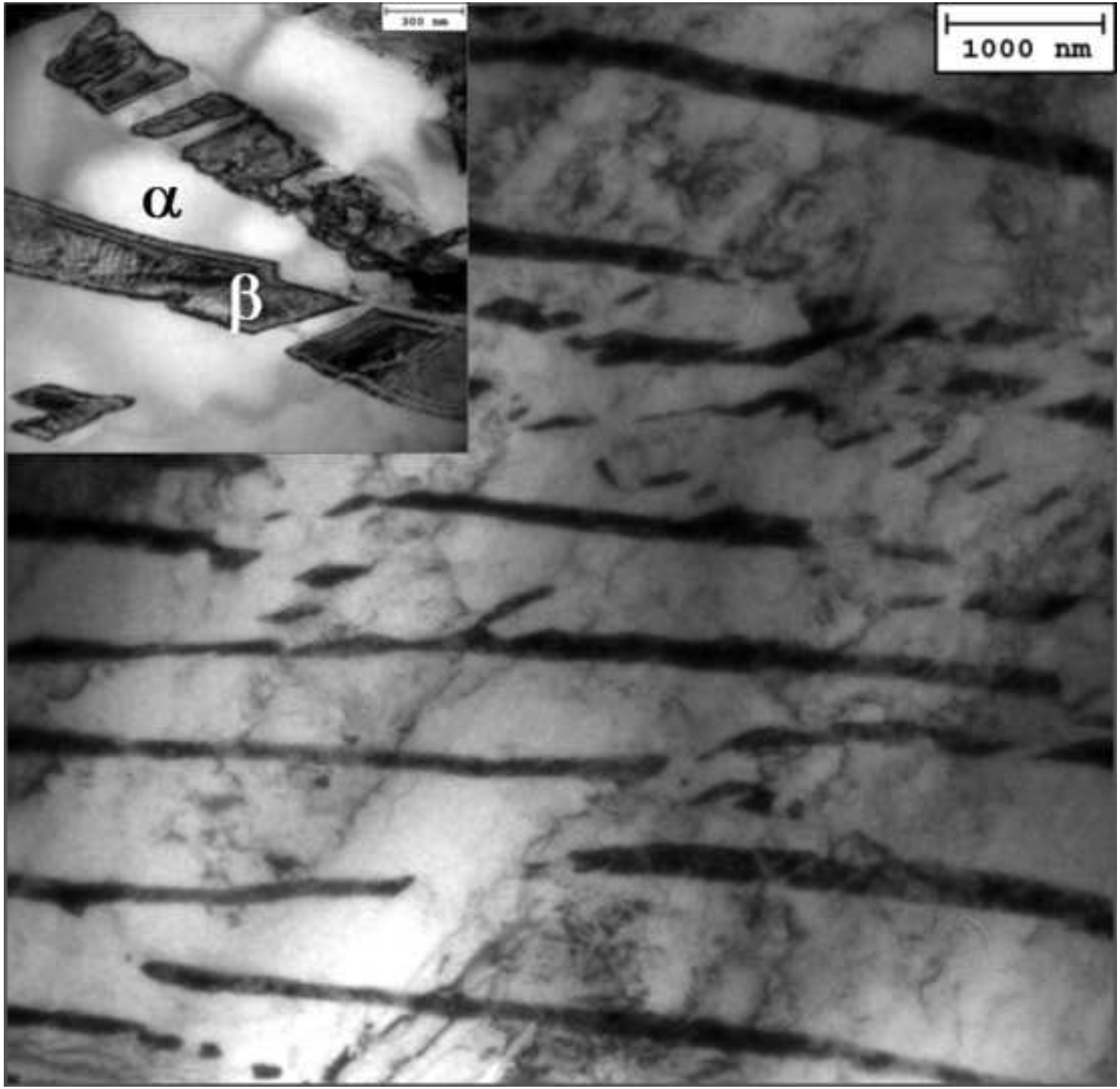

Figure 11a

Click here to access/download;Figure(s);Fig 11a (rev1).tif

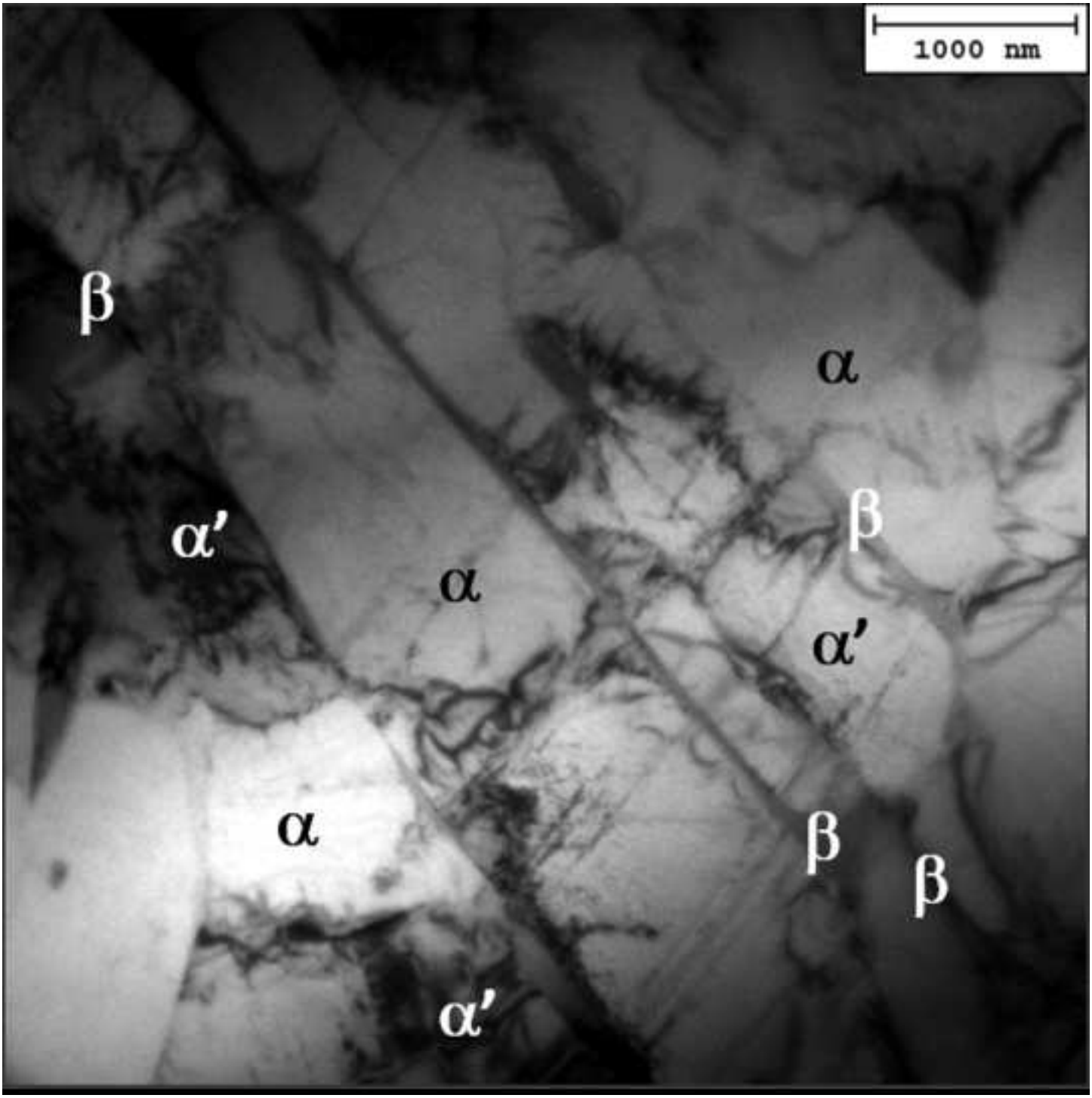

Figure 11b

Click here to access/download;Figure(s);Fig 11b (rev1).tif

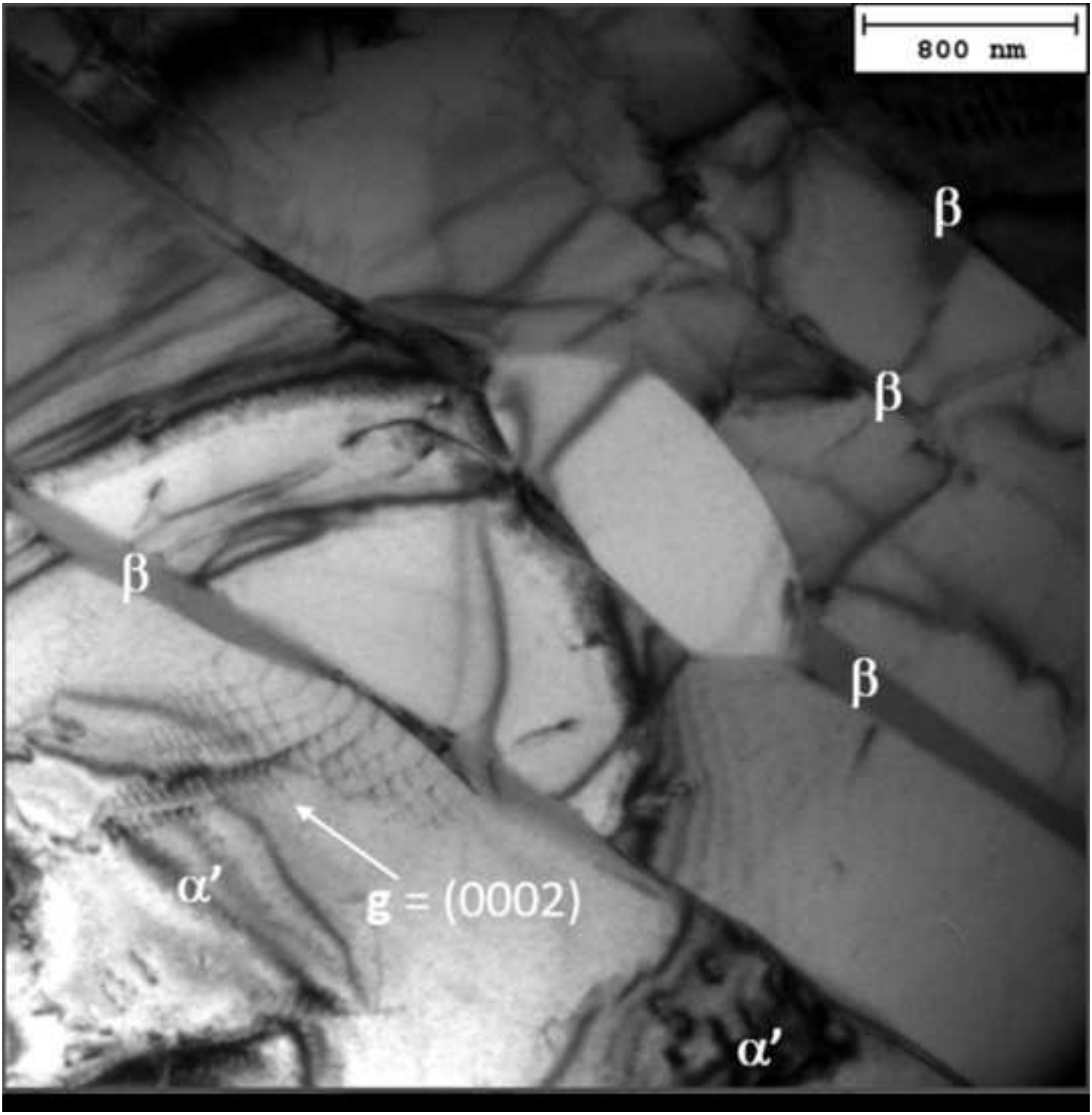

Figure 11c

Click here to access/download;Figure(s);Fig 11c (rev1).tif

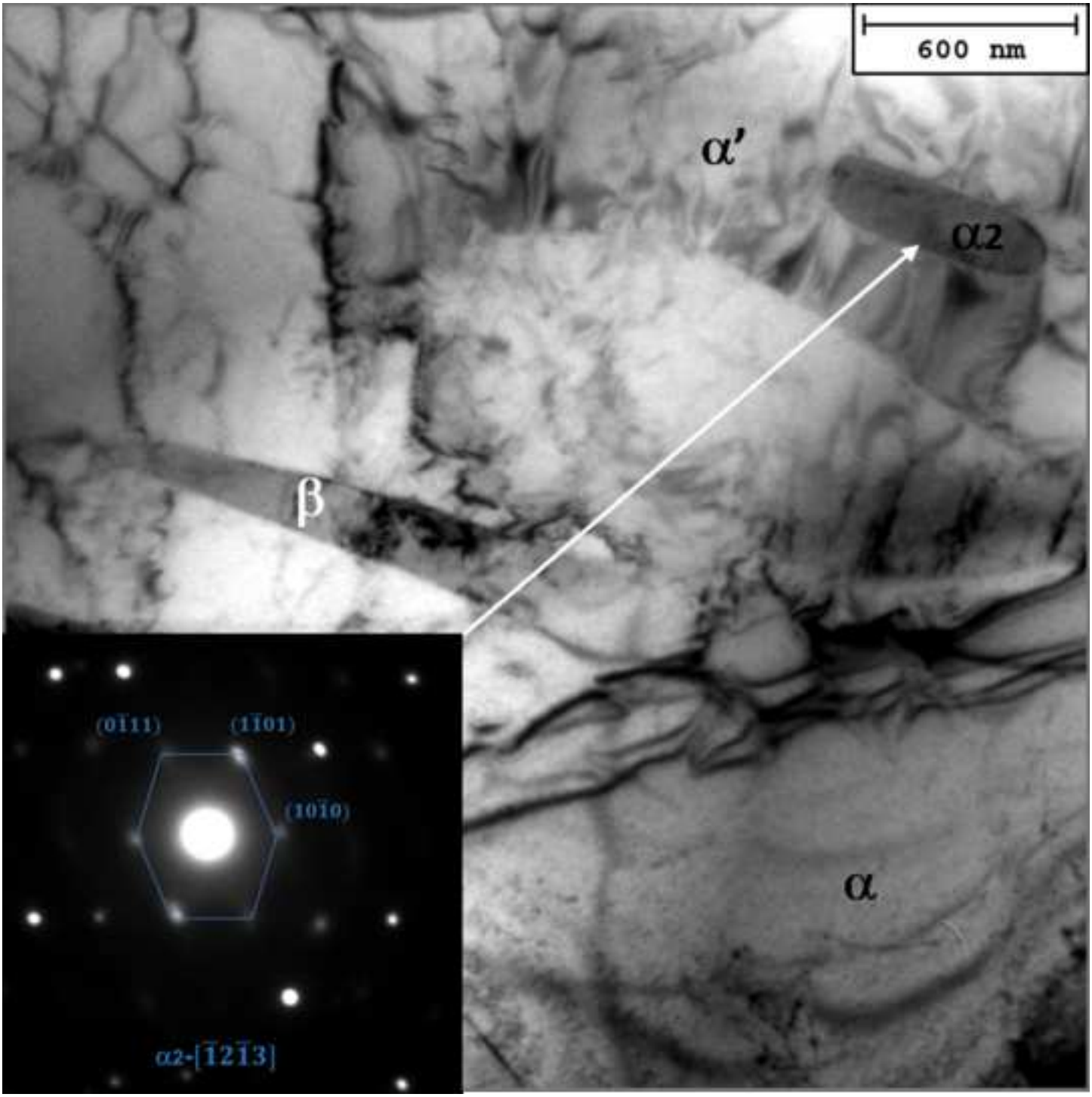

Figure 12a

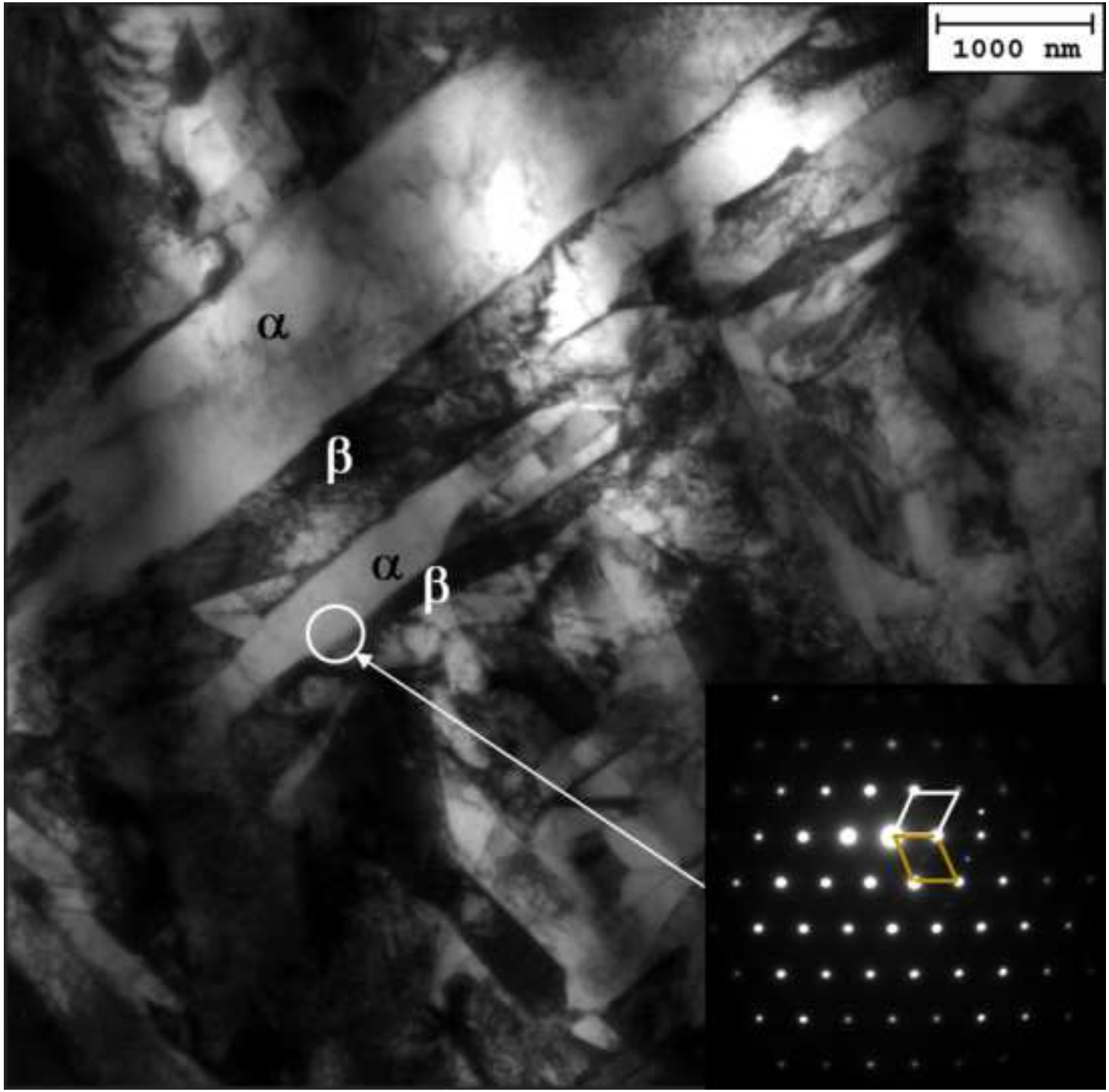

Figure 12b

Click here to access/download;Figure(s);Fig 12b.tif

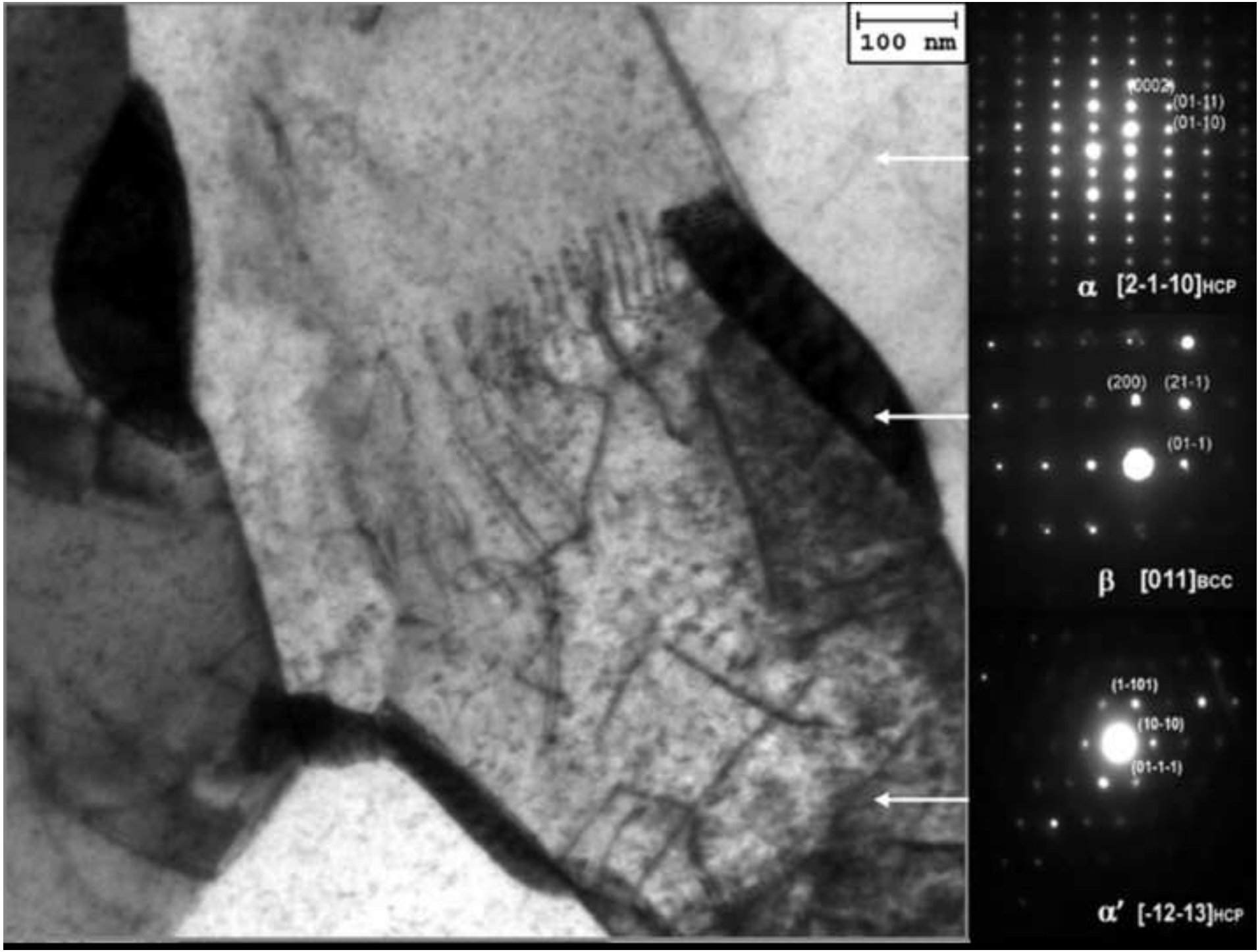

Figure 13

Click here to access/download;Figure(s);Fig 13.TIF

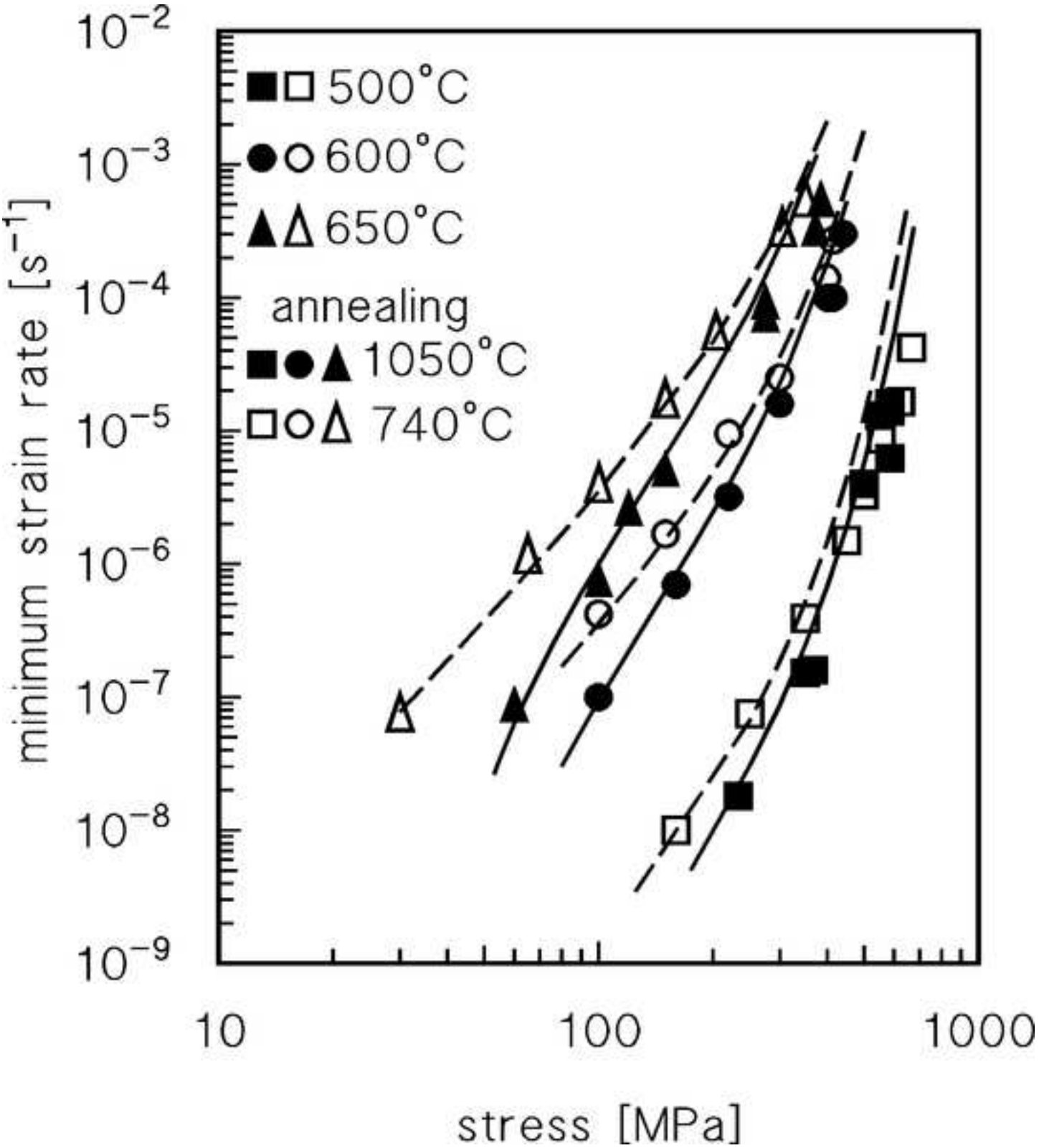

Figure 14

Click here to access/download;Figure(s);Fig 14.TIF

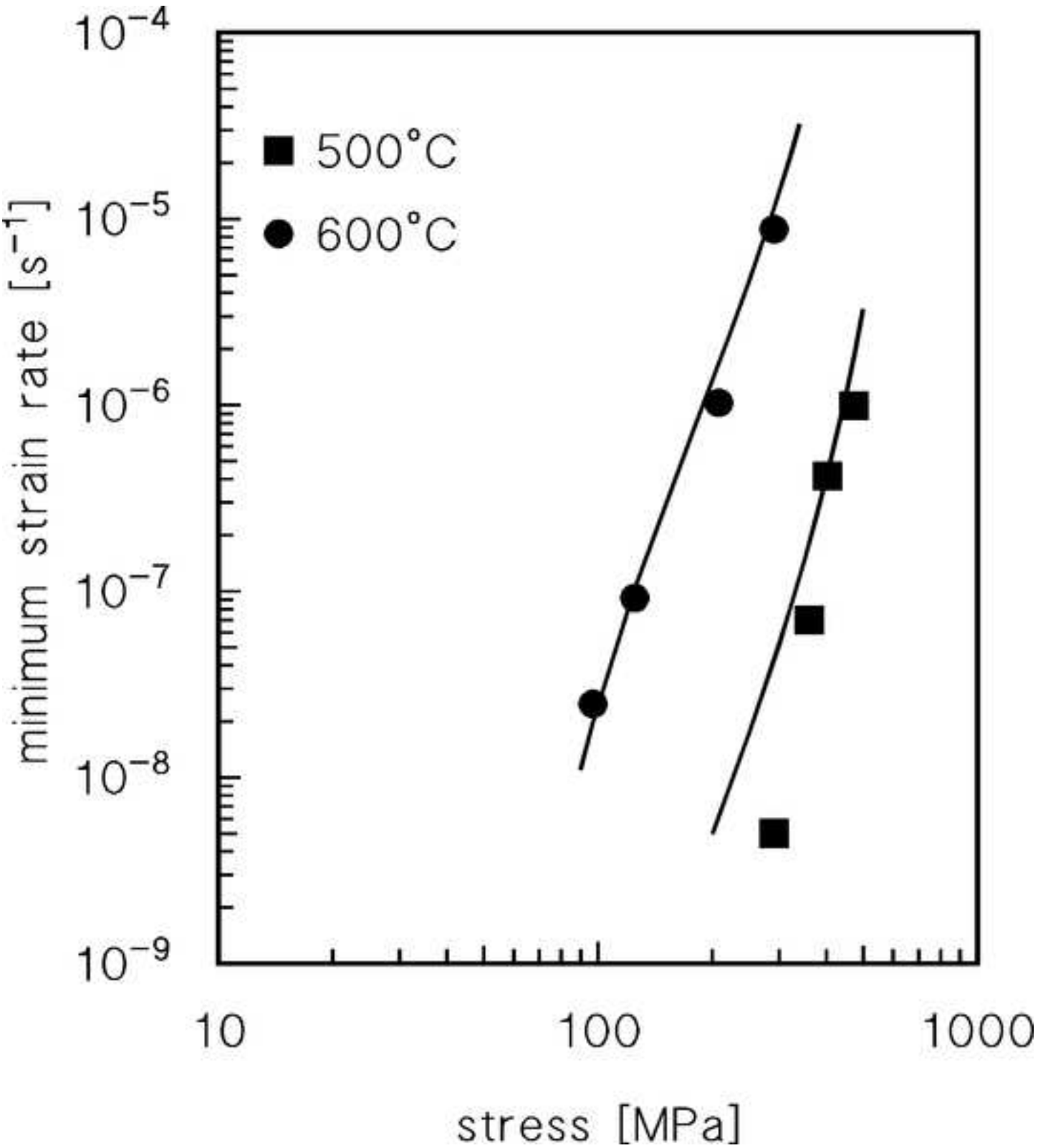

Figure A2.1a

Click here to access/download;Figure(s);AP1.TIF

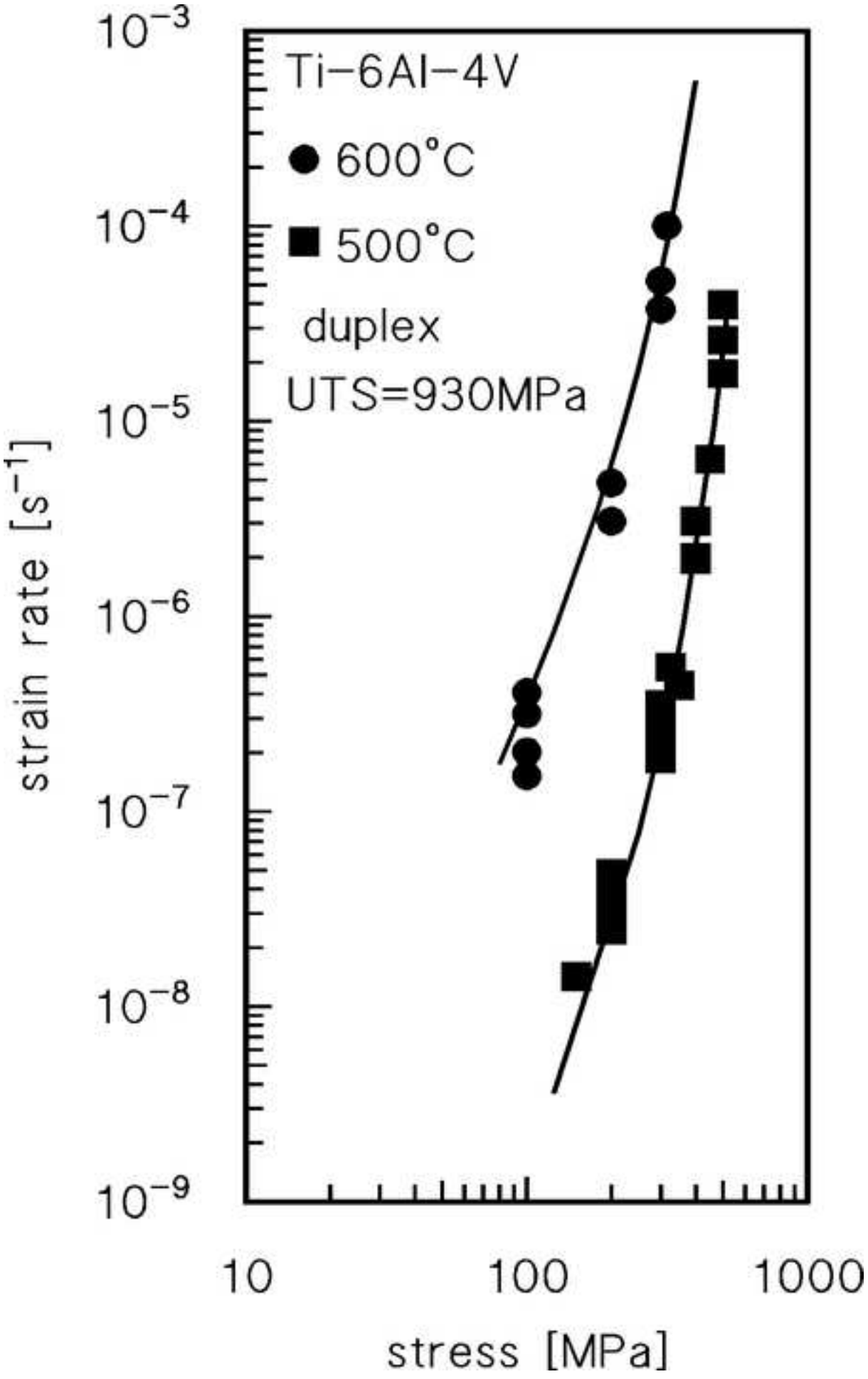

Figure A2.1b

Click here to access/download;Figure(s);AP2.TIF

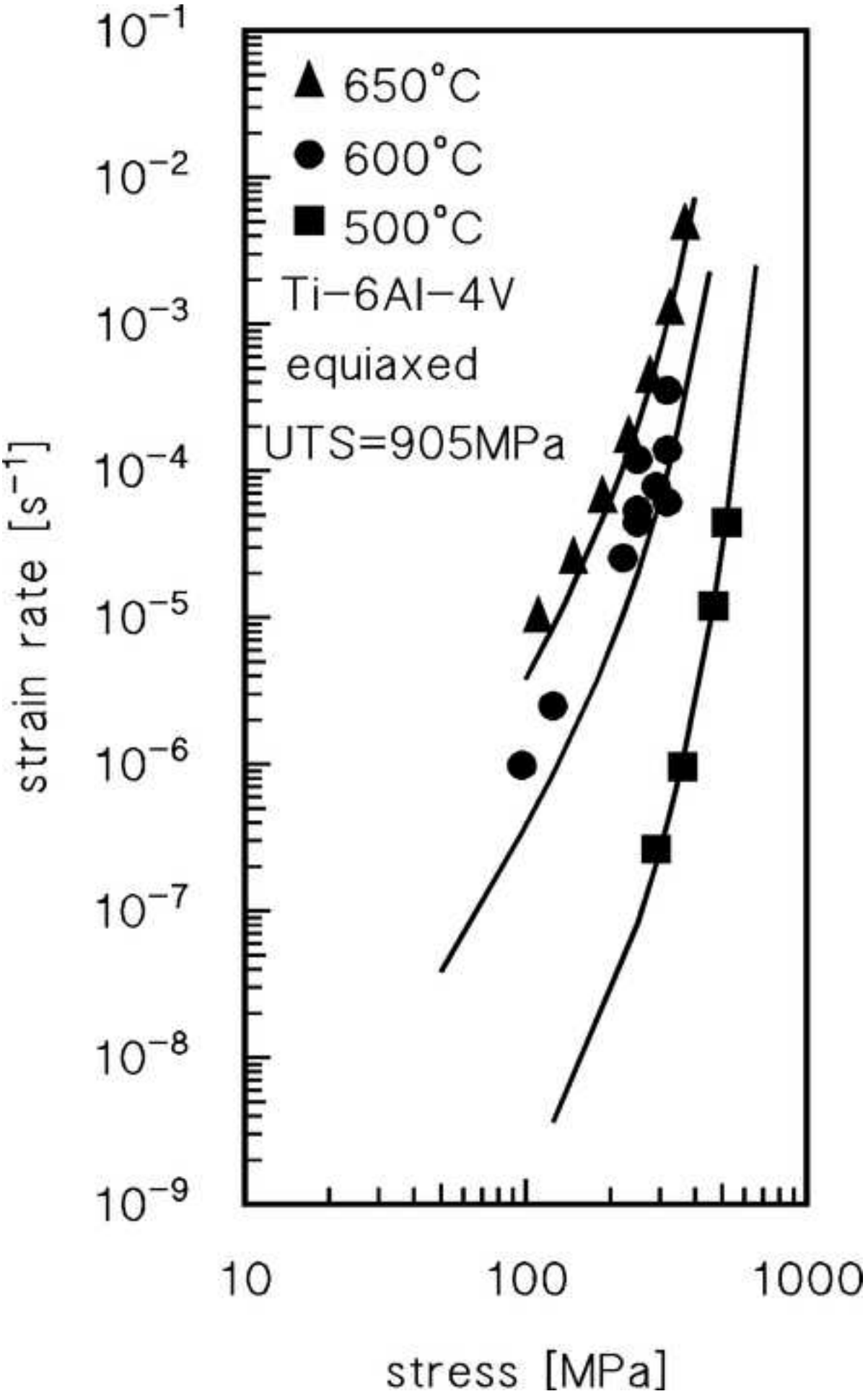

Figure A2.1c

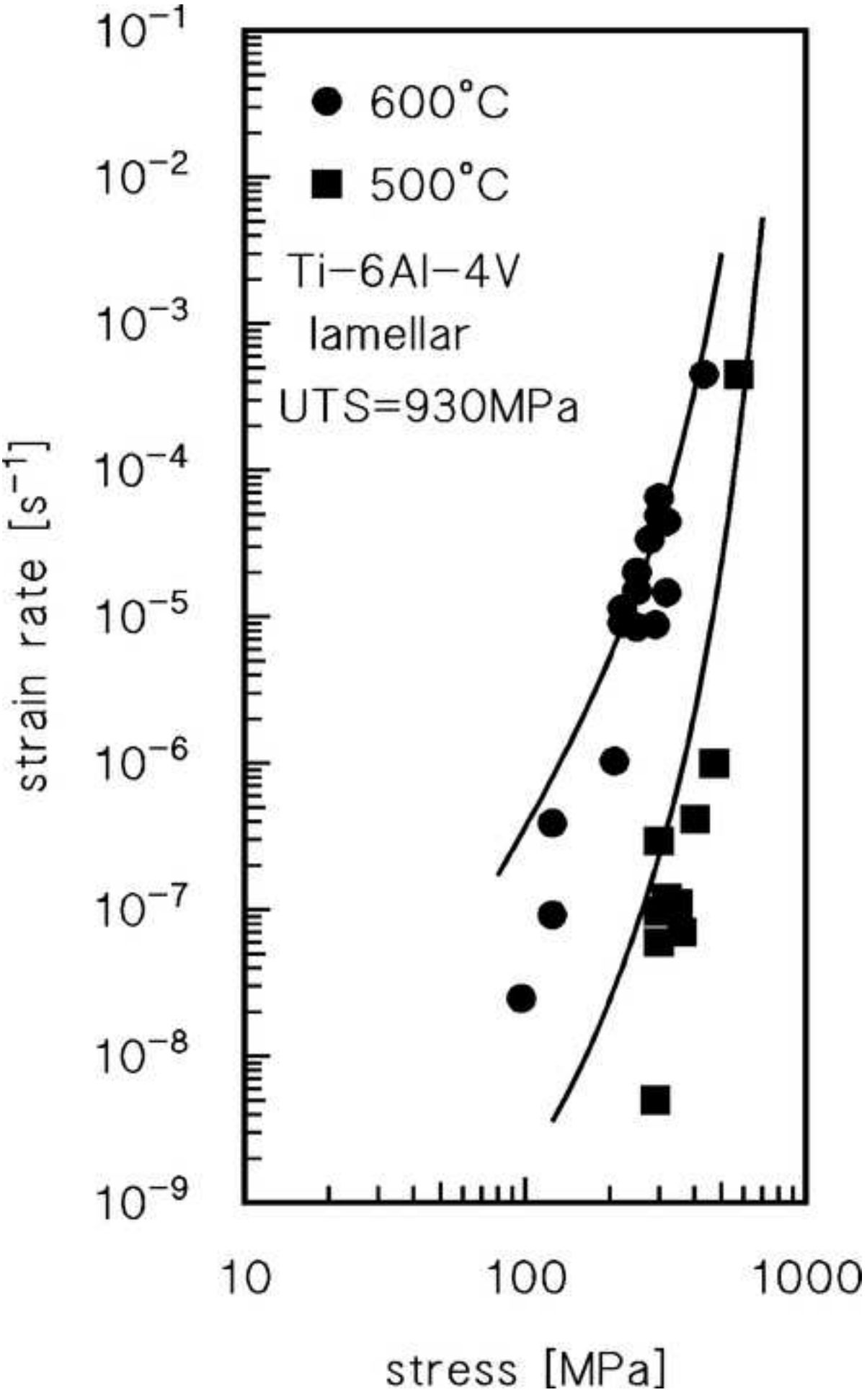

Table I. Volume fractions (% vol.) of β, α′, α_2, and α-phases in VLE samples crept at 650 °C/60 MPa (initial stress) and 500 °C/225 MPa.

crept sample	β	α’	α_2	α
500 °C and 225/577/233/368 MPa	~12.0	~2	~0.15	bal.
650 °C and 60/373 MPa	~9.5	~1	~0.08	bal.

Table II. Volume fractions (% vol.) of β, α, and α′ phases in VLE500, CLE600, and CLE650 samples.

Creep sample	β	α′	α
500 °C and 160/667 MPa	~3	~8	bal.
600 °C and 100 MPa	~4	<1	bal.
650 °C and 100 MPa	~8	<1	bal.

Declaration of interests

☒ The authors declare that they have no known competing financial interests or personal relationships that could have appeared to influence the work reported in this paper.

☐The authors declare the following financial interests/personal relationships which may be considered as potential competing interests:

ELSEVIER

Certificate of Elsevier Language Editing Services

The following article was edited by Elsevier Language Editing Services:

"Creep response of Ti-6Al-4V alloy produced by additive manufacturing: effect of annealing at 1050°C"

Authored by:

Marcello Cabibbo

Date: 18-Jul-2022

Serial number: LE-244504-E13D7F6F518B

CRediT author statement

S. Spigarelli: Conceptualization, Methodology, Formal analysis, Writing - Original Draft. **C. Paoletti:** Validation, Investigation. **E. Cerri:** Validation, Investigation. **E. Santecchia:** Methodology, Writing - Review & Editing, Visualization. **M. Cabibbo:** Conceptualization, Investigation, Writing - Original Draft.